KOMUNIKÁCIE
COMMUNICATIONS

Dear readers,

We live in a world driven by accelerating change, registered in addition to other spheres of our life, through science and technology including also the field of electrical and electronic engineering. During several past decades many new materials, technologies, devices and experimental methods have been developed. New materials including semiconductors, dielectrics, glasses, metals, ceramics, structures, composite and organic materials have been prepared for new exciting applications for new generations of microelectronic, optoelectronic, telecommunications and many other electrical and electronic device applications. Nano-structural technology goes through the information technology, solar cells, micro-sensor and biosensor technology, high-speed power devices, integrated circuits, etc. New device concepts for major areas of the current and future electrical applications lies in the understanding of the basic principles conditioning the rapid development in this field.

*In this issue of the journal **Communications** most of the articles present the work of both researchers at the Faculty of Electrical Engineering of Žilina University and some cooperative institutions and concern to the investigation of new materials, technologies and experimental techniques for electrical engineering. Thin silicon films for photovoltaic applications, carbon nanotubes, silicon MOS structures and organic wafers for perspective applications, nondestructive techniques of conducting materials, optical field scanning method and some other problems are presented here as a view at our research work and simultaneously as the contribution to electrical and electronic engineering development.*

Peter Bury

J. Müllerová – P. Šutta – S. Jurečka *

THIN-FILM SILICON IN PHOTOVOLTAICS: THE ROLE OF STRUCTURE AND MICROSTRUCTURE

Structure and microstructure of hydrogenated silicon thin films and the influence of the hydrogen dilution of silane plasma at the PEVCD deposition on the film properties were investigated. The results show that at dilution between 20 and 30 the transition between amorphous and crystalline phase occurs. The sample becomes a mixture of amorphous silicon, polycrystalline silicon with nano-sized grains and voids with decreasing hydrogen concentration at grain boundaries and post-deposition oxygen contamination. The dominance of Si-H bonds and presence of interstitial oxygen and oxygen bonded in surface Si-OH groups was observed.

1. Introduction

Solar cells convert solar energy into electricity – either directly through the photovoltaic effect (photovoltaic cells or PV cells) or via a two-step process converting solar energy first into heat or chemical energy. The PV industry and market progress rapidly owing to the global energy consumption demands, the need for renewable and sustainable power, as well as owing to the reducing technological costs. Growing PV market reflects the world-wide needs for non-polluting long-lasting electricity sources for remote devices, e.g. satellites, remote places, e.g. remote settlements, campers or small devices of everyday use, e.g. watches, calculators, cameras etc.

The main criteria to select the beneficial cell material are efficiency, stability and costs. Definitely the most used material in photovoltaics is silicon. Silicon PV industry takes advantage of material abundance, non-toxicity, and the possibility to share research efforts with microelectronic industry. Silicon in PV cells is used as:
- monocrystalline silicon (mc-Si) and polycrystalline silicon (poly-Si, polysilicon) – the cells are the most effective Si-based solar cells, however, they need expensive wafer-based production technologies suffering from substantial waste of material,
- amorphous silicon (a-Si) in the thin-films configuration – the cells are produced by the module-based technology, essential layers are deposited on the substrate mostly by the conventional chemical vapour deposition (CVD), mainly by plasma-enhanced CVD (PECVD) or hot-wire assisted CVD. Thin film technologies allow reducing the amount of silicon used and using the material of poorer quality and hence reduce costs per watt of power output.

Today, the vast majority of PV market is based on crystalline silicon. The conversion efficiencies of a-Si based thin-film cells and panels are lower in comparison with mc-Si and poly-Si cells. However, they take advantage of reduced production costs, and therefore they still attract a lot of attention of researchers and producers in the PV competition with conventional sources of electricity.

Amorphous silicon is characterised by higher absorption of light than c-Si and allows the deposition on low-cost substrates (glass, metals, plastics) at low temperatures (<250 °C). Differently from c-Si, the loss of structure order in a-Si results in defects (dangling bonds and distorted Si-Si bonds in both lengths and angles). Defects bring about energy levels in the energy gap where charge carriers recombine and limit the photocurrent. It was discovered that in a-Si deposited under hydrogenation conditions like PECVD and hot-wire CVD using the silane (SiH_4) precursor, hydrogen atoms saturate dangling bonds and weak bonds thus remove defects and result in a defect-free energy gap. CVD deposition techniques allow depositing hydrogenated amorphous silicon (a-Si:H) thin films with tailored structure and physical properties for photovoltaics and optoelectronics [1, 2, 3].

Nevertheless a-Si:H solar cells suffer from light-induced metastability – the Staebler-Wronski effect discovered in 1977 [4]. The microscopic origin of this photodegradation is still under extensive studies. The so-called protocrystalline or edge Si, i.e. amorphous Si near and above the onset of microcrystallinity prepared by CVD under additional amount of hydrogen – the so-called hydrogen dilution of silane plasma – attracts attention. H_2 dilution of SiH_4 is the gas flow ratio $D = [H_2] / [SiH_4]$ and results in films with higher stability. The hydrogen-dilution PECVD improves both material and solar cell stability. Therefore, solar cells photodegrade less than other samples prepared by other methods and thicker layers can be deposited at reduced deposition rates. Structure of small crystallites of $10 \sim 100$ nm embedded in a-Si network and mostly terminated by hydrogen is observed. This structure makes

* **J. Müllerová[1], P. Šutta[2], S. Jurečka[1]**
[1]Department of Engineering Fundamentals, Faculty of Electrical Engineering, University of Žilina, ul.kpt. J. Nálepku 1390, 031 01 Liptovský Mikuláš, Slovakia
[2]University of West Bohemia, New Technologies - Research Centre, Univerzitní 8, 306 14 Plzeň, the Czech Republic
E-mail: mullerova@lm.utc.sk

defect density lower and reduces recombination of photo-excited carriers.

The formation of microcrystalline boundary feels the deposition conditions, substrate material and film thickness. One of the up-to-now rare theoretical models of hydrogen-induced phase transition shows [5] that the crystallisation is due to the chemical rearrangement of a-Si:H network under additional hydrogen. Physical and technological aspects of the transition from amorphous to polycrystalline silicon are of great importance. As material properties are strongly dependent on exact deposition conditions, deposition parameters (e.g. substrate temperature, rf power, excitation frequency) can be set to favour the crystallisation.

This work reports on experimental studies of the structure, hydrogen and oxygen microstructure of a-Si:H thin films deposited by PECVD on glass from hydrogen diluted silane plasma.

2. Experimental

Undoped Si:H thin films were deposited at the Delft University of Technology, the Netherlands, on clean Corning 1737 glass substrates by 13.5 MHz rf excited parallel plate PECVD industrial deposition system [6] (rf power 13.5 W). The deposition was performed at the substrate temperature 194 °C and the total chamber pressure 200 Pa from hydrogen to silane plasma under varying dilution D. A series of 6 samples was investigated (Table 1). The thickness of the samples was kept at approximately the same value ~ 400 nm to avoid the thickness influence on the film properties.

The surface and cross-section morphology were inspected by AFM – atomic force microscopy (NT-MDT SPM Solver P7 LS in the contact repulsive mode) and SEM – scanning electron microscopy (QUANTA 200). Structure analysis was investigated by X-ray diffractometry (X-ray diffractometer Bruker AXS D8 with a 2D detector using CoKα radiation), Raman scattering (488 nm Ar$^+$ laser [7]) and FTIR – Fourier transform infrared spectroscopy (DIGILAB FTS 3000MX Excalibur spectrophotometer in the horizontal attenuated total reflection mode).

3. Results and discussion

Structure and surface morphology

According to the Raman spectra (Fig. 1), the samples deposited at $D \geq 30$ are mixed phase material. The lattice expansion and finite dimensions of the crystallites in the films manifest themselves in Raman components – one of the peak intensity I_{520} close to the wavenumber $\bar{v} = 520$ cm^{-1} belonging to crystalline Si, another of the peak intensity I_{480} at 480 cm^{-1} belonging to amorphous Si. The ratio $x_c = \dfrac{I_{520}}{I_{520} + I_{480}}$ is considered as the degree of crystallinity. The degree of crystallinity increases with increasing dilution (Table 1). From the shift of the Raman peak at 520 cm^{-1} by the procedure described in [8], the grain size can be

calculated. The grain size is $L_R = \sqrt{\dfrac{88.43}{|\Delta \bar{v}|}}$ where the Raman peak shift position is $\Delta \bar{v} = \bar{v} - 520.7$ cm^{-1} (Table 1). Tensile stress leads to the Raman peak shift to smaller wavenumbers and higher stress causes a higher peak shift. Thus, crystallisation induces tensions in the samples under study.
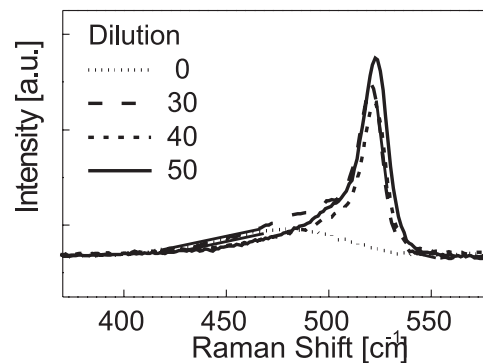

Fig. 1 Raman spectra of the undiluted sample and the samples deposited under higher dilution.

X-ray diffraction (XRD) data provide the same observation of the progressive formation of crystalline Si with increasing D as Raman spectra. In the XRD patterns of the first three samples at $D < 30$ no diffraction lines of crystalline Si are present. We conclude that the samples are either amorphous or with negligible part of the crystalline phase. The XRD scans of the samples at $D \geq 30$ in Fig. 2 show three diffraction lines ascribed to (111), (220), and (311) of crystalline silicon. This suggests that the films become polycrystalline. For the comparison the XRD scan of the amorphous glass substrate is added to the plots in Fig. 2.

From the broadening of diffraction lines the average microstrain (relative microdeformation) and the average size of the coherently diffracting domains were deduced by the procedures outlined in [9] (Table 2). The size of the coherently diffracting domains or simply the grain size is defined as the average size of crystallites perpendicular to the diffracting plane. For the calculations, ceramic Al$_2$O$_3$ from NIST (National Institute for Standards and Technology) was used as an instrumental standard. From the shift of the diffraction lines in consideration to the position of the standard diffraction lines, the biaxial lattice stress (so-called macrostress) was calculated. When the diffraction line shifts to the lower 2ϑ angle than that of the standard, the thin film is under tensile stress while the shift to the higher angle induces compressive stress. The X-ray diffraction analysis shows that all three mixed-phase films are primarily under tensile stress (Table 2).

AFM analysis of the sample frames 2×2 μm^2 shows surface features appearing with increasing dilution as can be seen in the 3D AFM images (Fig. 2, 3 for the samples at $D = 30$ and $D = 50$). Vertical relief structure can be evaluated from AFM data by the

Samples under study. The degree of crystallinity and average grain size determined from Raman scattering.　　　　Table 1

sample	dilution D	thickness [nm]	rms roughness [nm]	degree of crystallinity [%]	peak shift [cm^{-1}]	average grain size [nm]
#1	0	390	–	–	–	–
#2	10	394	0.756	–	–	–
#3	20	385	1.013	–	–	–
#4	30	388	3.629	61	3.2	5.2
#5	40	402	5.476	73	1.9	6.8
#6	50	397	5.021	82	1.1	9.3

Residual stress – macrostress and microstrain.　　　　Table 2

sample	dilution D	diffraction line position [deg]			grain size [nm]	average microstrain
#4	30	33.73	55.88	66.23	10 ± 3	0.02
#5	40	34.16	56.09	66.19	10 ± 3	0.02
#6	50	33.63	55.81	66.25	40 ± 5	0.005
Instrumental standard		33.15	55.28	66.25		
biaxial stress		tensile	tensile	compressive		

calculation of the rms roughness (Table 1) which shows the maximum at $\sim D = 40$ at which the amorphous-to-crystalline transition may be accomplished. This increase may be connected with growing crystalline grains according to the geometrical model of conical microcrystalline conglomerates [1]. The thin film prepared under dilution D between 20 and 30 may be considered as a film on the boundary between amorphous and crystalline phase. The lateral dimensions of the largest features are ~ 200 nm for the film prepared at $D = 30$. With D increasing over this value the lateral size of grains decreases (~ 100 nm for the samples at $D = 40$, $D = 50$), they finally touch each other to form a smoother surface.

Fig. 3 AFM image of the 2 × 2 μm^2 surface of the sample # 4 (dilution 30).

Fig. 2 XRD scans of the samples prepared at $D \geqq 30$ and of the glass substrate.
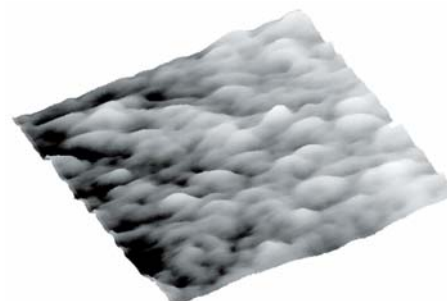
Fig. 4 AFM image of the 2 × 2 μm^2 surface of the sample # 6 (dilution 50).

The size of crystalline grains determined from the XRD analysis and from Raman spectra (Table 1, Table 2) is much smaller than that of surface fea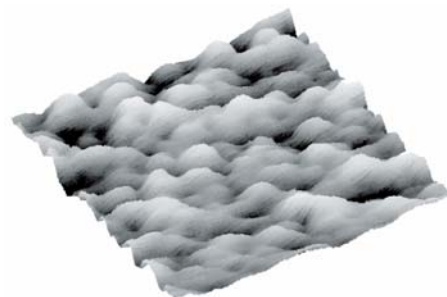tures inspected by AFM measurements. We conclude that features seen by AFM are polycrystalline aggregates of nano-sized crystalline grains for the samples prepared at $D \geqq 30$.

For the comparison we insert the SEM cross-sectional micrograph of the sample deposited at $D = 50$ on crystalline (111) Si substrate (Fig.5). The sample has similar optical properties and structure as the sample #6 on glass [3]. SEM image evidences compact film with high packing density of conical conglomerates and negligible porousity.

Fig.5 SEM cross-sectional micrograph of the almost fully crystallized polysilicon – sample deposited at the dilution 50 at n^+ (111) Si substrate.

Microstructure

According to the structure analysis, the samples prepared at $D \geq 30$ are polysilicon composed of nano-sized grains and grain boundaries formed by amorphous Si, hydrogen and voids (Fig. 6).

Fig.6 Mixed-phase hydrogenated Si. Crystalline grains of silicon (large circles) terminated by hydrogen (small circles) and embedded in the amorphous tissue.
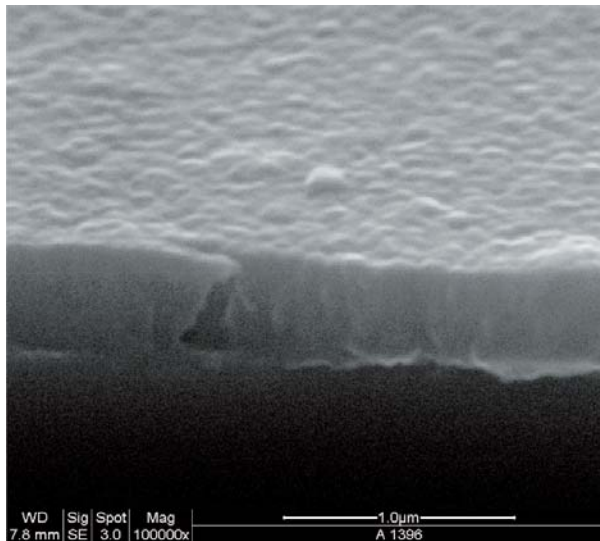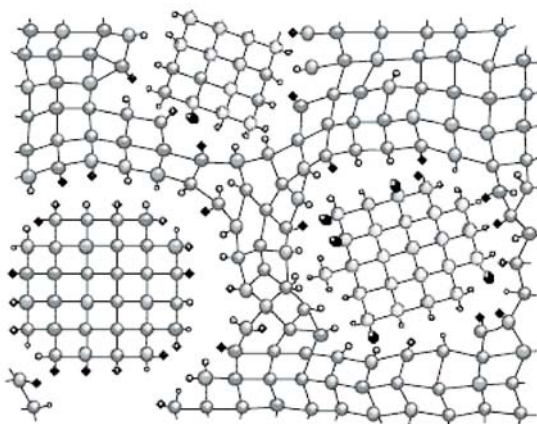*(Drawing from National Institute of Advanced Industrial Science & Technology Tsukuba, Japan).*

FTIR absorbance spectra exhibit absorption peaks corresponding to Si:H or Si-O bonds and revealing the microstructure of hydrogen and oxygen in grains and at grain boundaries. The attention was focused on the broad absorbance band at wavenumbers $\bar{v} \sim 2000$ cm^{-1}, which is the convolution of predominant Si:H stretching vibrations centered at ~ 2000 cm^{-1} and SiH$_2$ at ~ 2090 cm^{-1}. More loose SiH$_2$ bonds are typical for polycrystalline silicon. Integral intensities of two deconvoluted peaks are proportional to bonded atoms densities.

Properties of polysilicon as a function of hydrogen microstructure are represented by the microstructure factor

$$\mu = \frac{\int I_{SiH_2}(\bar{v})d\bar{v}}{\int I_{SiH_2}(\bar{v})d\bar{v} + \int I_{SiH}(\bar{v})d\bar{v}}$$

which is commonly considered as a figure of merit of the quality of the films when being < 10 % [10]. The concentration of H atoms bonded to Si is $N = A_x \int \frac{\alpha(\bar{v})}{\bar{v}} d\bar{v}$, where A_x is the proportionality constant for specific vibrational mode [11], $\alpha(\bar{v})$ is the wavenumber-dependent absorption coefficient. Hydrogen concentration in atomic percent is

$$C = \frac{A_x}{N_{int}} \int \frac{\alpha(\bar{v})}{\bar{v}} d\bar{v}$$

N_{int} is the total atomic concentration of the films (5×10^{22} cm^{-3} for c-Si). The microstructure factor and hydrogen concentration (calculated with $A_x = 9 \times 10^{19}$ cm^{-2}) versus dilution are in Fig. 7. Hydrogen concentration declines with increasing dilution and thus with progressing crystallization.

Nano-grains obviously attract air oxygen. Post-deposition oxygen contamination of Si:H films usually detrimentally results in conductivity changes and enhanced porosity of the samples [12]. FTIR measurements show that all films are contaminated with certain amount of oxygen. In the absorbance spectra the pronounced stretching vibrations of the interstitial oxygen in the O-Si-O bonds at ~ 1000 cm^{-1} and about one order less intense surface vibrational features extended from 3000 cm^{-1} to 3800 cm^{-1} attributed to asymmetric streching vibrations of Si-OH species are present. The area under the broad band of surface Si-OH groups called silanols at ~ 3100 cm^{-1} is the oxygen-related parameter proportional to the surface oxygen density. It reaches its maximum at $D \sim 20$ and then decreases. The same behaviour attributed to interstitial oxygen was observed analysing the absorption band at ~ 1000 cm^{-1} (Fig.8). In Fig. 8 one can also see the similar dilution dependence of the area under the absorption peaks at ~ 850 cm^{-1} referred to the relatively weak bending vibrations of Si-H bonds. Patterned regions in Fig. 7 and Fig. 8 at $D \sim 20 \div 30$ indicate the protocrystalline material recommended for photovoltaic application.
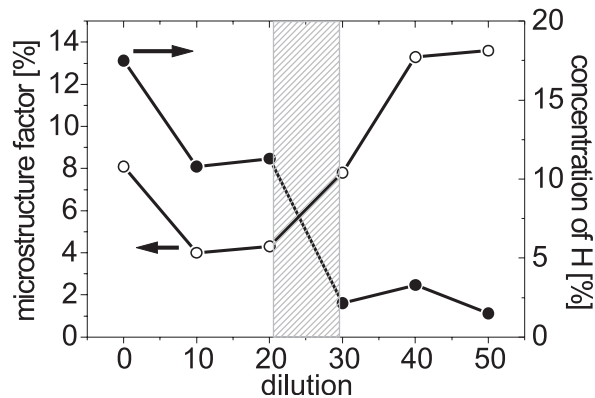
*Fig. 7 Microstructure factor and the hydrogen concentration
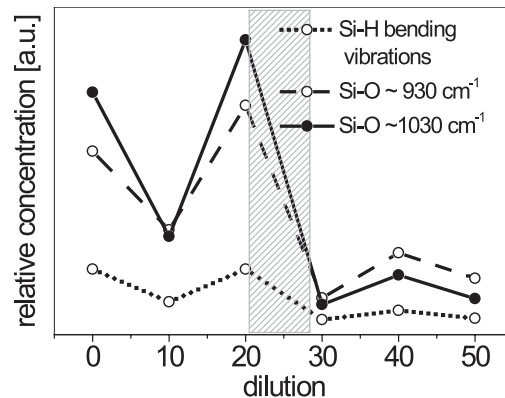as the function of dilution.*

*Fig.8 Relative concentrations of hydrogen and oxygen representing
microstructure versus dilution.*

3. Conclusions

In PECVD deposition of Si:H thin films for photovoltaic applications, remarkable changes in structure and microstructure due to the increasing hydrogen dilution were detected. The samples prepared at the dilution under 20 remain within the amorphous regime while the dilution over 30 favours the crystallisation and tensile stress. The films prepared at $D \geq 30$ were identified as polycrystalline Si. Grains in nanometer scale recognized by XRD analysis and Raman scattering exist within the features seen by AFM. The grain size increases with increasing dilution.

The protocrystalline regime recommended for photovoltaics occurs between dilutions 20 and 30 whilst other deposition parameters, esp. rf power, deposition temperature and the film thickness are kept constant. FTIR spectroscopy reveals primarily monohydride SiH bonding with increasing part of dihydride SiH$_2$ while the dilution rises. With increasing dilution and the crystallinity, the hydrogen concentration decrease. In spite of the microstructure factor being over 10 % in polycrystalline films, the inevitable film porosity and increasing presence of oxygen were not observed.

References

[1] KOČKA, J., FEJFAR, A., MATES, T., FOJTÍK, P., DOHNALOVÁ, K., LUTEROVÁ, K., STUCHLÍK, J., STUCHLÍKOVÁ, H., PELANT, I., REZEK, B., STEMMER, A., ITO, M.: *Phys. Stat. Sol. (c)*, 1, No.5, 1097, 2004.
[2] KOVAL, R. C., KOH, J., LU, Z., JIAO, L., COLLINS, R. W., WRONSKI, C. R.: *Appl. Phys. Lett. 75*, No.11, 1553, 1999.
[3] MÜLLEROVÁ, J., JUREČKA, S., ŠUTTA, P.: *Acta Physica Slovaca,* 55, No. 3, 351, 2005.
[4] STAEBLER, D. L., WRONSKI, C. R.: *Appl. Phys. Lett.*, 31, 292, 1977.
[5] SRIRAMAN, S., AGARWAL, S., AYDIL, E. S., MAROUDAS, D.: *Nature 418,* 62, 2002.
[6] NÁDAŽDY, V., DURNÝ, R., THURZO, I., PINČÍK, E., NISHIDA, A., SHIMIZU, J., KUMEDA, M., SHIMIZU, T.: *Phys. Rev. B 66,* 195211, 2002.
[7] NÁDAŽDY, V.: *Personal communication.*
[8] PARK, Y.-B., LI, X., RHEE, S.-W., PARK, D.-W.: J. *Appl. Phys. 90,* 1, 219, 2001.
[9] VAN ZUTPHEN, A. J. M. M., ŠUTTA, P., TICHELAAR, F. D., VON KEITZ, A., ZEMAN, M., METSELAAR, J. W.: *J. Crystal Growth,* 223, 332, 2001.
[10] STANOWSKI, B., SCHROPP, R. E. I.: *Thin Solid Films,* 383, 125, 2001.
[11] PEREYRA, I., CARRENO, M.N.P., TABACSNIK, M. H., PRADO, R. J., FANTINI, M. C. A.: *J. Appl. Phys.*, 84, 5, 2371, 1998.
[12] PERSHEYEV, S. K., O'NEILL, K. A., ANTHONY, S., ROSE, M. J., SMIRNOV, V., REYNOLDS, S.: *Mat. Res. Soc. Symp.* Proc., 808, A9.10.1, 2004.

Drahoslav Barančok – Július Cirák – Pavol Tomčík – Ján Vajda – Martin Weis *

ELECTRICAL CHARACTERIZATION OF THIN LAYER MATERIALS: DESTRUCTIVE AND NON-DESTRUCTIVE IRREVERSIBLE PROCESSES IN LANGMUIR FILMS

Summary Well-defined Langmuir-Blodgett films prepared by reproducible technique are still highly attractive for exploitation in investigation of subjects as diverse as chain packing, phase transitions, two-dimensional physics, biosensors and membrane physics. During last 15 years the Maxwell displacement current (MDC) measuring technique was developed for dynamic study of monolayers. In experiment MDC flows through the metal electrode/air gap/Langmuir monolayer/water surface structure. Spontaneous formation of the monolayer was observed and significant differences between destructive and non-destructive processes are discussed.

1. Introduction

The Langmuir-Blodgett (LB) technique can be exploited to prepare well-ordered monomolecular layer and multilayer films of amphiphilic organic materials. In this technique an insoluble monolayer is formed at the air/water interface by the movable barrier to a specified surface pressure-area state and subsequently transferred onto a solid substrate. Recently with increasing interest in the low-dimensional systems, applications were used in the field of physics, chemistry and biology [1, 2]. For all these applications it is essential to have a uniform film with well-defined parameters prepared by reproducible technique. Hence, the investigation of irreversible phenomena in the Langmuir film is of prior necessity.

Generally we distinguish between two classes of structural changes induced by mechanical stimulation of the Langmuir film, the transitions between different two-dimensional phases [3], and those in which dimensionality changes from the degree of two to three [4]. The latter class is a destructive process at high pressures caused by the fracture collapse, or at lower pressures (but still above the equilibrium spread pressure [5]) by the slow collapse [6].

In this paper we investigate the formation of a simple fatty acid monolayer at the air-water interface on a pure water subphase and also the significant difference between the non-destructive and destructive (slow collapse) irreversible processes.

2. Experiment

The computer-controlled Langmuir trough (Type 611, Nima Technology, England) was used. Stearic acid molecules (Fluka, Switzerland) were spread over the subphase (bidistilled deionized water, 15 MΩ.cm) from a chloroform solution. The Langmuir film was compressed at a rate of 0.002 nm^2/min per molecule. The
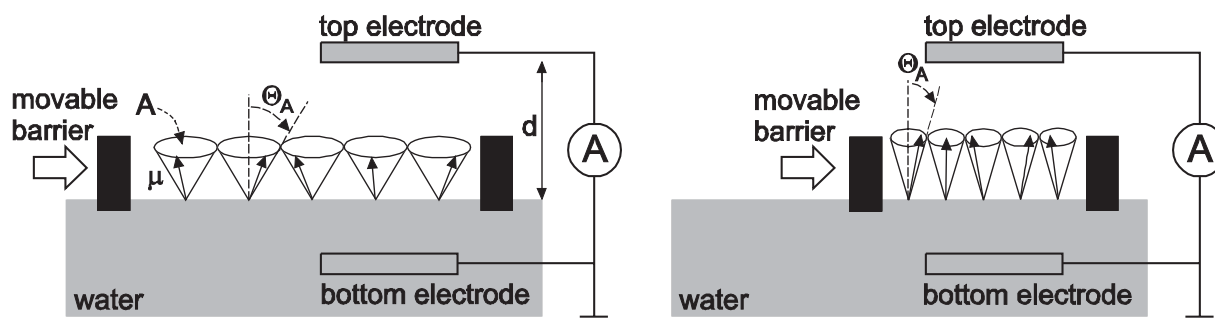
Fig. 1 Sketch of the experimental setup for the displacement current measurement. Rod-like polar molecules execute precessional motion on the water surface with the maximum tilt angle Θ_A (A and μ stand for the area per molecule and the dipole moment of molecule, respectively), which is controlled by the movable barrier. The electrical shielding of the top electrode is not shown.

* **Drahoslav Barančok, Július Cirák, Pavol Tomčík, Ján Vajda, Martin Weis**
  Faculty of Electrical Engineering and Information Technology, Slovak University of Technology
  Ilkovičova 3, 812 19 Bratislava, Slovak Republic, E-mail: Barancok@elf.stuba.sk

slow collapse experiment was carried out in the isobaric regime, keeping the surface pressure constant at 30 mN/m for 35 minutes.

Monolayer processes were studied using the Maxwell displacement current (MDC) technique [7,8].

The displacement electric current I flows through a short-circuited capacitor being formed by two parallel plates, the one in air above the monolayer detached at a certain spacing (1 mm in our case), the other immersed in the water subphase below the organic monomolecular layer. Compression of the monolayer, carried out by a movable barrier, results in the change of the number of molecules N under the electrode as well as in the mean orientational change of the direction of molecular electric dipoles $\langle\cos\Theta\rangle$. If we consider the organic film as a system of electric dipole moments then it is possible to calculate the induced charge on the upper electrode by the method of images

$$Q_i = \langle\mu_z\rangle NG = \mu\langle\cos\Theta\rangle NG \qquad (1)$$

where μ is the dipole moment of one molecule (μ_z is projection of μ to the normal), N is the number of molecules under the top electrode and G is the geometrical factor of the experimental arrangement. The $\langle\cos\Theta\rangle$ stands for the statistical mean value of $\cos\Theta$, where Θ is the angle between the dipole moment vector and the normal. Detailed analysis of the dipole moment projection of simple fatty acid was described in [9].

As shown in our previous studies [9], the current flowing in the outer circuit can be expressed as a time change of the induced charge

$$I = \frac{\partial Q_i}{\partial t} = \mu NG \frac{\partial\langle\cos\Theta\rangle}{\partial t} + \mu\langle\cos\Theta\rangle G \frac{\partial N}{\partial t} \quad (2)$$

By integrating the displacement current with respect to time, the induced charge Q can be obtained and in this way we also evaluated the vertical component of the molecular dipole moment. Thus, the dipole moment projection to the normal should be calculated as

$$\mu_z = \mu\langle\cos\Theta\rangle = \frac{1}{GN}\int I dt \qquad (3)$$

The displacement current technique is sensitive only to dynamic charge processes, which in this arrangement are caused by lateral compression of the monolayer. Therefore any time-independent charge (e.g. polarized water surface or additional substances in subphase) distributed at the interface has no effect. This is advantage in comparison with conventional electrical measurements, e.g. the Kelvin probe method.

3. Results

Langmuir film was prepared by standard procedure and was left for 15 min for solvent evaporation. Measured signals for first four compressions are presented in Fig. 2. On subsequent compressions the signal already remained the same. Although the amplitude of the signal was changed, the area under the current-time isotherm (current-area for constant compression rate) is conserved. The stabilization of the signal (formation of the monolayer) is therefore caused by homogenization of material distribution, not by a destructive process.

The destructive process was modeled by the slow collapse of the Langmuir film. The monolayer collapses were monitored as the relative area loss (A/A_0) with respect to time while keeping the monolayer at a constant surface pressure of 30mN/m. Recordings of the MDC signals before and after the monolayer degradation are shown in Fig. 3.

Detailed analysis of the change of the dipole moment projection is possible if Eq. 3 is rewritten to the form

$$\mu_z = \frac{1}{GN}\int I dt = \frac{1}{GN}\int \frac{I}{\beta} dA \qquad (4)$$

where $\beta = dA/dt$ is the compression rate per one molecule. Due to the collapse, the number of molecules on the water surface was changed. Hence, at a constant compression rate regime (speed of
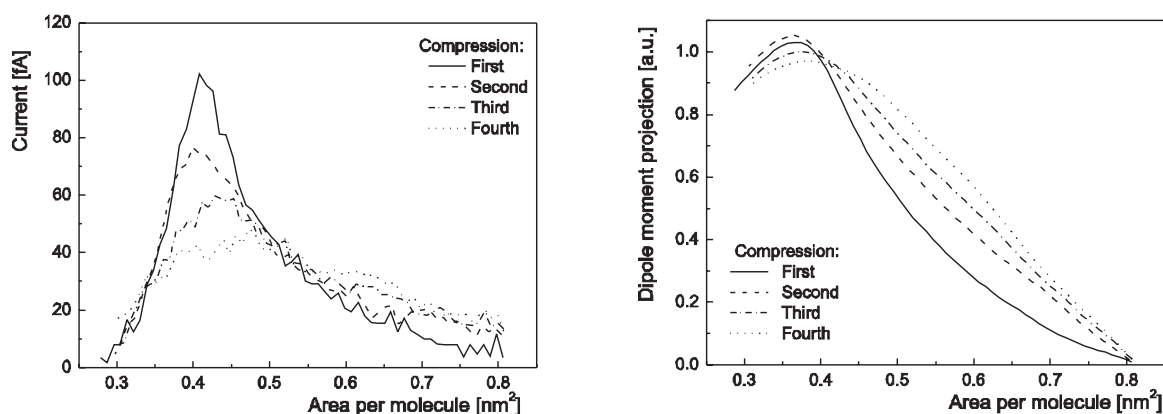

Fig. 2 (top) MDC signals of formation of a stearic acid monolayer during first four compressions. (bottom) Calculations of the dipole moment projection by Eq. 3.
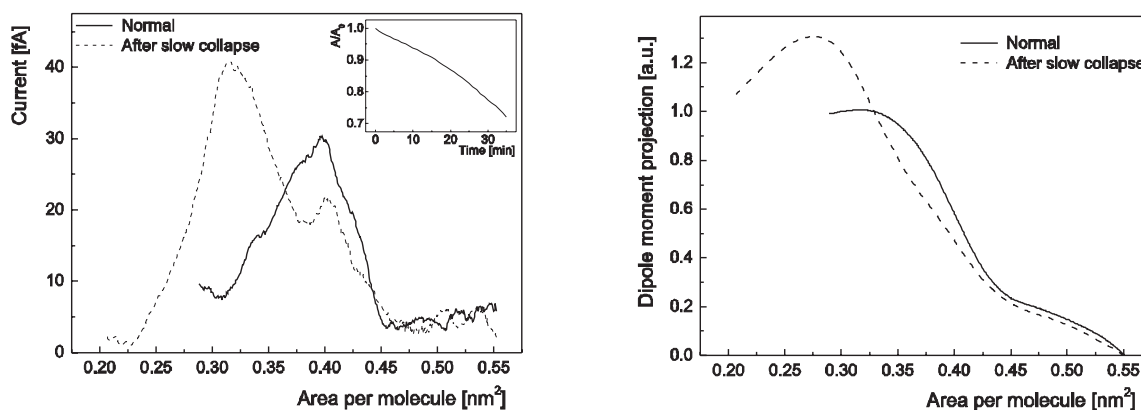
Fig. 3 Left – MDC signals of a stearic acid monolayer before and after the slow collapse. In the insert the relative area loss-time isobar is shown during the slow collapse process.
Right – calculations of the dipole moment projection were accomplished using Eq. 4.

the movable barrier) the compression rate per one molecule was increasing. In our previous work [9] we showed that the ratio I/β is conserved. Therefore, the amplitude of the signal as well as the dipole moment (related with the area under current-area isotherm) rise owing to the change of the compression rate β and the number of molecules N. It is remarkable that the change of the MDC signal is directly proportional to the relative area loss-time isobar.

4. Conclusions

For the first time the MDC method was used for studying monolayer collapse. It was shown that its application is highly effective and unambiguously distinguished between destructive and non-destructive processes in the monolayer. The experiment performed on a stearic acid monomolecular film situated on the water surface recognizes homogenization and formation as well as the degree of degradation of the Langmuir film. The destructive process is characterized by the increase of the amplitude and by the shift of the peak towards lower areas. It leads to a significant rise in the calculated dipole moment. The effect of monolayer formation is very important also for the LB technique. It pointed out the need for multiple compressions before LB deposition for building samples with reproducible properties.

References

[1] SACKMANN, E.: Science, 271 (1996), 43.
[2] LIPOWSKY, R.: Nature, 349 (1991), 475.
[3] VOLLHARDT, D., FAINERMAN, V.: Colloids Surf. A 176 (2001) 117.
[4] VOLLHARDT, D.: Colloids Surf. A 143 (1998) 185.
[5] GAINES, G. L.: Insoluble Monolayers at Liquid/Gas Interfaces (Wiley-Interscience, New York, 1966).
[6] SMITH, R. D., BERG, J. C.: Colloid Interface. Sci. 74 (1980) 273.
[7] MAJIMA, Y., IWAMOTO, M.: Rev. Sci. Instrum. 62(9) (1991) 2228.
[8] BARANČOK, D., CIRÁK, J., TOMČÍK, P., VAJDA, J.: Phys. Stat. Sol. 169(2) (1998) 267.
[9] VAJDA, J, WEIS, M., BARANČOK, D., CIRÁK, J., TOMČÍK, P.: App. Surf. Sci. 229/1-4 (2004) 183.

D. Pudiš – I. Martinček – I. Turek – M. Michalka – J. Kováč, jr. – V. Gottschalch – D. Káčik *

SCANNING OF OPTICAL FIELDS USING NEAR-FIELD SCANNING OPTICAL MICROSCOPY

The Near-field scanning optical microscopy is a high-resolution diagnostics for the optical field characterization. In our experiments we focus on the optical field characterization of semiconductor laser diodes based on multiple quantum well structure as well photonic crystal fibers. The parameters of optical field of laser diode in the near- and far-field zone as well the local spectral analysis of the quantum well laser devices in the near-field will be studied. The mode distribution across photonic crystal fiber was scanned using near-field scanning optical microscopy. This experimental technique in combination with an analysis of optical field in the near-field region could be an effective optical tool for the final diagnostics of laser devices and photonic crystal fibers.

1. Introduction

Near-field scanning optical microscopy (NSOM) is a promising diagnostics of optical microscopies, which can provide optical resolution better than the Rayleigh diffraction limit [1]. NSOM uses optical fiber tip with an aperture that is much smaller than the wavelength (of the detected light. Typically, an optical fiber is shaped to a small tip with an aperture in the range of 100 nm. The application of near-field imaging and spectroscopy to optical and optoelectronic devices provides subwavelength information on a device structure, performance and output properties [2, 3, 4]. The emission profile is obtained by coupling the emitted radiation into the fiber-tip moving along the investigated emitter. The near-field properties could be determined by placing the fiber tip very close to the sample surface (in order of 10–100 nm).

Laser devices based on multiple quantum well (MQW) structures became attractive in last decade because of their excellent optical properties. We present the characterization of a MQW laser structure based on GaAs material with InAs monolayers. The mode spectrum of laser devices based on this structure as well band calculations were published in [5]. In this paper we focus on the characterization of InAs/GaAs MQW laser device using NSOM. The profile of optical field as well local spectral analysis of MQW laser diodes is directly investigated.

Photonic crystal fibers (PCF) are at the top of interest because of their distinct guiding mechanism of light. PCF consists of an array of microscopic air holes in the glass fiber reminiscent of a crystal lattice [6]. We employ NSOM diagnostics to characterize the lateral modes in the PCF.

2. Experimental

In the experimental part we focused on the preparation of high-quality optical fiber tips for NSOM investigations. The technology of etching in hydrogenfluorid acid and pulling in small flame, respectively, were used for the preparation of the high quality tapered optical fiber tips. A quality of fiber tips was examined by the Scanning electron microscopy (SEM). The near-field of the MQW laser structures and the mode shape of the fundamental and the higher-order lateral mode of PCF were investigated using the fabricated fiber tips.

The MQW laser structures have been grown by low-pressure metal-organic vapor phase epitaxy (MOVPE) on (001) oriented n-type GaAs substrates. The layer structure with the detailed wave-guide arrangement is shown in fig. 1. The structure consists of a 150 nm n-doped GaAs buffer layer followed by 625 nm n-doped $Al_xGa_{1-x}As$ confinement layer, the MQW active region and 625 nm p-doped $Al_xGa_{1-x}As$. The structure was covered with a 15 nm GaAs layer. The 90 nm thick active region contains 9 InAs monolayers spatially separated by 2.5 nm thick GaAs barriers [5]. Al composition in $Al_xGa_{1-x}As$ confinement layers was varied to form the graded-index waveguide.

The gain guided metal stripe lasers were fabricated for the experimental emission studies. The stripes width of 5 μm in SiO_2 mask and AuBe/Ti/Au p-contact layer was deposited. The device fabrication was completed by thinning of the wafer to 150 μm and evaporation of bottom AuGe/Au n-contact. The samples were cleaved perpendicular to metal stripes to have cavity facets.

* **D. Pudiš[1], I. Martinček[1], I. Turek[1], M. Michalka[2], J. Kováč, jr.[3], V. Gottschalch[4], D. Káčik[1]**
[1]Dept. of Physics, Faculty of Electrical Engineering, University of Žilina, Veľký diel, 010 26, Žilina, Slovakia,
[2]International Laser Centre, Ilkovičova 3, Bratislava 812 19, Slovakia,
[3]Dept. of Microelectronics, Faculty of Electrical Engineering and Information Technology, Slovak University of Technology, Ilkovičova 3, Bratislava, Slovakia
[4]Faculty of Chemical and Physics, University of Leipzig, Linnéstrasse 3-5, 04103 Leipzig, Germany, E-mail: pudis@fyzika.utc.sk

For the NSOM investigations the laser diode was mounted on the micro-mechanical positioning stage. The beam profile was scanned in the vertical (in the growth direction) and lateral (in the plane of layer structure) direction in the front of the laser facet using the prepared optical fiber tips (Fig. 2). The resonator parameters of the laser diode are stripe length $d = 235$ μm, stripe width $w = 22$ μm.
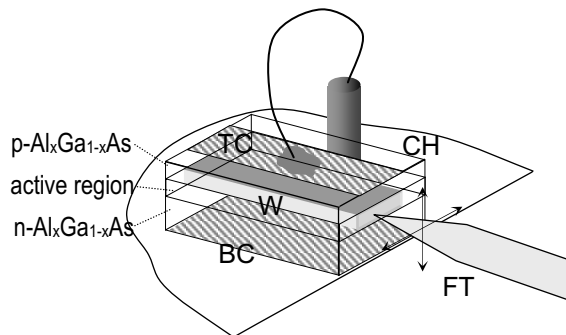

Fig.1 The laser diode and a detail of the NSOM experiment on the front laser facet; CH, laser diode chip; FT, fibre-tip; TC, top contact; BC, bottom contact; W, gain guided waveguide.
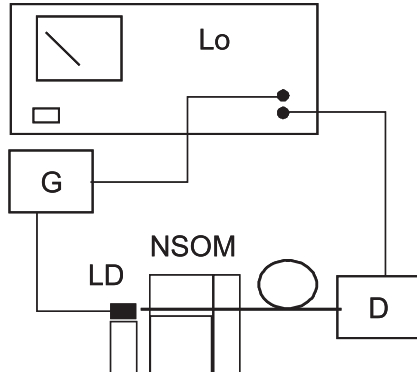

Fig.2 Experimental setup of the NSOM experiment; LD, laser diode; NSOM, positioning stage; G, pulse generator; D, Si-detector; Lo, Lock-in amplifier. For the local spectral analysis the Si-detector and Lock-in amplifier by spectral analyzer was replaced.

The mode spectrum as well the near-field shape of stripe laser diode was investigated using the NSOM diagnostics and the spectral analyzer with the spectral resolution of 0.07 nm. The operation spectral region of these quantum well laser diodes is in the range of 910–930 nm and FWHM of mode is ~ 0.2 nm [5].

The optical near-field region of laser diode was recorded using the optical fiber tip mounted on the 3D mechanical positioning stage with step 50 nm. The tip diameter used for field detection was better than 200 nm [7]. The fiber tip was placed close to the front laser facet (< 50 nm). Two experimental setups were used to analyze the near-field shape and the laser emission spectra of the laser device:

i) For the near-field shape investigations of the laser diode the experimental arrangement with Si-detector was used (Fig. 2).
ii) The spectral analysis measurements were investigated using the spectral analyzer Anritsu HS 9710B with spectral range of 0.6–1.7 μm (Fig. 1) [8, 9].

The spectrum was analyzed using NSOM experiment at different positions of the fiber tip on the front laser facet. The detail scheme of an experiment is shown in Fig. 1. The mode laser spectrum was recorded at different vertical positions of the NSOM fiber tip on the front laser facet. The vertical step of the experiment was set to 300 nm. The horizontal position of the fiber tip was set to get a maximal intensity.

Modes in PCF were excited using the InAs/GaAs MQW laser diode at wavelength $\lambda = 923$ nm. In the experimental setup for mode investigation the PCF was fixed on the steady holder instead of the laser diode (Fig. 1). The optical field of two different lengths 150 cm and 7 cm of PCF was scanned to show the propagation of fundamental and higher-order lateral modes. The PCF under studies has the core diameter ~ 13 μm, the average hole diameter 2.6 μm and pitch 7.1 μm [10].

3. Experimental results

Prepared optical fiber tips were studied by SEM Their quality was examined by scanning of optical field of MQW laser structures and PCF in the near-field region using NSOM arrangement.

From SEM images the fiber tip diameter was determined to be less than 100 nm for tapered fibers prepared using technology of pulling in small flame and less than 800 nm using etching technology. Detection properties of optical fibers prepared using both of technologies were compared from the measurements of the near-field profile of MQW laser diode. In the near-field profile scanned in the vertical direction the ghost peaks were observed for the etched fiber tips as is shown in fig. 4. Their origin is probably caused by the surface inhomogenities arisen during the etching process. Therefore, tapered optical fibers prepared by pulling technology in the small flame were used in the forthcoming near-field investigations.

The near-field investigation of the laser diode shows Gaussian shape of the optical field scanned in the vertical and horizontal direction (Fig. 5a). The light propagation in the z-axis is shown in Fig. 5b as an intensity image and can be theoretically described by equation [4]

$$W^2(z) = W_0^2 \left[1 + \left(\frac{z}{z_0} \right)^2 \right],\qquad(1)$$

where W_0 is beam waist in the near-field region and z_0 is confocal parameter given by

$$z0 = \pi W_0^2 / \lambda.\qquad(2)$$

a) b)
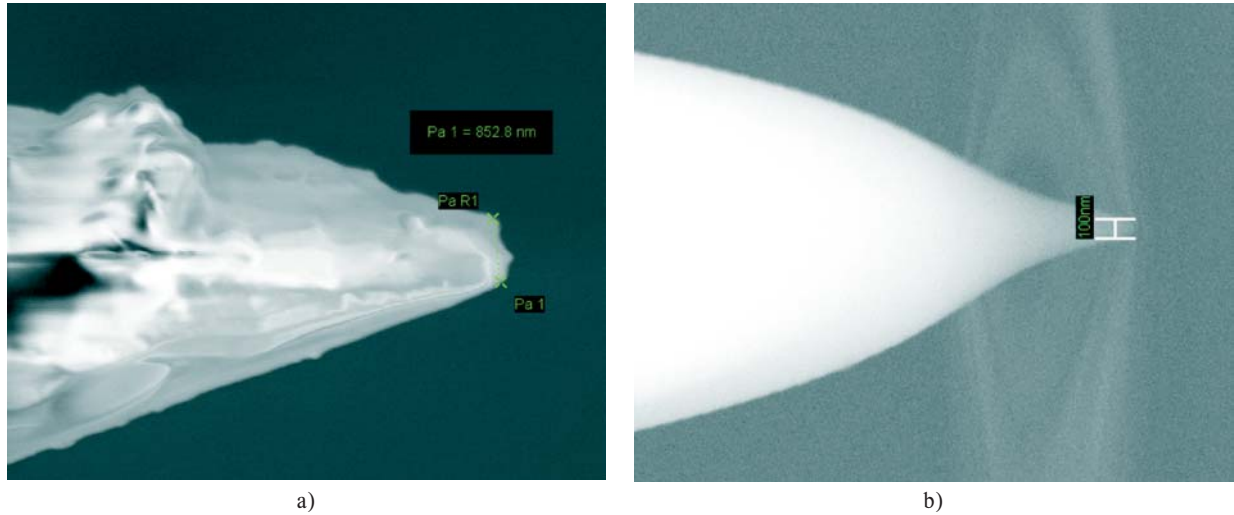
Fig.3 The SEM image of the prepared fiber tips using a) etching and b) pulling in small flame.
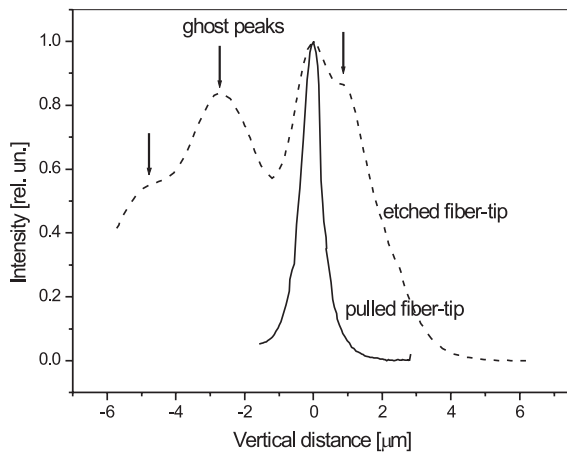
Fig. 4 Profile of the optical field of the laser structure recorded in the near-field region using the etched and pulled optical fiber tips.

The emission wavelength (was determined from the spectral measurements to be 923 nm. The divergence angle θ_0 of the propagating light is a function of the emission wavelength and beam waist

$$\theta_0 = \lambda/\pi W_0. \tag{3}$$

From the measured optical field distribution in the near- and far-field region (Fig. 5a and 5b) the following parameters were estimated $2W_0 = 1.97$ μm, $z_0 = 3.30$ μm and $\theta_0 = 0.298$ rad.

The measured mode spectrum of the laser diode is shown in Fig. 6a for different vertical positions of the fiber tip on the front laser facet. The vertical step of record was 300 nm. For these vertical measurements the horizontal position of the fiber tip was set to obtain the maximum intensity of a signal. The corresponding density image of the mode spectrum distribution is shown in Fig.

a) b)
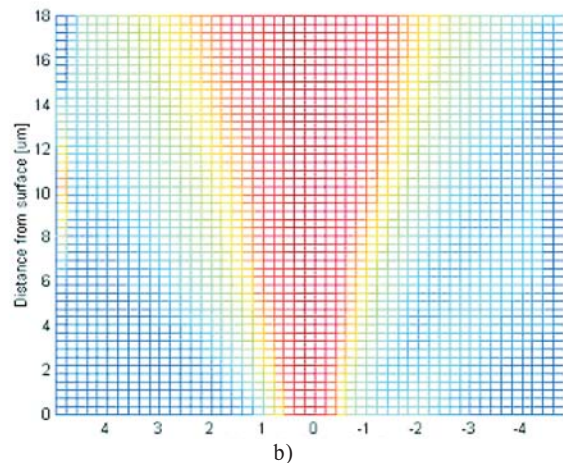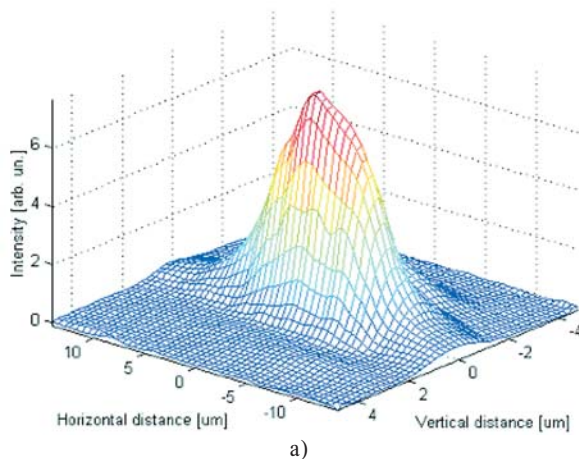
Fig. 5a) The optical field scanned in the vertical and horizontal direction. b) Intensity image of the optical field distribution scanned in the vertical direction in different distances from the front laser facet.

6b. Modes in the laser spectrum correspond to longitudinal modes for the Fabry-Pérot resonator. Their wavelength separation could be determined from the simple approach

$$\Delta\lambda \approx \frac{\lambda^2}{2nd}, \tag{4}$$

where λ is the wavelength one of adjacent modes, n is refractive index in the resonator and d is the resonator length. The mode separation of the investigated laser diode for adjacent modes (maximum at wavelength $\lambda = 919.8$ nm) was determined from measured spectra $\Delta\lambda = 0.5$ nm. This experimental result corresponds to the theoretical calculation $\Delta\lambda = 0.507$ nm, following equation (4) and taking into account the waveguide parameters of the laser diode, stripe length $d = 235$ μm and refractive index of active region $n_{(GaAs)} = 3.55$.

In all range of the vertical scanning only longitudinal modes corresponding to Fabry-Pérot wavelengths were observed. The laser mode spectrum was measured at different driving currents for all vertical positions of the fiber tip. A corresponding current dependence taken in the vertical position $+300$ nm is shown in Fig. 7. The longitudinal mode intensity of the peak at 919.8 nm increased with the driving current increase while the intensity of other modes lightly declines. In these current dependencies the additional peaks were observed for the current $I = 55$ and 60 mA. Their position in spectral dependencies does not correspond to the longitudinal Fabry-Pérot resonator wavelengths. Their behavior as well as origin was described in [9]. We suppose their relation with the higher-order lateral modes of a planar waveguide. Higher-order lateral modes are typically observable for current densities above kink region in the dependence of optical power vs.

a)   b)
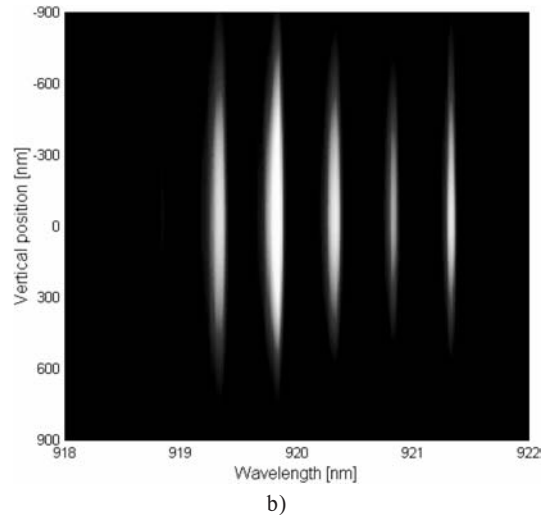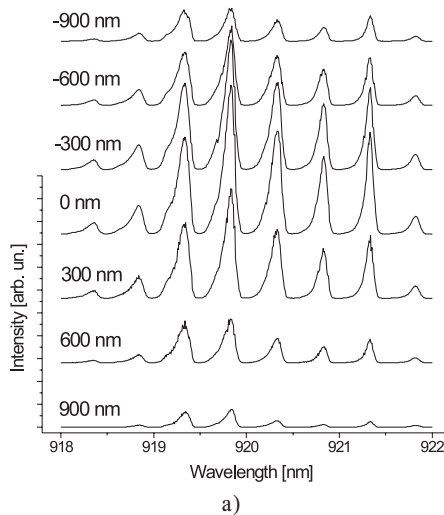
Fig. 6 a) Laser mode spectrum at different vertical positions of the fiber tip at driving current I = 50mA, b) interpolated density image.
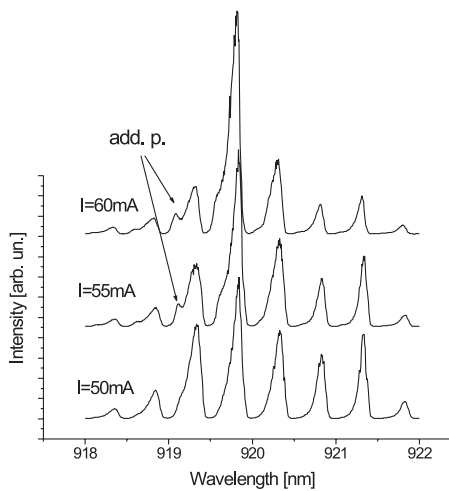

Fig. 7 The laser mode spectrum at different driving currents recorded at the vertical position +300 nm. First higher-order lateral modes are shown as weak additional peaks (add. p.).
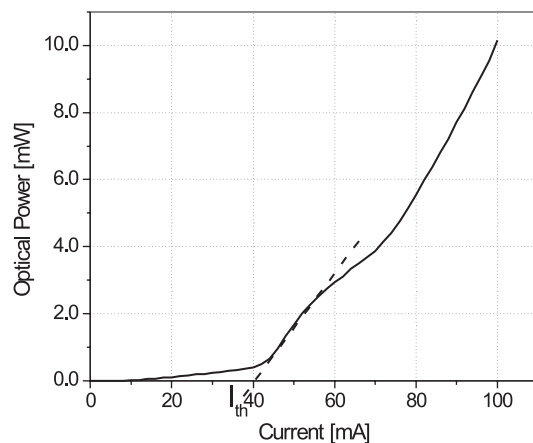
Fig. 8 Dependence of optical power vs. driving current with estimated threshold current value I_th = 40 mA.
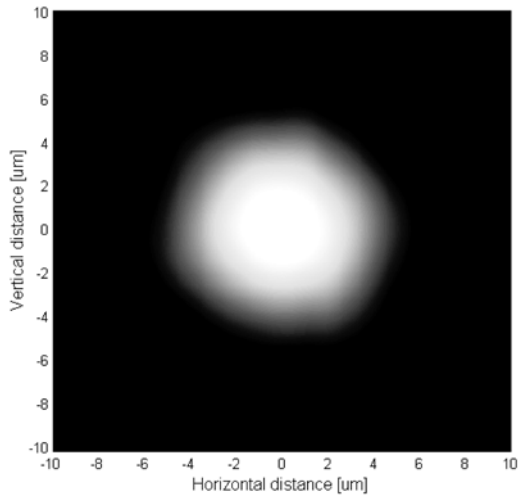
Fig. 9 The fundamental lateral mode in PCF reflects the hexagonal symmetry of the air holes spacing in the PCF structure.

ture. However, the optical field of the 7 cm long PCF is a combination of the fundamental and the first higher-order lateral mode. All three possible symmetries of the first higher-order lateral mode are shown in Fig. 10.

4. CONCLUSION

The NSOM measurements using the prepared optical fiber tips could provide the high-resolution characterization of the optical field of semiconductor lasers. The NSOM was employed to obtain the near- and far-field profile of the InAs/GaAs MQW laser structures. From near- and far-field of the laser structure the parameters of optical field were determined. In the near-field region of InAs/GaAs MQW laser structures the spectrum was analyzed. From the locally analyzed spectra in the near-field the lateral modes in the spectrum were identified.

The NSOM experiment was employed for the near-field characterization of lateral modes in PCF. In the intensity image of the
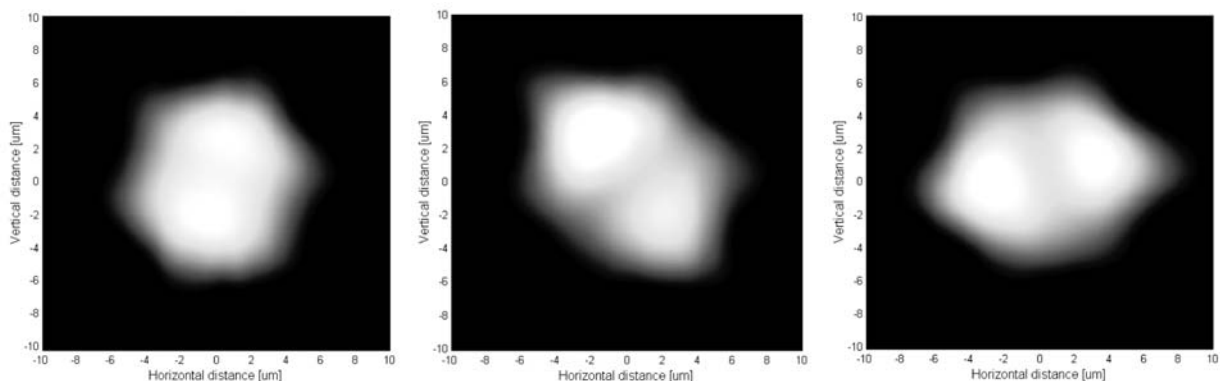
Fig. 10 Intensity image of the first higher-order lateral mode of PCF as a combination with fundamental lateral mode.
All three possible symmetries of first higher-order mode are shown.

driving current [11]. It corresponds to the dependence of the optical power vs. driving current shown in Fig. 8.

The lateral modes in PCF were investigated by the horizontal and vertical scan. The intensity image of the scanned optical field in horizontal and vertical direction is shown in Fig. 9. According to the basic principles of wave propagation in optical fibers the radiation of higher-order lateral modes was expected for 150 cm long fiber [12]. Only fundamental lateral mode was observed for the 150 cm long fiber. The shape of the fundamental mode of the optical field reflects the hexagonal symmetry of the PCF struc-

PCF optical field the fundamental lateral mode as well as the first higher-order lateral mode was observed.

We expect that the NSOM technique will be a useful tool for waveguide optimization of semiconductor lasers and analysis of lateral modes in PCF.

References

[1]   PAESLER, M. A., MOYER, P. J.: *Near-field optics*, (New York: John-Wiley&sons, Inc.)., 1996, pp.21–31
[2]   CAMPILLO, A. L., HSU, J. W. P., WHITE, C. A., JONES, C. D.: *Appl. Phys. Letter,* 80, 2002, p. 2239
[3]   BRYANT, G. W., SHIRLEY, E. L., GOLDNER, ET AL., *Phys. Rev. B,* 58, 1998, p. 2131

[4] HERZOG, W. D., ŰNLÜ, M. S., GOLDBERG, B. B., ET AL.: *Appl. Phys. Letter* 70, 1997, p. 668

[5] KOVÁČ, J., KVIETKOVÁ, J., KOVÁČ, J. Jr., ET AL.: *Laser Physics,* Vol. 14, No. 2, 2004, pp. 1–6

[6] LAEGSGARD, J., HANSEN, K. P., NIELSEN, M. D., ET AL.: *In Proceedings of SBMO/IEEE MTT-S IMOC*, 2003, pp. 259–261

[7] PUDIŠ, D., MARTINČEK, I., TUREK, I., ET AL.: *In Proceedings of 10th International Workshop on Applied Physics of Condensed Matter,* 2004, pp. 215–218

[8] PUDIS, D., MARTINCEK, I., TUREK, I., ET AL.: *Will be published in Laser Physics,* 15, No. 12, 2005

[9] PUDIŠ, D., MARTINČEK, I., KOVÁČ, J. JR., ET AL.: *Advances in Electrical and Electronic Engineering,* Vol. 4.,No. 2, 2005, pp. 97–100

[10] KÁČIK, D., TUREK, I., MARTINČEK, I. ET AL.: *Intermodal interference in a photonic crystal fibre,* Opt. Express 12, 3465–3470, 2004

[11] SINGH, J.: *Optoelectronics,* (NewYork: The McGraw-Hill Companies, Inc.), 1996

[12] GHATAK, A., THYAGARAJAN, K.: *Introduction to fiber optics,* Cambridge University Press, 1998, pp. 132–178.

Ctibor Musil – Július Štelina *

METHODS OF DETERMINATION OF THE SIGN OF THE THERMO-DIFFUSION COEFFICIENT IN DISPERSED LIQUIDS

In this paper three methods of determination of the sign of the thermo-diffusion coefficient (Soret constant) are presented. The first method uses the relation for Soret constant which was derived from the thermo-diffusion equation. This relation permits determination of the sign of the Soret constant as well as its approximate value. The second method is based on the time dependence of the decay of the created diffraction grating. The last method is based on the measurement of the transmission of light by the dispersion liquid.

1. Introduction

When the nanoparticles with the diameter of $(10 \div 20)$ nm are placed in a liquid medium they are dispersed and at the same time a temperature and concentration gradient are created. As a result there will be forces acting on the particles and, therefore, the diffusion and thermo-diffusion flux of the particles will rise. According to the first Fick law the value of the density of flux of the nanoparticles in one-dimensional case can be expressed by the equation

$$i = -D \cdot \frac{\partial n}{\partial x} - D \cdot S \cdot n \cdot \frac{\partial T}{\partial x} \qquad (1)$$

where the first expression on the right hand side is the diffusion flux and the second one on the right hand side is the thermo-diffusion flux of the particles. D is the diffusion constant of the particles, S is the thermo-diffusion coefficient (the Soret constant) and T is temperature. It is possible to show experimentally that if a gradient of temperature is created in the sample, the particles can accumulate, (when specific conditions are fulfilled), at the place where the temperature is lower ($S > 0$) or at the place where the temperature is higher ($S < 0$).

The explanation of the reason why $S < 0$ is known for gasses, but for liquids a satisfying theory is unknown. That is the reason why there is permanent interest in the solution of this problem in the world [1], [2].

In this paper we present three methods used for the determination of the sign or value of the thermo-diffusion coefficient.

2. Arrangement of an experimental apparatus

For the determination of the sign and value of the Soret constant the experimental apparatus which is depicted in Fig. 1 was used.
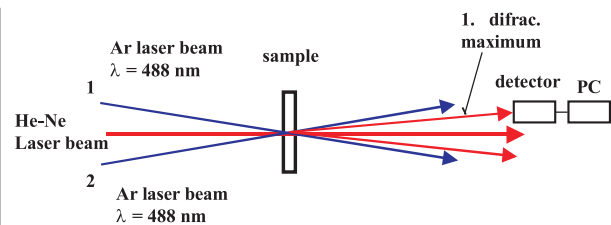
Fig. 1 Schematic arrangement of the experimental apparatus.

In order to create the particle diffraction grating and also to increase the temperature of the disperse liquid at the place of measurement the Ar laser beam with $\lambda = 488$ nm and $(0 \div 120)$ mW power was used. To create the diffraction grating, the laser beam was divided into two crossed beams. At the point where the two beams are crossing the periodical light field arises due to their interference. The periodical thermal field arises because the light energy is absorbed in the sample. Consequently, due to the diffusion and thermo-diffusion of the nanoparticles the particle diffraction grating in the liquid is created.

3. Methods of measurements

a) Method of direct calculation

If we take the sample in the form of a thin layer of the investigated liquid and create the temperature difference $\Delta T = T_2 - T_1$ between two places with coordinates x_1 and x_2, the stationary concentration difference Δn arises. Eq. (1) for the stationary case gives

$$i = 0 = -D \cdot \frac{\partial n}{\partial x} - S \cdot D \cdot n \cdot \frac{\partial T}{\partial x}. \qquad (2)$$

After solving this equation for S we obtain

$$S = \frac{1}{n} \cdot \frac{dn}{dT}. \qquad (3)$$

* Ctibor Musil, Július Štelina
Department of Physics, Faculty of Electrical Engineering, Žilina University , Univerzitná 1, 010 26 Žilina, Slovak Republic
E-mail: stelin@fel.utc.sk

If we assume a small linear change of temperature which is connected with small changes of concentration then the relation (3) can be expressed as

$$S = \frac{1}{n} \cdot \frac{\Delta n}{\Delta T} . \tag{4}$$

The experimental determination of the local value of n is not simple. This one is, however, closely related with the light absorption coefficient α which can be measured directly. Using the equation

$$\frac{\Delta n}{n} = \frac{\Delta \alpha}{\alpha} \tag{5}$$

one gets for the Sorret constant

$$S = \frac{1}{\alpha} \cdot \frac{\Delta \alpha}{\Delta T} \tag{6}$$

where all the quantities necessary for the evaluation of S may be obtained from the experiment.

Moreover, the absorption coefficient can be determined from the relation

$$\alpha = \frac{1}{L} \cdot \ln \left| \frac{U}{U_1} \right|, \tag{7}$$

where L is the sample thickness, U is the signal produced by the detector when the laser beam is passing across the empty cell and U_1 is the signal produced by the detector when the laser beam is passing through the cell in which the sample is placed. After substituting U expressed by equation (7) into relation (6), we obtain

$$S = \frac{1}{\Delta T} \cdot \frac{\ln \left(\dfrac{U_1}{U_2} \right)}{\alpha \cdot L}, \tag{8}$$

where U_1, U_2 are signals from the detector after the laser beam passed through the sample at the temperatures T_1, T_2, respectively [3].

b) The time dependence method of the decay of the grating

If we take the sample in the form of a thin layer of colloidal liquid (thickness of 60 μm) in the interference field of two laser beams (Fig. 1), due to the absorption of light the temperature grating in the sample will be created and the nanoparticles will start repartitioning in the temperature field created according to the sign of the thermo-diffusion coefficient (Soret constant S) and they will start to create an absorption grating [4].

After cutting out the interference field of the crossed beams, the temperature grating will vanish in about 3 ms and the diffraction absorption grating will decay as depicted in Fig. 3.

If one screens one beam of the Ar -laser only the remaining laser beam will be absorbed in places of particle accumulation (grating) and the temperature in these places will remain higher than in the places where the particles concentration is lower. If $S < 0$, the thermo-diffusion flux will be greater than the diffusion

flux and the grating decay will be slowed down or the grating will even be reconstructed (Fig. 2) [4]. From the behaviour of the time dependence depicted in Fig. 3 it follows that $S > 0$ and the effective diameter of the nanoparticles can also be determined.
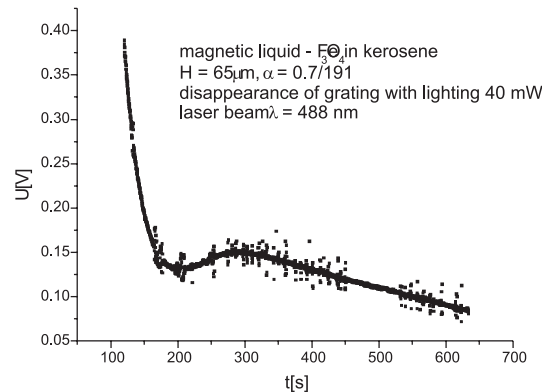
Fig. 2 The time dependence of decay of the lighting particles grating when S < 0.
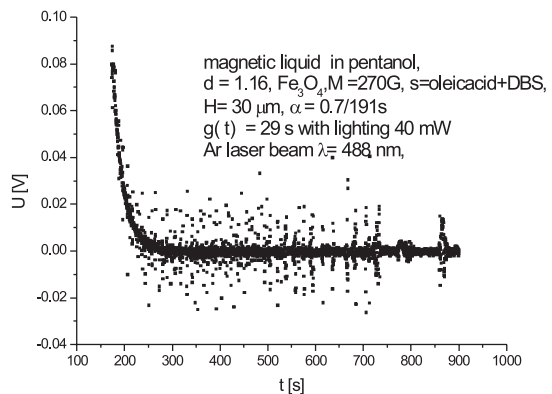
Fig. 3 The time dependence of decay of the lighting particles grating when S > 0.

c) Method of measurement of light transmission

In this method the sample of disperse liquid of the thickness cca (60 ÷ 100) μm is being heated by means of the absorption of the laser beam of high intensity at the point of its passing through the sample (Fig. 4). In this same place the diagnostic beam (e. g. 5 mW He -Ne laser beam) passes through the sample as well.

In the case $S > 0$ the particles are ejected from the place of heating [4] and the intensity of the diagnostic beam grows. If $S < 0$, the dispersed particles accumulate in the place of heating and the intensity of the diagnostic beam decreases (Fig. 5).

4. Experimental results

For the disperse liquid with nanoparticles Fe_3O_4 based on kerosene at the temperature 24 °C we found $S < 0$ with value
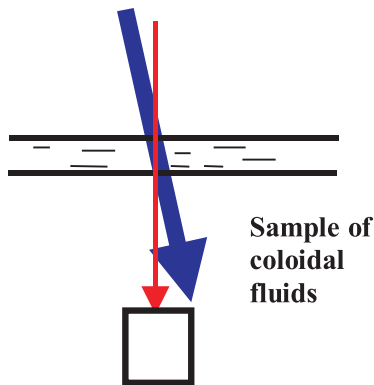
Fig. 4 Schematic arrangement for reading dates to determine the light absorption in the sample.
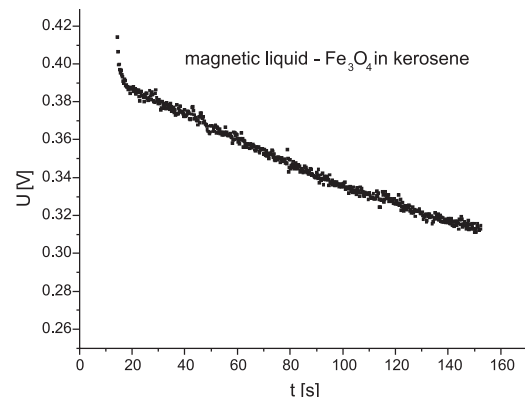
Fig. 5 The time dependence of detection signal through the sample (S < 0) if that is heating.

about 0.023 K^{-1} using all three methods. For the disperse liquid with nanoparticles Fe_3O_4 dispersed in pentanol we found $S > 0$ at the temperature 24.5 °C using method b). For the disperse liquid of tempera paint (Kraplak dark) based on water we found $S > 0$ at the temperature 21.5 °C using method b).

5. Conclusions

On the basis of the obtained results we conclude that the presented methods are suitable for determination of the sign and approximate magnitude of the Soret constant. The accuracy of the first method depends mainly on the accuracy with which the initial and final temperatures of the liquid T_1 and T_2 and the voltages U_1 and U_2 are determined in the stationary regime of the liquid sample in the presence of the Ar laser beam.

Except for the fast determination of the sign of the Soret constant, these methods can also serve for the study of the thermo-diffusion and kinetic phenomena connected with it in the liquids in which nanoparticles are present.

References

[1] LANDAU, L. D., LIFŠIC, E. M.: *Hydrodynamics* (in Russian), Moskva, Nauka 1986
[2] DE GANS, B., KITA, R., WIEGAND, S., LUETTMER-STRATHMANN, J.: *Phys. Rev.*, Lett. 91, 2455501, 2003
[3] ŠTELINA, L., MUSIL, C.: *Metod for specification sign and value of Soret constant factor in colloid fluids (in Slovak)*, ADVANCES in Electrical and Electronic Engineering, ŽU, No.1, Vol. 3/2004, Žilina, pp. 55-58
[4] ŠTELINA, J., MUSIL, C., BRACINÍK, J., KOPČANSKÝ, P., TIMKO, M., KONERACKÁ, M.: *Influence of the sign of Soret constant on the formation and decay of the nanoparticle structures in dispersion fluids,* 11th International Workshop on APCOM, Malá Lučivná, 2005, pp. 230-234
[5] KOPČANSKÝ, P., TIMKO, M., POTOČOVÁ, I., KONERACKÁ, M., JURÍKOVÁ, A., TOMAŠOVIČOVÁ, N., ŠTELINA, J., MUSIL, C., BRACINÍK, J.: *The determination of the hydrodynamic diameter of magnetic particles using FRS experiment,* Jour. of Magnetism and Magnetic Materials, 289, pp. 97-100, 2005

S. Jurečka – J. Müllerová *

THIN FILM OPTICAL PARAMETERS DETERMINATION BY THE DYNAMICAL MODELLING AND STOCHASTIC OPTIMIZATION METHOD

We report on a new method of experimental data processing to obtain optical parameters of thin films. Dynamical modelling of the spectral reflectance can be performed interactively in a graphical environment by the genetic search in wide interval of parameter space and then refined by the genetic algorithm method, by the Nelder-Mead downhill simplex method or Marquardt-Levenberg method. Optical parameters of hydrogenated amorphous silicon (a-Si:H) thin film used in solar cell technology are determined by this new method. The spectral reflectance is a function of optical properties and the thickness of the film. Optical parameters found by our approach do not depend on the initial spectral reflectance estimation.

1. Introduction

The theoretical and experimental studies on the optical behaviour of thin films deal primarily with optical reflection, transmission and absorption properties, and their relation to the optical constants of films. The theoretical reflectance R_t can be calculated from the optical properties and thickness d of the film. Normal incidence reflectometry is often used for several reasons: good spatial resolution, high throughput and accuracy. Optical properties of any material can be described by the complex index of refraction, $N = n - ik$, where n is the refractive index and k is the extinction coefficient. Both n and k depend on the wavelength of light λ. In many thin-film applications, namely in solar cell technologies, the optical constants n and k are strongly correlated to the deposition process conditions and their broadband determination is needed to design the solar cell structures. Experimental and theoretical reflectance can be matched by fitting for the film thickness and optical properties. The optimization problem is formulated as

$$\min_3 \left\{ \sum \left[R_o(\lambda) - R_t(n, k, \lambda, d) \right]^2 \right\} \qquad (1)$$

where R_o denotes measured reflectance values. The optimization issue is to find the system of parameters that satisfy the desired optical specifications. Numerical methods are flexible and can handle complicated problems. The numerical computations are based on merit functions that can be defined according to quantities of interest. Considering the computational cost involved, and furthermore the constraints to calculate the gradient information for this specific optical thin-film model, algorithms that can substantially reduce computation without using derivatives are preferable. In our approach the dynamical modelling and stochastic optimization approach (DMSO) is used.

2. Dynamical modelling and stochastic optimization method

The spectral reflectance (SR) of a thin quasi-ideal single homogeneous isotropic film on a thick partly absorbing substrate is given by

$$R = \frac{A + Bx + Cx^2}{D + Ex + Fx^2}.$$

In this equation $x = \exp(-\alpha d)$ is the absorbance, $\alpha = (4\pi k_1)/\lambda$ is the absorption coefficient [1] and

$$A = [(1 - n_1)^2 + k_1^2][(n_1 + n_2)^2 + (k_1 + k_2)^2]$$
$$B = 2[A'\cos\varphi + B'\sin\varphi]$$
$$C = [(1 + n_1)^2 + k_1^2][(n_1 - n_2)^2 + (k_1 - k_2)^2]$$
$$D = [(1 + n_1)^2 + k_1^2][(n_1 + n_2)^2 + (k_1 + k_2)^2]$$
$$E = 2[C'\cos\varphi + D'\sin\varphi]$$
$$F = [(1 - n_1)^2 + k_1^2][(n_1 - n_2)^2 + (k^1 - k_2)^2]$$
$$A' = (1 - n_1^2 - k_1^2)(n_1^2 - n_2^2 + k_1^2 - k_2^2) + 4k_1(n_1k_2 - n_2k_1)$$
$$B' = 2(1 - n_1^2 - k_1^2)(n_1k_2 - n_2k_1) - 2k_1(n_1^2 - n_2^2 + k_1^2 - k_2^2)$$
$$C' = (1 - n_1^2 - k_1^2)(n_1^2 - n_2^2 + k_1^2 - k_2^2) - 4k_1(n_ik_2 - n_2k_1)$$
$$D' = 2(1 - n_1^2 - k_1^2)(n_1k_2 - n_2k_1) + 2k_1(n_1^2 - n_2^2 + k_1^2 - k_2^2)$$
$$\varphi = (4\pi n_1 d)/\lambda$$

In the DMSO method, the optical parameters are determined in several steps. In the first step we prepare an initial spectral reflectance model in graphical environment by interactive dynamical modification of the reflectance model parameters. Alternatively automatic stochastic search in wide interval of parameter hyperspace can be used to create an initial reflectance model. The stochastic optimization is based on the genetic algorithm (GA). The next step uses stochastic optimization refinement of result reflectance reached in the previous modelling by the Nelder-Mead or Marquardt-Levenberg optimization:

* S. Jurečka, J. Müllerová
  Department of Engineering Fundamentals, Faculty of Electrical Engineering, kpt. Nálepku 1390, 03101 L. Mikuláš, Slovakia,
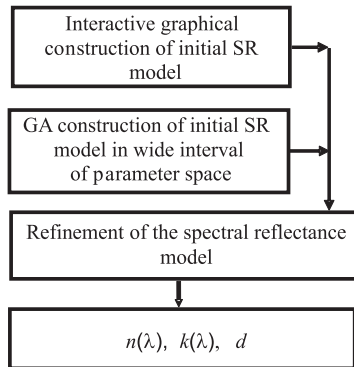 E-mail: jurecka@lm.utc.sk

Fig. 1 Dynamical modelling method of the initial spectral reflectance model estimation

The step of dynamical modelling speeds up the calculations of the reflectance function parameters and enables constructing the theoretical reflectance model with comfort and high quality. Besides this, stochastic algorithms enable also comfortable incorporation of necessary physical constraints into the optimization method. We used genetic algorithm with binary representation of the theoretical reflectance model variables [2]. There are many different settings associated with predictions in optical parameters solutions. Most of these settings are maintained automatically using rules of the GA that create the best results. To speed up the achievement of the best solution we used visual construction of the spectral reflectance model. The values of the theoretical reflectance model parameters are dynamically modified and corresponding theoretical model is graphically displayed and compared with an experimental reflectance curve. This visual modelling step provides good estimation of the initial reflectance model and substantially reduces computation time and stochastic search of the model parameters values.

GA procedure refines the initial mathematical model by minimizing the differences between theoretical and experimental values. The initial reflectance estimation introduces a set of parameters based obviously on the properly selected dispersion model of the refractive index n and the extinction coefficient k [3,4], e.g.

$$n = n(p_1, p_2, p_3. p_4, \lambda), \qquad k = k(p_1, p_2, p_3. p_4, \lambda).$$

Therefore, the spectral reflectance model is represented by variables

$$X = [p_1, p_2, p_3. p_4, \lambda].$$

A set of correction values $\Delta = [\Delta p_1, \Delta p_2, \Delta p_3. \Delta p_4, \lambda]$ is used in each GA iteration step for setting new trial reflectance model variables $X' = X - \Delta$. The implementation of the GA algorithm minimizes the differences (1) by stochastic exploring the correction parameters hyperspace in the interval $\langle -0.2X, 0.2X \rangle$ for each variable in the spectral reflectance function. Alternatively in case of the high quality of the initial spectral reflectance mathematical model was obtained in the first step of the DMSO method

the conventional numerical optimization methods can be implemented (Marquardt-Levenberg or Nelder-Mead simplex methods):
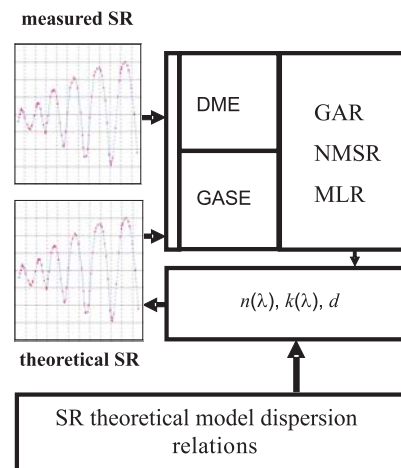
Fig. 2 DMSO method implementation
DME - Dynamical Modelling Initial SR Model Estimation
GASE - Genetic Algorithm Search SR Estimation
GAR - Genetic Algorithm method SR Refinement
NMSR - Nelder-Mead Simplex method SR Refinement
MLR - Marquardt-Levenberg method SR Refinement

3. Experimental results

The described method was used to extract the refractive indices of a series of undoped a-Si:H thin films with approximately the same thickness $\sim$ 400 nm (Table 1). The samples were deposited at the Delft University of Technology, the Netherlands, on Corning 1737 glass substrates by PECVD industrial deposition system [5,6] from hydrogen (H_2) to silane (SiH_4) plasma under varied H_2/SiH_4 gas flows (the dilution D).

Samples under study   Table 1

dilution D	thickness [nm]
0	390
10	394
20	385
30	388
40	402
50	397

Optical properties of the dilution series are obviously affected by the changing structure [6]. The refractive indices for all samples under study were determined from the experimental spectral reflectance determined by the DMSO method (Fig. 3). At all wavelengths, we observe the decreases of the refractive index with increasing dilution For the sample prepared at $D = 40$, approximately the same spectral refractive indices were revealed as for the
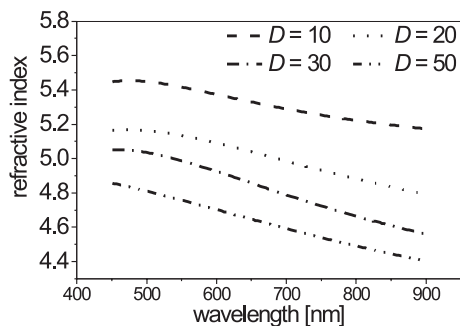
Fig. 3 Refractive indices of the a-Si:H thin film samples.
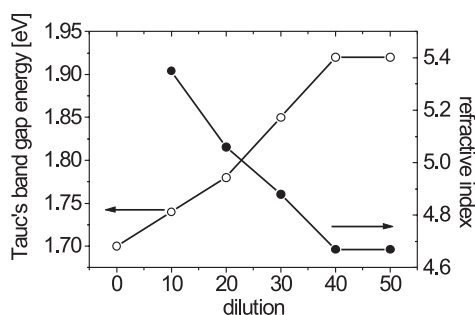
Fig. 4 Refractive index (at 633 nm) and the Tauc's optical band.

sample at $D = 50$, therefore this plot was not incorporated into the Fig. 3.

Fig. 4 illustrates the dilution-dependent refractive index at 633 nm and Tauc's optical band gap determined from the experimental spectral transmittance in the vicinity of the absorption edge [6]. The data for Tauc's optical band gap as one member of the set of dispersion model parameters acquired from the course of DMSO method are in good agreement with the values plotted in Fig. 4.

Thus, the DMSO method yields quickly and reliably information useful for all applications of the samples under study where optical properties matter. The observed decrease of refractive index may be probably due to the voids – sites with missing radicals of $SiH_4 - H_2$ decomposition. The band gap appears to increase with increasing dilution. The increase of E_g at the amorphous-crystalline boundary is due to the appearance of indirect gap electronic structure of the crystalline silicon.

4. Conclusions

The DMSO method was introduced for the thin film optical parameter determination. Experimental spectral reflectance data of a series of a-Si:H thin films were analysed. DMSO method succeeded in theoretical reflectance model refinement very good. It does not converge to a local optimum of the refined model. The combination of dynamical modelling and stochastic optimization of the initial mathematical model compared with the experimental data speeds up calculations and enables checking for meaningful optical parameters.

References

[1] SWANEPOEL, R.: J. *Phys. E*, 34, 1214, 1983.
[2] GOLDBERG, D. E.: *Genetic Algorithms in Search, Optimization and Machine Learning.* Addisom-Wesley, 1989.
[3] FRANTA, D., OHLÍDAL, I., MUNZAR, D.: *Acta Physica Slovaca,* 48, No. 4, 451, 1998
[4] JELLISON, G. E.: *Thin Solid Films,* 313 – 314, 33, 1998
[5] NÁDAŽDY, V, DURNÝ, R., THURZO, I., PINČÍK, E., NISHIDA, A., SHIMIZU, J., KUMEDA, M., SHIMIZU, T.: *Phys. Rev.* B 66, 195211, 2002.
[6] MÜLLEROVÁ, J., JUREČKA, S., ŠUTTA, P.: *Acta Physica Slovaca,* 55, No. 3, 351, 2005.

L. Harmatha – Ľ. Stuchlíková – P. Písečný *

RADIATION HARDNESS OF MOS STRUCTURES EXPOSED TO HIGH-ENERGY IONS

MOS structures exposed to 305 MeV Kr and 710 MeV Bi ions irradiation with fluences of 10^9 cm^{-2} and 10^{10} cm^{-2} were investigated by capacitance measuring methods (C-V, C-t), completed by quasistatic low-frequency C-V and DLTS measurements.

The irradiated MOS structures were functional in spite of a high density of radiation defects. The electric activity of the defects brought a sharp decrease in the generation parameters t_r and τ_g. The parameters of six deep levels were detected in the MOS structures exposed to 710 MeV Bi ions irradiation. Five of these levels with energies 0.52 eV, 0.14 eV, 0.17 eV, 0.25 eV, 0.27 eV were radiation defects.

Keywords: Silicon; high-energy ion implantation; irradiation; MOS structure; capacitance method; DLTS

1. Introduction

Recently there has been a growing interest in the use of high-energy heavy ion irradiation for electronic materials modification [1]. The issues involved in high-energy ion implantation are open both on the fundamental [2] as well as on the applied aspects of the process [3]: the understanding of defect creation and its kinetics on the one hand, and the application of deep implantation on the other hand.

This study is also very useful for knowledge of the radiation hardness of electronic devices in a high radiation environment in a reactor laboratory or in the outer space.

The scope of this paper is to investigate the effect of the 305 MeV Kr and 710 MeV Bi ion irradiation on the electrical properties of MOS structures.

We used the capacitance-voltage C-V method to determine the flat-band voltage U_{FB} and the free carriers concentration profile $n(x)$ in the structures before and after irradiation. The kinetics of the generation process that takes place in the space charge region was diagnosed by the non-equilibrium C-t method [4]. Parameters obtained from this method, the relaxation time t_r, the generation lifetime of minority charge carriers τ_g and the surface generation velocity S_g characterize the electrical behaviour of defects in the MOS structure.

The energy distribution of the insulator-semiconductor interface trap density D_{it} was obtained from the low frequency C-V curve. We used the quasistatic charge-voltage method [5].

In particular, deep level transient spectroscopy (DLTS) [6] proved to be highly applicable because of its good sensitivity, and specific defect centers with well-defined signatures can be monitored to concentrations of $\sim 10^{-5}$ below the dopant concentration. We used the standard capacitance DLTS method with electrical excitation.

2. Experiment

An n-type Czochralski-grown antimony doped (100)-oriented homogeneous wafer of silicon with resistivity 2–5 Ωcm and thickness 300 μm was used as a substrate of the MOS structure. The gate SiO_2 layers were prepared by thermal oxidation in the atmosphere of dry oxygen at 1050 °C for 90 minutes. The thickness of the SiO_2 layer was about 100 nm. All gates were vapour deposited and patterned photolithographically. After manufacturing the MOS structures, the sample was annealed in $N_2 + H_2$ at 460 °C for 20 minutes. The ohmic contact from the backside of the wafer was prepared by vapour deposition of Al.

Afterwards, the MOS structures were exposed to 305 MeV Kr ion irradiation with a fluence of 10^9 cm^{-2} (samples D1) and a fluence of 10^{10} cm^{-2} (samples D2) and to 710 MeV Bi ion irradiation with a fluence of 10^9 cm^{-2} (samples D8) and with a fluence of 10^{10} cm^{-2} (samples D6) at the Joint Institute for Nuclear Research in Dubna, Russia [7].

The non-irradiated MOS structure (D0) and the irradiated MOS structures (D1, D2, D6, D8) were characterized by C-V, low-frequency C-V and C-t methods. High frequency capacitance-voltage C-V and non-equilibrium capacitance-time C-t measurements were performed using the 4280 1 MHz C Meter/C-V Plotter Hewlett-Packard [8]. Quasistatic low frequency C-V measurements were performed using the Keithley 595 Quasistatic CV Meter. The MOS structures (D0) and irradiated (D6, D8) were also investigated by a standard DLTS method. This method is a high-frequency transient capacitance thermal scanning method, where the capac-

* L. Harmatha, Ľ. Stuchlíková, P. Písečný
Department of Microelectronics, Faculty of Electrical Engineering and Information Technology, Slovak University of Technology, Ilkovičova 3, 812 19 Bratislava, Slovakia, fax: ++421-2-654 23480, E-mail:ladislav.harmatha@stuba.sk

itance transient effect in the potential barrier of a semiconductor is caused by an electrical excitation pulse. DLTS measurements were performed using a BioRad boxcar detection system.

3. Results and Discussion

The MOS structures (sample D0) used in this experiment were of high quality, having a low density of defects. This presumption was verified by many measured DLTS spectra under different measuring conditions (Fig. 1).
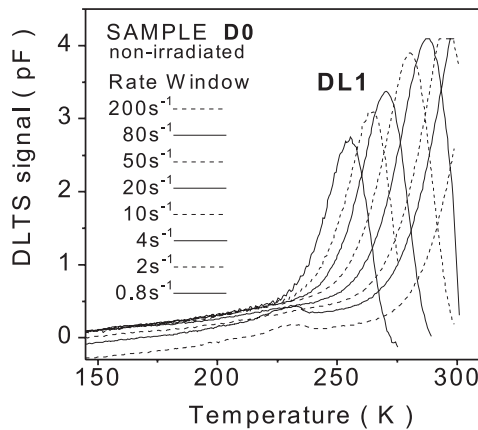
Fig. 1. Typical measured DLTS spectra of the sample D0 at optimal measuring conditions ($U_R = -1$ V, $U_F = -0.25$ V, $t_F = 0.8$ ms). DL1 is the determined energy deep level.

We found only one deep level DL1 (0.61 eV) with a very low concentration of 2×10^{13} cm^{-3}. This deep level corresponds to the presence of Au (0.59 eV) [9].

In C-V measured curves (Fig. 2), we observed a rise in the positive defect charge in the oxide and at the interface with the silicon substrate, which resulted in an increased flat band voltage (Tab. 1).

The antimony doped MOS structures had the same or only slightly lower concentration of impurities, N_D, after irradiation with
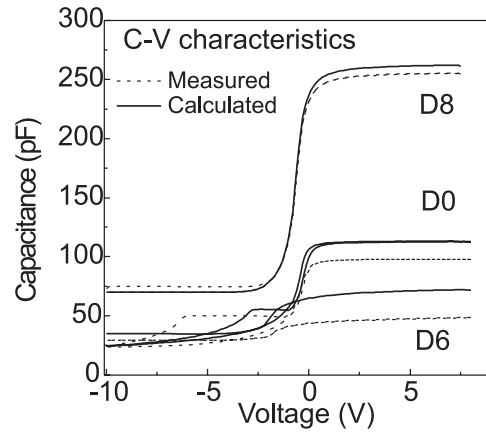
Fig. 2. MOS structures D0, D6, D8 measured and calculated C-V curves; the calculated C-V curves include a correction for the effect of conductance upon the measurement of the capacitance.

Kr and Bi ions. Significant changes in the parameters of the MOS structure were observed in the non-equilibrium state. In C-t measurements we observed a marked decrease of the relaxation time, tr, see Fig. 3.
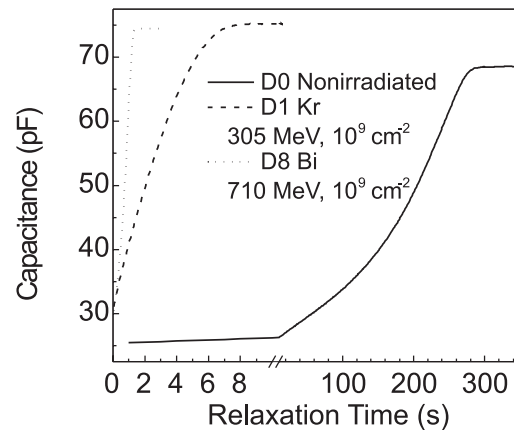
Fig. 3. MOS structures D0, D1, D8 measured C-t curves of MOS structure before and after irradiation by Kr and Bi ions with the same fluence 10^9 cm^{-2}

Parameters extracted from C-V, low-frequency C-V and C-t measurements on MOS structures. Tab. 1
The values of D_{it} were determined for the level 0.22 eV above the midgap (Fig. 6).

Sample	U_{FB} (V)	N_D (m^{-3})	t_r (s)	τ_g (μs)	S_g (ms^{-1})	D_{it} (m^{-2}eV^{-1})
D0 – nonirradiated	-0.1	1.22×10^{21}	487	472	2.2×10^{-3}	9.1×10^{14}
D1 – Kr, 305 MeV, 10^9 cm^{-2}	-0.4	1.1×10^{21}	10	3.9	3.1×10^{-3}	2.4×10^{15}
D2 – Kr, 305 MeV, 10^{10} cm^{-2}	-1.2	0.98×10^{21}	1.9	0.8	1.3×10^{-1}	1.3×10^{16}
D8 – Bi, 710 MeV, 10^9 cm^{-2}	-0.5	1.1×10^{21}	1.7	1.3	4.5×10^{-1}	1.86×10^{16}
D6 – Bi, 710 MeV, 10^{10} cm^{-2}	no C-V	–	no C-t	–	–	no lf C-V

The rise in the density of radiation defects is expressed quantitatively through parameters τ_g and S_g (Tab. 1). The highest density of electrically active defects was found in the case of Bi ions with higher energies than those of Kr. Remarkable differences in the generation parameters were observed also in dependence on the fluence of irradiation. In Fig. 4 one can see the shortening of the time of relaxation after irradiation by Kr ions with a higher fluence.
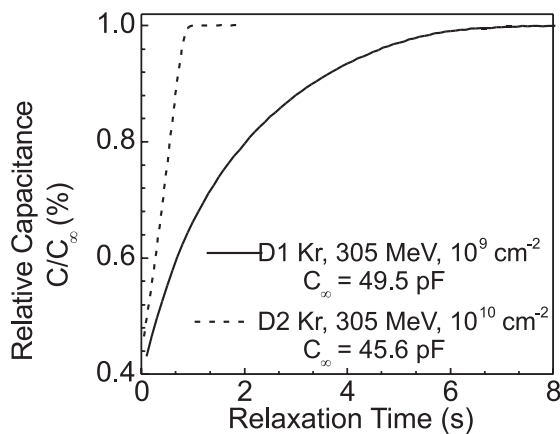
Fig. 4. MOS structures D1 and D2 measured C-t curves of MOS structure after Kr ion irradiation with fluences $10^9\ cm^{-2}$ and $10^{10}\ cm^{-2}$.

In the case of irradiating with ions of Bi with a fluence of $10^{10}\ cm^{-2}$ a significant increase in the conductivity of the insulating layer was observed (Fig. 5).
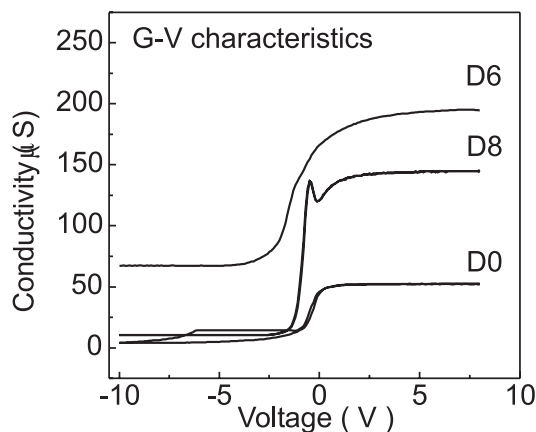
Fig. 5. MOS structures D0, D6, D8 measured G-V curves - conductivity from applied voltage.

C-V measurements and the calculation of D_{it} (Fig. 6) reveal that the growing dose and energy of implanted ions increase the density, D_{it}. A similar trend can be observed also in the change of

the surface generation velocity, S_g. One can deduce that the quality of the Si – SiO$_2$ deteriorates. In spite of that the irradiated MOS structures still remain their capacitance properties and functionality.
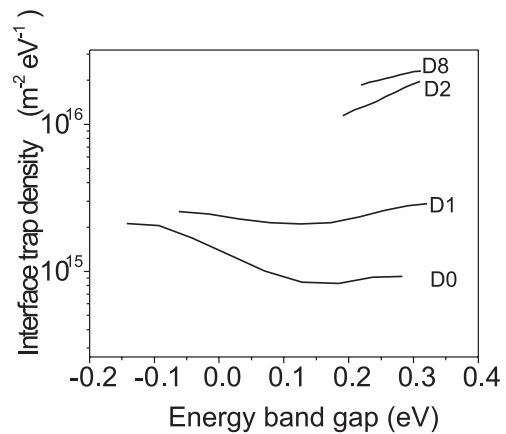
Fig. 6. The energy distribution of the Si–SiO$_2$ interface trap density. **D0** - nonirradiated, **D1** - Kr, 305 MeV, $10^9\ cm^{-2}$, **D2** - Kr, 305 MeV, $10^{10}\ cm^{-2}$ and **D8** - Bi, 710 MeV, $10^9\ cm^{-2}$.

The measured DLTS spectra of the MOS structures after Bi ion irradiation with fluences $10^9\ cm^{-2}$ and $10^{10}\ cm^{-2}$ (D6 and D8) exhibit a strong deviation from an exponential dependence (Fig. 7).
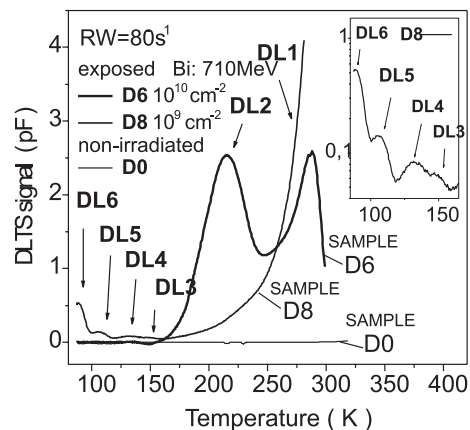
Fig. 7. Typical measured DLTS spectra of the samples D0, D6, D8 for rate window 80 s^{-1} at the same measuring conditions (reverse voltage $U_R = -3\ V$, filling pulse $U_F = -1.1\ V$, and pulse time $t_F = 0.8\ ms$). DL1-DL6 are the determined energy deep levels.

This can be caused by the presence of several mutually influencing deep energy levels. Six peaks labelled DL1, DL2, DL3, DL4, DL5 and DL6 were detected. These deep levels DL1-DL6 are traps of majority charge carriers (electrons). The values of the activation enthalpies (En of electron deep levels and the capture

Parameters of the measured deep levels extracted from the Arrhenius diagram.   Tab. 2

Deep Levels	activation enthalpies ΔE_n (eV)	cross section σ_n (cm^{-2})	concentration (cm^{-3})			Temperature at RW = 100 s^{-1}	Similar traps in literature
			sample D0	sample D6	sample D8		
DL1	0.611	1.8×10^{-15}	2×10^{13}	3×10^{15}	1×10^{15}	305.4	Au, 0.59eV [8]
DL2	0.523	1.9×10^{-13}	no detect	1×10^{15}	4×10^{14}	223.0	E - centre [8]
DL3	0.269	2.9×10^{-16}	no detect	no detect	7×10^{13}	152.1	V^{-2} [9]
DL4	0.246	1.2×10^{-16}	no detect	no detect	9×10^{13}	134.2	V^{-2} [9]
DL5	0.171	1.3×10^{-15}	no detect	no detect	2×10^{14}	107.8	A – centre [8]
DL6	0.143	4.9×10^{-16}	no detect	no detect	7×10^{14}	88.1	A – centre [8]

cross section for electrons σ_n were determined from the Arrhenius diagram using the known equations [6] (they are listed in Tab. 2).

In principle it was shown, see Fig. 7, that the deep energy deep DL1 was found in all the three investigated samples D0, D6, D8, while the deep energy level DL2 can be detected only in the structures irradiated by Bi ions. We can suppose that it was a radiation defect with an activation enthalpy of 0.52 eV, which probably corresponds to an E – centre (vacancy- phosphorous) in irradiated Si [9]. This deep level dominates in structure D6.

DL3, DL4, DL5 and DL6 peaks were detected only in D8 structures irradiated by Bi ions with fluency 10^9 cm^{-2}. These are radiation defects. We suppose that DL3 (0.27 eV) and DL4 (0.25 eV) deep level are divacancies V^{-2} in Si [10] created by the implantation process and DL5 (0.17 eV) and DL6 (0.14 eV) correspond probably to the A – centre (vacancy-oxygen) in irradiated Si [11].

4. Conclusion

From the capacitance C-V and C-t measurements we found that MOS structures irradiated by high energies and doses of Kr and Bi ions were functional in spite of a high density of radiation defects. In the case of Bi ions with a higher energy than that of Kr ions, the conductivity of the insulating layer increased. We did not observe a decrease in the concentration of shallow impurities in irradiated MOS structures. The radiation defects created at the Si-SiO$_2$ interface increased the trap density and their electrical activity.

We detected six deep levels in MOS structures irradiated by Bi ions with energy 710 MeV and fluency 10^9 and 10^{10} cm^{-2}. Five of them, DL2-DL6, were produced by radiation. DL3-DL6 levels cannot be detected under higher fluency (10^{10} cm^{-2}). Our interpretation of this fact is following: irradiation with a fluency of 10^{10} cm^{-2} caused gettering of DL3-DL6 defects. This fluency also causes great oxide layer damage. At the same time, the concentration of DL2 defect in structure D6 rose strongly.

References

[1] SCRIVASTAVA, P.C., PANDEY, S. P., SINHA, O. P., AVASTI, D. K., ASOKAN, K.: *Nuclear Inst. and Methods in Physics Research B*, 1999, vol. 156, pp. 105–109.
[2] NEUSTROEV, E. P., ANTONOVA, I. V., POPOV, V. P., STAS, V. F., SKURATOV, V. A., DIDYK, A. YU.: *Nuclear Instr. and Methods in Physics Research B*, 2000, vol. 171, pp. 443–447.
[3] YARYKIN, N., CHO, C. R., ZUHR, R., ROZGONYI, G.: *Physica B,* 1999, vol. 273–274 pp. 485–488.
[4] ZERBST, M.: *Z. Angew. Physics,* 1966, vol. 22, pp. 30–36.
[5] PÍSEČNÝ, P., ŤAPAJNA, M., HARMATHA, L., VRBICKÝ, A.: *Journal of Electrical Engineering, 2004,* vol. 55, pp. 95–99.
[6] LANG, D. V.: *J. Appl. Phys.,* 1974, vol. 45, pp. 3014–3023.
[7] NEUSTROEV, E. P., ANTONOVA, I. V., OBODNIKOV, V. I. POPOV, V. P., SKURATOV, V. A., SMAGULOVA, S. A., DIDYK, A.YU.: *Nuclear Instr. and Methods in Physics Research B,* 1998, vol. 146, pp. 323–328.
[8] GURNIK, P., HARMATHA, L.: *J. Electrical Engineering,* 1997, vol. 48. pp. 52–56.
[9] FUKUOKA, N., YONEYAMA, M., HONDA, M., ATOBE, K.: *Jpn. J. Appl. Phys.,* 1993, vol. 32, pp. 2059–2062.
[10] WATKINS, G. D.: *The lattice vacancy in silicon.* In: Deep Centers in Semiconductors (Si). Edited by S. T. Pantelides, Gordon and Breach Science Publishers, 1986, pp. 147–183
[11] STAŇO, J., ŽIŠKA, M.: *Solid State Phenomena,* 2002, vol. 82–84, pp. 453–458.

Ladislav Janoušek – Tomáš Marek – Daniela Gombárska *

EDDY CURRENT NON-DESTRUCTIVE EVALUATION OF CONDUCTIVE MATERIALS

Non-destructive methods of material properties evaluation are presented in the paper. The methods are useful especially for increasing the safety of sophisticated and environment threatening facilities and, consequently, for decreasing the operating expenditures of those facilities. The attention is paid mainly to the method that utilises eddy currents induced in the surface layer of conducting samples by means of a small flat coil. The eddy current testing method is theoretically described and results of its particular application are presented in the paper.

1. Introduction

The present-day period is characteristic of a fast development of sophisticated technologies. The technologies strongly influence not only industry but also global living surroundings. Due to their price and possible consequences of their breakdown a permanent inspection of their integrity and function becomes more and more important. The inspection has many aspects and thus different approaches are utilised. A non-destructive testing (NDT) of materials properties plays an important role among them as a tested structure is not damaged during the inspection and usually there is no need for disassembling of the tested structure. Accordingly, the NDT is used for in-service inspection as well as for evaluation of manufacturing processes. Reliable inspection methods are very important because of two closely related aspects. The first and the most important one is the safety. Discovering structural anomalies and preventing accidents is the basic task of the NDT. The second aspect is economical because an effective utilisation and safe prolongation of life-span of expensive facilities such as nuclear reactors, dams, space devices, aircraft, submarines, sophisticated medical devices, information databases etc. can be based on a periodical monitoring of their health.

The most important task of the non-destructive evaluation consists in the discovering of different defects arisen during production or service of a component due to fatigue, overloading or influence of extreme conditions. Different methods are utilised for the purpose. It depends on a character of a material being tested as well as on a structure and a location of an expected defect which of the methods is the most reliable one. The methods differ mainly in resolution and sensitivity to various kinds of defects (e.g. surface or volume).

The methods of non-destructive evaluation can be divided into several main groups:
- *Mechanical waves techniques* – mechanical vibrations of an inspected body are investigated, namely, propagation of surface or volume mechanical waves in a sample or emission of acoustic waves from the body. Resolution of mechanical wave methods is limited by a wavelength or a frequency of the wave.
  - Ultrasonic defectoscopy.
  - Acoustic emission.
  - Investigation of resonance spectra of mechanical vibrations.
- *Electromagnetic waves techniques* – interaction of an electromagnetic wave with an inspected body is evaluated, mainly propagation, reflection and scattering of the electromagnetic wave caused by non-homogeneities in a sample.
  - Optical methods (e.g. microscopic investigation, holographic and interferometric methods) are very effective mainly in a case of investigation of a sample deformation or changes of quality of its surface.
  - Infra-red thermography is used for investigation of non-homogeneous thermal profile of a sample caused by electrical or mechanical losses (e.g. heating of bearing or breaks, heating of electric joints or electric devices).
  - X-ray investigation represents very effective and powerful means of defectoscopy. Influence of a sample structure on the X-rays propagation through the sample is investigated. The method is sensitive to internal defects of conducting samples like welded joints, parts of motors, railway carriages wheels, organic samples, etc.
- *Nuclear methods.*
  - Radioactive sampling method works based on addition of a radioactive substance (liquid or gas) into a flowing fluid and consequent dosimetric evaluation of the fluid propagation thorough an investigated system or penetration into investigated defects.
  - Nuclear magnetic resonance is a method which is able to discover special atoms in a sample, e.g. hydrogen atoms of the water. The method is effectively used for the investigation of living structures (plants or animals).
- *Computer tomography methods* represent modern tools developed in connection with evolution of powerful computers. Tomography imaging consists in computer aided processing of a huge amount of data obtained by a successive detection of radiation emitted by an investigated body. A source of a signal might be

* **L. Janoušek, T. Marek, D. Gombárska**
Department of Electromagnetic and Biomedical Engineering, Faculty of Electrical Engineering, University of Žilina, Univerzitná 1, 010 26 Žilina, Slovakia, E-mail: janousek@fel.utc.sk, marek@fel.utc.sk, gombarska@fel.utc.sk

X-rays, nuclear magnetic resonance signal, radioactive emission etc. The computer tomography is a tool for 3D-imaging of a sample internal structure.

- *Electromagnetic inductive methods* employ interaction between the alternating electromagnetic field with an electro-dynamic structure of a conducting material.
  - Acoustic wave which propagates through a sample can be generated by an electromagnetic field in a surface conductive layer of the sample. A special probe used for generating and detecting of the wave is known as EMAT (Electromagnetic-Acoustic Transducer). The method combines advantages of the ultrasonic inspection together with an advantage of a non-contact inductive method for the ultrasound generation and detection. Detailed description of the method together with some results of its development was published in [1 – 5].
  - External electromagnetic field generates strongly attenuated electromagnetic wave known as the skin effect in the surface layer of a conducting sample. It is connected with existence of induced eddy currents. Non-destructive eddy current testing (ECT) is utilized for non-contact inspection of conducting bodies. This method is described in detail in [6 – 12] and in the present paper.

2. Eddy Current Testing

The principle of the ECT method underlies in the interaction of the induced eddy currents with a structure of an examined body. The alternating electromagnetic field generated by a suitable coil penetrates into a surface layer of the body to an effective depth given by an expression:

$$\delta = \sqrt{\frac{2}{\omega\mu\sigma}},$$

where ω is the angular frequency, μ and σ are the permeability and the conductivity of a material, see Fig. 1.
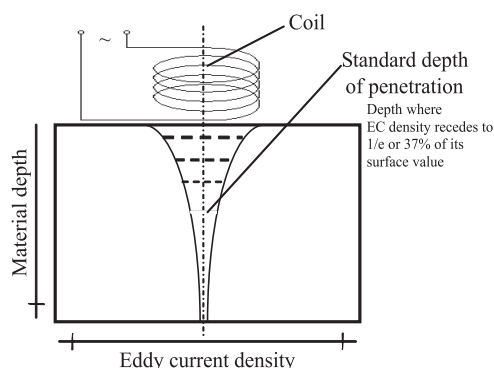

Fig. 1 Depth of penetration

The eddy currents (EC) are influenced by defects and other non-homogeneities in the tested sample. The electromagnetic field generated by the EC can be detected by the same coil (self inductance ECT probe of the absolute type) and is evaluated as a change in the coil's impedance. The impedance is influenced not only by the sample properties but also by a configuration of the coil and by a lift-off distance of the coil from the sample surface. Evaluation of the obtained signal is a challenge of the method. A relation between the detected change in the impedance of the coil and a structure of the tested sample is very complex and has to be evaluated by means of special transformation procedures performed using dedicated computer codes (inverse problem) developed based on the forward simulations of ECT tasks.

The ECT method is effectively used only for the examination of surface breaking defects because the EC amplitude exponentially decays with the depth in the tested sample. A surface layer that can be effectively inspected by the ECT goes from several decimals of mm (100 kHz range) up to several mm (kHz range). Selection of the inspection frequency depends on an estimated character as well as on an expected depth of defects. On the other hand, the resolution of the method is limited by the electromagnetic wavelength, which is comparable with the effective skin depths $\lambda = 2\pi\delta$ and thus it is dependent on frequency. Usually multi-frequency examination is used during an inspection employing the ECT method.

The input impedance and thus the primary current of the excitation circuit are affected by material properties of a specimen, geometrical arrangement of a probe itself and the lift-off distance from the surface of a sample. When the last two parameters are kept constant during the inspection, the measured ECT signal depends on changes of the material properties in general and provides the information about the location of discontinuity, its shape and proportions.

The main advantages of the ECT method are [10]:
- sensitivity to small cracks and structural non-homogeneities;
- high resolution;
- versatility;
- inspection gives immediate results;
- portable equipment;
- non-contact inspection;
- inspection of complex structures.

On the other hand, the ECT has some limitations arising from its own physical principles. The primary limitation is given by applicability of the method to the inspection of conducting materials only. The EC depth of penetration is limited by the skin effect, therefore the method is applicable only for detection of surface and near subsurface defects or for the volumetric inspection of thin materials. Defects lying parallel to the coil's winding are hardly detectable. In addition, a surface roughness of a tested object influences the measured data and decreases the probability of detection as well as deteriorates the evaluation of the crack. However, because of the advantages listed above, the ECT is frequently used in many industrial fields. It is mainly applied in the non-destructive testing of various structural components. The ECT is also used for measurement of a thickness of conductive materials. For example, it can be used in evaluation of a wall thinning due to corrosion or in measurement of conductive material coating or paint-
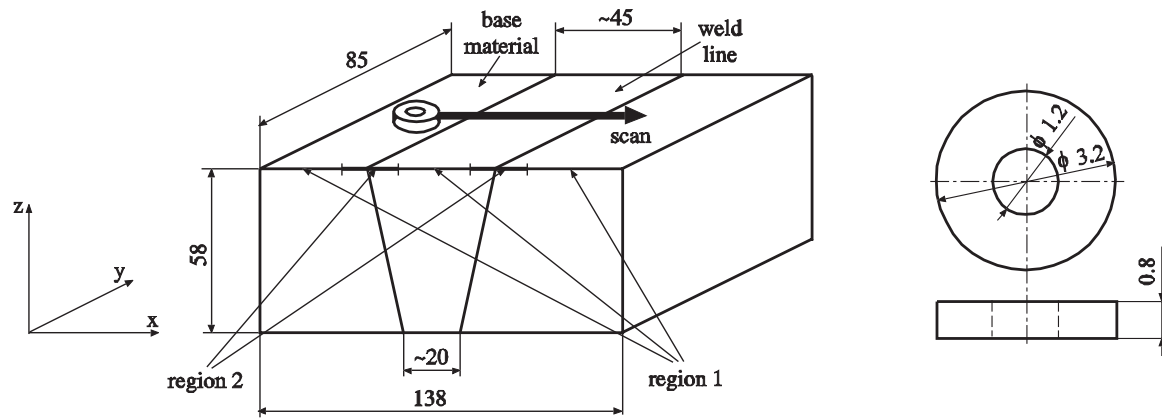
Fig. 2 Configuration and dimensions of the specimen and the pancake probe

ing thickness. The ECT is widely employed for an examination of the material properties during manufacturing process as well.

3. Measurement of the conductivity using ECT

This section deals with one of practical applications of the ECT; a measurement of conductivity is concerned here.

A welded specimen, shown in Fig. 2, is inspected in the study and its conductivity is estimated based on the measured values. The specimen base material is Alloy 600. The material is frequently used in structural components of nuclear power plants where the ECT is applied for non-destructive testing. The electromagnetic parameters, i.e. conductivity and relative permeability, of the base material are generally known. However, one of basic elements in such components is weld. The conductivity variation in the weld

is unknown while the relative permeability is the same as the one of the base material, i.e. $\mu_r = 1$. To be able to deal with such configuration in numerical simulations using the finite element method, a numerical model of the specimen with known parameters has to be built.

A circular coil, so called self-inductance absolute pancake probe, shown in Fig. 2, is used for this study. The probe scanned over the surface of the specimen as depicted in Fig. 2 across the weld line. A professional ECT instrument ASWAN was used to drive the probe and at the same time to pick-up the signal. The length of the scanning line was 90 mm and the probe moved with a lift-off of 0.25 mm. The signals for three frequencies of 200, 300 and 400 kHz were gained at the same time and they were stored in a PC for further analyses. The real part and the imaginary part of the detected signal for the frequency of 200 kHz are shown in Fig. 3.

a)

b)
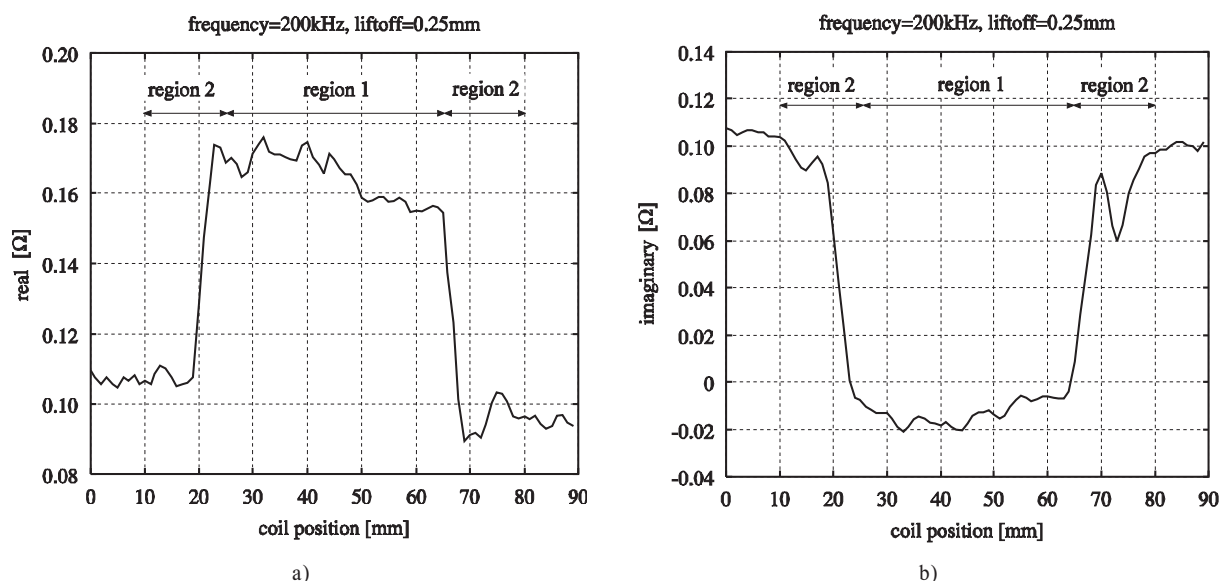
Fig. 3 Detected signal across the weld line: (a) real part, (b) imaginary part.

Fig. 4 The reconstructed profile of conductivity.

Fig. 5 Lissajous plot, comparison between the measured
and simulated signals.

Two assumptions are made to reconstruct the conductivity variation across the weld line:

- The surface of welded specimen is divided into two regions. The first (Fig. 2 - region 1, part of the base material, middle part of the weld) is quasi stable one, where the signal variation is small. The second, transient one (Fig. 2 - region 2) covers a heat affected zone and the boundary of the weld, where the signal variation is large.
- The conductivity is supposed to vary just in one direction perpendicular to the weld line.

According to these assumptions, two different prediction methods have been proposed for the two regions separately [13]. The conductivity distribution along the quasi stable regions is estimated based on the relationships derived from a uniform model. It was proved that such method can deal also with no uniform distribution of the conductivity if the conductivity variation is limited. A neural network approach is utilized to tackle the conductivity profile recognition 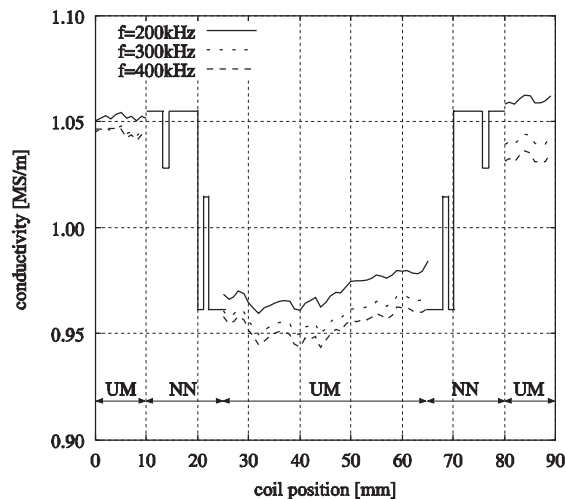along the transient regions. More description about the methods can be found in [13]. All the input data for both the approaches were acquired by numerical simulations using the finite element method.

The reconstructed profile of conductivity across the weld line is shown in Fig. 4. The conductivity in the quasi stable regions (region 1) was estimated based on the uniform model (UM) for all the three frequencies. As it can be seen the weld features the conductivity that is by approximately 7–8 % lower than the one of the base metal. In the transient regions (region 2), the conductivity profile was estimated by using the neural network (NN) for

a frequency of 200 kHz. The conductivity changes sharply at the border of the weld line.

To prove the results of the conductivity profile reconstruction a finite element model of the target with taking into account the estimated profile of conductivity was built and the probe signal under the same conditions as the one used in the experiment was simulated. Both the signals, i.e. experimental and simulated ones, are shown in Fig. 5. The numerical results well coincide with the measured ones.

Conclusion

The importance of the non-destructive testing (NDT) of materials was emphasized in the paper. Different NDT methods were described focusing mainly on utilization of the eddy current phenomena in the non-destructive evaluation of conductive materials. The basic principle of the method was explained and possible application areas of its utilization were shown. The welded structure made of Alloy 600 was inspected by means of the eddy current NDT. The conductivity profile in the base material as well as in the weld was reconstructed from the measured data. It was found out that the conductivity of the weld is approximately by 8 % lower than the one of the base material. The numerical simulations of the signal using the finite element method based on the reconstructed profile of conductivity were presented. The comparison of the measured and simulated signals confirmed the validity of the gained results.

References

[1] ČÁPOVÁ, K., ČÁP, I.: *Electroacoustic Method of Thin Surface Layer Investigation,* Advanced Computational Electromagnetics and Mechanics 9, IOS Press Ohmsha, 1995, ISSN 1383-7281, pp. 292–300.

[2] ČÁPOVÁ, K., ČÁP, I.: *Acoustically Excited Electromagnetic Wave in Metal.* Studies in Applied Electromagnetics and Mechanics 13. IOS Press Ohmsha (Amsterdam, Berlin, Oxford, Tokyo, Washington D.C), 1998, ISSN 1383-7281, pp. 811–814.

[3] ČÁPOVÁ, K., ČÁP, I.: *Material Anisotropy Investigation Using Anomalous Electromagnetic Generation of Acoustic Wave.* Electromagnetic, Studies in Applied Electromagnetics and Mechanics 14, IOS Press Ohmsha (Amsterdam, Berlin, Oxford, Tokyo, Washington D.C.), 1998, ISSN 1383-7281, pp. 74–81.

[4] ČÁPOVÁ, K., ČÁP, I., FAKTOROVÁ, D.: *Special Problems of Material Non-destructive Testing by Electromagnetic Acoustic Transducer.* JSAEM Studies in Applied Electromagnetics and Mechanics, 9, 2001, Tokyo Japan, pp. 541–542.

[5] ČÁPOVÁ, K., ČÁP, I., FAKTOROVÁ, D.: *Special Problems of Electromagnetic-acoustic Transducer for Material Non-destructive Testing,* International Journal of Applied Electromagnetics and Mechanics,15, 2002, IOS Press, pp. 73–77.

[6] MAREK, T., FAKTOROVÁ, D., ČÁPOVÁ, K.: *The Eddy Current Method using in Nondestructive Testing,* In proceedings of Advanced Methods in Theory of Electrical Engineering. Plzeň, Czech Republic, Sept. 2005, ISBN 80-7043-392-2, pp. C13–C18.

[7] http://www.un.org/esa/sustdev (accessed on 2005/09/14).

[8] http://www.ndt.net/article/ecndt98/aero/028/028.htm (accessed on 2005/09/14).

[9] http://www.ndt.net/article/pacndt98/18/18.htm (accessed on 2005/09/15).

[10] http://www.ndt.net/article/wcndt00/papers/idn345/idn345.htm (accessed on 2005/09/15).

[11] http://www.ndt-ed.org/EducationResources/CommunityCollege/communitycollege.htm (accessed on 2005/09/16).

[12] AULD, B. A. AND MOULDER, J. C.: *Review of Advances in Quantitative Eddy Current Nondestructive Evaluation,* Journal of Nondestructive Evaluation, March 1999, Vol. 18, No. 1, Plenum Press, New York and London, ISSN 0195-9298, pp. 3–36.

[13] JANOUSEK, L. Et Al.: *Recognition of INCONEL Weld Conductivity Variation by means of eddy current testing,* Studies in Applied Electromagnetics and Mechanics, Vol. 24, 2004, IOS Press, ISSN 1383-7281, pp. 286–293.

Branislav Dobrucký – Pavol Špánik – Róbert Šul *

IMPROVEMENT OF POWER ELECTRONIC STRUCTURE CHARACTERISTICS USING SiC TECHNOLOGY – OVERVIEW

This paper is dedicated to the recent unprecedented boom of SiC electronic technology. The contribution deals with a brief survey of those properties. In particular, the differences (both good and bad) between SiC electronics technology and well-known silicon VLSI technology are highlighted. Projected performance benefits of SiC electronics are given for several large-scale applications at the end of the contribution. The basic properties of SiC material were discussed already at the beginning of 1980's, also in our work place [1].

1. Introduction

Silicon carbide (SiC) based semiconductor electronic devices and circuits are presently being developed for the use in high-temperature, high-power, and/or high-radiation conditions under which conventional semiconductors cannot adequately perform. Silicon carbide's ability to function under such extreme conditions is expected to enable significant improvements to a far-ranging variety of applications and systems. These range from greatly improved high-voltage switching for energy savings in public electric power distribution and electric motor drives to more powerful microwave electronics for radar and communications to sensors and controls for cleaner-burning more fuel-efficient jet aircraft and automobile engines. In the particular area of power devices, theoretical appraisals have indicated that SiC power MOSFET's and diode rectifiers would operate over higher voltage and temperature ranges, have superior switching characteristics, and yet have die sizes nearly 20 times smaller than correspondingly rated silicon-based devices. However, these tremendous theoretical advantages have yet to be realized in experimental SiC devices, primarily due to the fact that SiC's relatively immature crystal growth and device fabrication technologies are not yet sufficiently developed to the degree required for reliable incorporation into most electronic systems. The widely spread usage of power semiconductors manufactured of SiC is one of the most promising developments at this market today. Because of the outstanding performance of this new material high voltage blocking active switches are under investigation [1], [7], [11].

This paper briefly surveys the SiC semiconductor electronics technology. In particular, the differences (both good and bad) between SiC electronics technology and well-known silicon VLSI technology are highlighted. Projected performance benefits of SiC electronics are highlighted for several large-scale applications. Key crystal growth and device-fabrication issues that presently limit the performance and capability of high temperature and/or high power SiC electronics are identified.

2. SiC Material Fundamental Properties

SiC is a material with outstanding properties for power semiconductor application. Beside research activities including different power semiconductor switch types, unipolar JFET devices for blocking voltage of more than 1200V are applicable as samples promising switching loss reduction above all [11].

In comparison with a similar table in [1] one can see that, the new material 4H-SiC with energy bandgap 3.2 eV has been developed and is mostly used in applications (see below in chapters 4 and 5).

The wide bandgap energy and low intrinsic carrier concentration of SiC allow SiC to maintain semiconductor behavior at much higher temperatures than silicon, which in turn permits SiC semiconductor device functionality at much higher temperatures than silicon. As discussed in basic semiconductor textbooks [1], semiconductor electronic devices function in the temperature range where intrinsic carriers are negligible so that conductivity is controlled by intentionally introduced dopant impurities. Furthermore, the intrinsic carrier concentration ni is a fundamental prefactor to well-known equations governing undesired junction reverse-bias leakage currents [7].

As temperature increases, intrinsic carriers increase exponentially so that undesired leakage currents grow unacceptably large, and eventually at still higher temperatures, the semiconductor device operation is overcome by uncontrolled conductivity as intrinsic carriers exceed intentional device dopings. Depending upon a specific device design, the intrinsic carrier concentration of silicon generally confines silicon device operation to junction temperatures less than 300 °C. SiC's much smaller intrinsic carrier concentration theoretically permits device operation at junction temperatures exceeding 800 °C, and 600 °C SiC device operation has been experimentally demonstrated on a variety of SiC devices.

* B. Dobrucký, P. Špánik, R. Šul
Faculty of Electrical Engineering, Dept. of Mechatronics and Electronics, University of Zilina,
E-mail: branislav.dobrucky@fel.utc.sk, pavol.spanik@fel.utc.sk, robert.sul@fel.utc.sk

Comparison of Selected Important Semiconductor of Major SiC Polytypes with Silicon and GaAs [7].   Tab. 1

Property	Silicon	GaAs	4H-SiC	6H-SiC	3C-SiC
Bandgap [eV]	1.1	1.42	3.2	3.0	2.3
Relative Dielectric Constant	11.9	13.1	9.7	9.7	9.7
Breakdown Field $ND = 10^{17}$ cm^{-3} [MV/cm]	0.6	0.6	//c-axis: 3.0 //c-axis: 3.2	| c-axis: > 1	>1.5
Thermal Conductivity [W/cmK]	1.5	0.5	3 – 5	3 – 5	3 – 5
Intrisic Carrier Concentration [cm^{-3}]	1010	1.8 x 106	$\sim 10^{-7}$	$\sim 10^{-5}$	~ 10
Electron Mobility @ $ND = 10^{16}$ cm^{-3} [cm^{-2}/Vs]	1200	6500	//c-axis: 800 | c-axis: 800	//c-axis: 60 | c-axis: 400	750
Electron Mobility @ $NA = 10^{16}$ cm^{-3} [cm^{-2}/Vs]	420	320	115	90	40
Saturated Electron Velocity [10^{17} cm/s]	1.0	1.2	2	2	2.5
Donor Dopants & Shallowest Ionization Energy [meV]	P: 45 As: 54	Si: 5.8	P: 45 As: 80	P: 85 As: 80	N: 50
Acceptor Dopants & Shallowest Ionization Energy [meV]	B: 45	Be, Mg, C: 28	Al: 200 B: 300	Al: 200 B: 300	Al: 270

The structure of 6H-SiC new material is shown in Fig. 1.
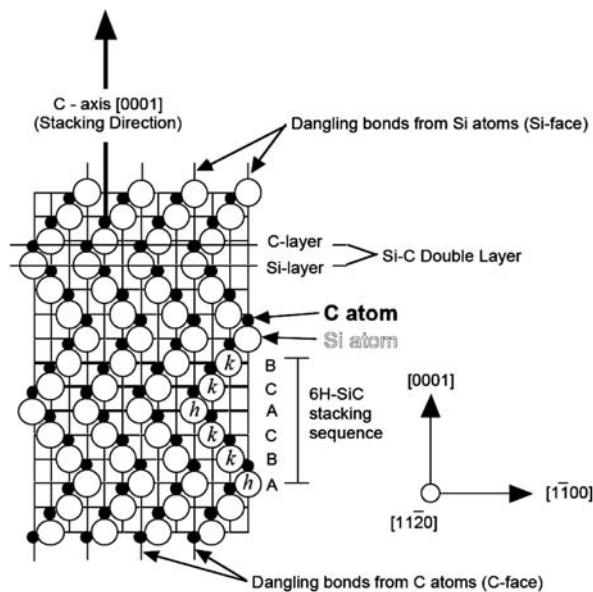
Fig. 1 Schematic cross-section [(1120) plane]
of the 6H-SiC polytype [7]

3. Comparison of conduction characteristics of Si and SiC

While SiC's smaller on-resistance and faster switching helps minimize energy loss and heat generation, SiC's higher thermal conductivity enables more efficient removal of waste heat energy from the active device (see Fig. 2). As heat energy radiation efficiency increases greatly with an increasing temperature difference between the device and the cooling ambient, SiC's ability to operate at high junction temperatures permits much more efficient cooling to take place, so that heatsinks and other device-cooling hardware (i.e., fan cooling, liquid cooling, air conditioning, etc.) typically needed to keep high-power devices from overheating can be made much smaller or even eliminated.
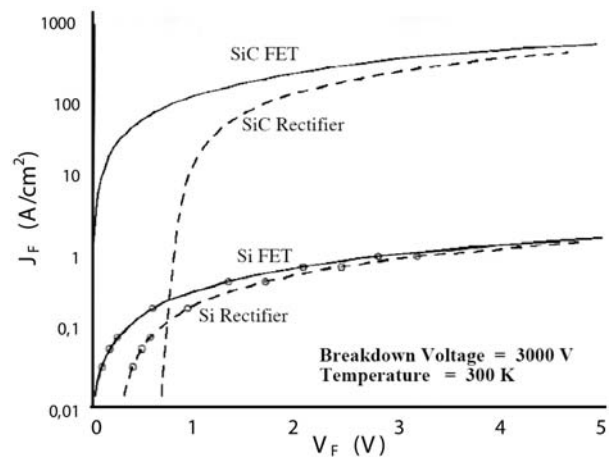
Fig. 2 Simulation experiment for forward conduction characteristics
of ideal Si and SiC 3000 V

While so far discussions have been focused on high-power switching for power conversion [10], many of the same arguments can be applied to devices used to generate and amplify RF signals used in radar and communications applications. In particular, the high breakdown voltage and high thermal conductivity coupled with high carrier saturation velocity allow SiC microwave devices to handle much higher power densities than their silicon or GaAs RF counterparts, despite SiC's disadvantage in low-field carrier mobility.

4. Advantages of SiC structure compared with Si material

As mentioned in Tab. 1, SiC is a wide-bandgap semiconductor, and this property of SiC is expected to yield greatly superior power electronics devices once processing and fabrication issues with this material are solved. Some of the advantages of SiC compared with Si based power devices are as follows:

- SiC-based power devices have higher breakdown voltages (5 to 30 times higher than those of Si) because of their higher electric breakdown field.
- SiC devices are thinner, and they have lower on-resistances. The substantially higher breakdownvoltage for SiC allows higher concentrations of doping and consequently a lower series resistance. For lowbreakdown voltage devices (∼ 50 V), SiC unipolar device on-resistances are around 100 times less; and at higher breakdown voltages (∼ 5000 V), they are up to 300 times less. With lower R_{on}, SiC unipolar power devices have lower conduction losses and therefore higher overall efficiency.
- SiC has a higher thermal conductivity and thus a lower junction-to-case thermal resistance, $R_{th\text{-}jc}$. This means heat is more easily conducted away from the device junction, and thus the device temperature increase is slower.
- SiC can operate at high temperatures because of its wider bandgap. SiC device operation at up to 600 °C is mentioned in the literature. Most Si devices, on the other hand, can operate at a maximum junction temperature of only 180 °C.
- Forward and reverse characteristics of SiC power devices vary only slightly with temperature and time; therefore, SiC devices are more reliable.
- SiC-based devices have excellent reverse recovery characteristics. With less reverse recovery current, the switching losses and electromagnetic interference (EMI) are reduced and there is less or no need for snubbers.
- SiC is extremely radiation hard; i.e., radiation does not degrade the electronic properties of SiC. [8]

5. Possibilities of application of SiC materials in power electronic systems

The structure of SiC Vertical Junction Field Effect Transistor is given in Fig. 3. Properties of this structure are as follows:
- Very high switchin speed
- High T capability (PN-isolation)
- Fast & robust PN body diode
- Volume mobility in the channel
- Doping: channel > drift region
- Suitable up to 3 – 4 kV
- Lowest R_{on} (today)
- No need for an external freewheeling diode

Cascode connection – basic connection V-JFET transistor (Fig. 4)

- 80 mΩ ON-resistance (25 °C) includes low voltage Si-MOSFET
- High short circuit capability
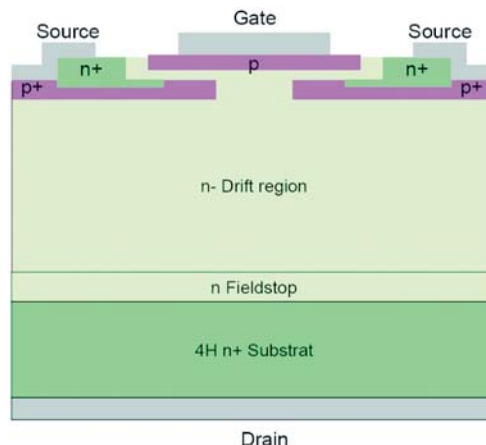
Fig. 3 Structure of SiC V-JFET

- Power almost totally on SiC V-JFET
- High T capability

Schematic diagram of the SiC Schottky diode structure, showing the field oxide, the overlapping metal electrode, and the epi-layer drift region (Fig. 5).
- Low-switch losses
- Breakdown voltages of 1000 to 1100 V
- High-Temperature Performance (over 300 °C)

Main applications:
- Power electronics
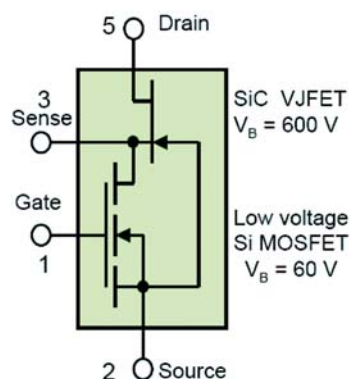
Fig. 4 Cascode SiC V-JFET + MOS FET
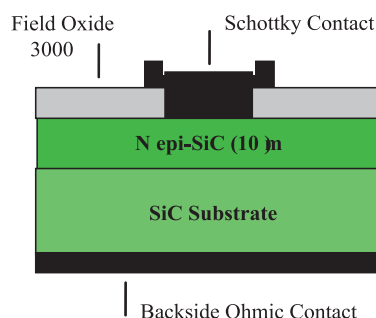
Fig. 5 Structure of SiC Schottky diode

Power supplies
Power converters
PFC
UPS
- Transmission and Distribution
Power active filters
FACTs
- Production of electric energy
Photovoltaic systems
Marine applications
Wind-power plant
- Motor drives
AC, DC drives
SRM, SMPM drives
- Automotive
- Power amplifiers
- Defence,
- Aviation,
- Space program
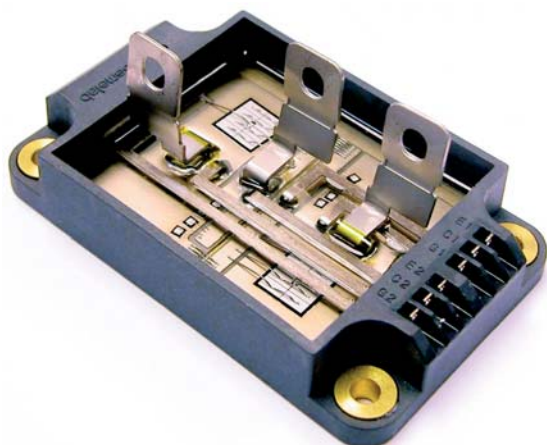
Fig. 6 SEMLab prototype 1200 V hybrid Si IGBT/SiC Schottky diode module [2]

Companies developing SiC devices:
- Diodes (Schottky/PIN) – Cree, Infineon/SiCED, Dynex, Eco-Tron, GF, Mitsubishi,
Rohm, Semisouth, Int. Rectifier, Rockwell, STMicroelectronics ...

Fig. 7 2004 – 2009 World market for SiC devices

- Transistors (JFET/SIT) – Northrop, Cree, Infineon/SiCED, Semisouth, Rockwell,
Hitachi, Intrisic, Toshiba, Fairchild, Mitsubishi, Rohm, Philips, Nippondenso ...
- Thyristors – Cree, GE

6. Conclusions

The new possibilities and characteristics of the SiC structure are discussed and reported in the paper.

The new survey [17] forecasts that the world market for Schottky diodes and power transistors will grow from $13 million in 2004 to over $53 million in 2009. Schottky diodes, supplied by US Cree Company and by Infineon in Europe, will penetrate the microelectronics market at a much higher rate than transistors, which are less mature. Rockwell Scientific and Cree supply SiC MOSFETs, and another 15 companies, mostly major chip manufacturers, are working on further development of these transistors.

References

[1] DOBRUCKÝ, B., RÁČEK, V., ŠPÁNIK, P., GUBRIC, R.: *Power Semiconductors Structures* (in Slovak), EDIS Editor Zilina (SK),1995

[2] LOCATELLI, M. L., GAMAL, S. H., CHANTE, J. P.: *Semiconductor Material for High Temperature Power Devices*, EPE Journal (4) 1994, No. 1, pp. 43–46

[3] GRECKI, M., NAPIERALSKI, A.: *Static Induction Transistor – A New High Speed Power Device.* In: Proc. PEMC '94, Warsaw, Sept. 1994, Vol. 2, pp. 836–841

[4] JANUSZEWSKY, S.: *Power Semiconductors Devices- State of Art & Recent Trends.* In. Proc. PEMC '94, Warsaw, Sept. 1994, Vol. 2, pp. 861–866

[5] HEUMANN , K.: *Trends in Semiconductor Devices and Impact on Power Electronics.* In Proc. PEMC'94, Warsaw, Sept. 1994, Vol.2, pp. 1288–1299

[6] BENDA, V.: *Power Semiconductors and Integrated Structures.* ČVUT Editor, Prague (CZ), 1994

[7] NEUDECK, P. G.: *SiC Technology,* NASA Lewis Research Center, Cleveland USA, 1998,

[8] TOLBERT, L. M., OZPINECI, B., ISLAM, S. K., PENG, F. Z.: *Impact of SiC Power Electronic Devices for Hybrid Electric Vehicles,* SAE 2002 Transactions, Journal of Passenger Cars: Electronic and Electrical Systems, 2003, pp. 765–771

[9] STEPHANI, D.: *The Industrial Utilization of SiC Power Devices – Aspects and Prospects,* Lecture given at the Workshop on Future Electron Devices (FED), Yokohama (JP), March 2003

[10] STEPHANI, D.: *Today's and tomorrow's industrial utilization of silicon carbide semiconductor power devices,* Revue de l'Électricité et de l'Électronique, Feb 2004, pp. 23–24

[11] DOMES, D., HOFMANN, W., LUTZ, J.: *A First Loss Evaluation using a vertical SiC-JFET and a Conventional Si-IGBT in the Bidirectional Matrix Converter Switch Topology*, of EPE'05 Conf., Dresden (DE), Sept. 2005, (CD-ROM)

[12] www.semlab.com

[13] www.infineon.com

[14] http://nina.ecse.rpi.edu/shur/SiC

[15] www.iem.ing.tu-bs.de/paper/2004/kohi_04.htm

[16] www.siced.de

[17] www.wtc-consult.de

M. Vojs – M. Veselý *

DIAMOND AND DLC LAYERS FOR A WIDE RANGE OF APLICATIONS

Summary: Diamond and diamond-like carbon (DLC) layers are nowadays of increasing importance for electrical and mechanical applications. In our laboratory we grow diamond on different substrates (Si, WC-Co) using Hot Filament Chemical Vapor Deposition (HF CVD) method improved by double biasing and DLC layers using pulsed arc system again on different substrates (Si, Ni, glass, Ti-6Al-4V, steel, WC-Co). Growth parameters facilitate to control crystallinity of diamond layers from microcrystalline to nanocrystalline type. Mechanical, electrical and optical parameters are possible to change using doping with hydrogen, nitrogen, or oxygen. The goal of this article is to summarize recent results achieved in our laboratory related to applications of diamond and DLC layers for their use in sensors of hard metal in water and medical implantable joints.

1. Introduction

Carbon is the sixth most abundant element in the universe. In addition, carbon is a very special element because carbon is your body, food you eat, clothes you wear, cosmetics you use and gasoline that fuels your car. Carbon, discovered in prehistory was known to the ancients, who manufactured it by burning organic material for charcoal production. In Fig. 1 there are four popular allotropes of carbon: amorphous carbon, graphite, diamond and fullerene (nanotubes) [1].
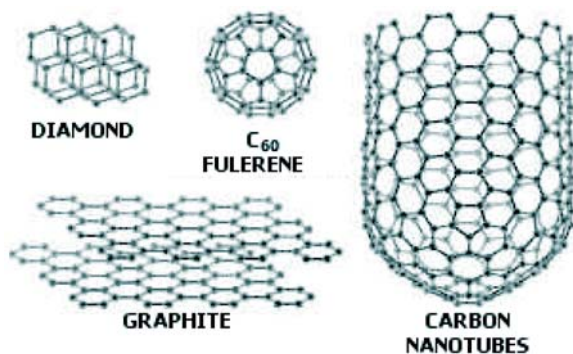
Fig. 1 Carbon Allotropes: Diamond, Buckminster fullerene, Carbon nanotube, and Graphite

Diamond and DLC have many excellent electrical, chemical, mechanical and biological properties [2]. Diamond is the hardest material known, it is extremely chemically inert and biologically compatible.

Electrical properties of diamond are: the highest electrical breakdown voltage, the highest thermal conductivity and the widest electromagnetic radiation transparency range of any material, as well as wide bandgap and high carrier mobilities. As an illustration of the excellent properties of diamond, Fig. 2 compares various wide-gap materials in terms of carrier mobility and thermal management properties, represented by surface area of the plotted circles. Recent progress in chemical vapor deposition (CVD) diamond technology has enabled the preparation of high-quality n-type CVD diamond layers using phosphorus as an n-type dopant and boron, nitrogen, hydrogen as p-type dopants. CVD diamond can therefore be considered as a new interesting conventional wide-gap semiconducting material having both n-type and p-type conductivity, which makes it attractive for numerous applications in high-temperature, high-voltage and high-frequency devices [3].
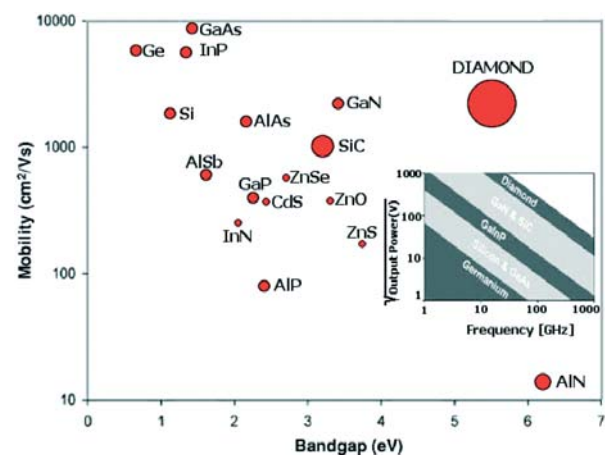
Fig. 2 Comparison of mobility materials together with thermal conductivity as represented by the surface area of the circles. The inset shows predicted performances, expressed as the square root of the output power, for high-frequency applications by using various semiconducting materials.

* M. Vojs, M. Veselý
Slovak University of Technology, Faculty of Electrical Engineering and Information Technology, Ilkovičova 3, 812 19 Bratislava, Slovak Republic,
Tel: +421 2 602 91 366; E-mail: marian.vojs@stuba.sk

The electrochemical approach is attractive because of sensitivity and dynamic range, portability and ease of application. Diamond and DLC is an attractive alternative electrode for electroanalysis on account of the reproducibility and chemical inertness, low background currents, and wide working potential window which this material exhibits in electrochemistry. One of the applications of diamond and DLC, carbon nitride CN_x, is for fast detection and determination of trace metals in solutions. Major importance lies in electrochemical analysis, where single or multiple heavy metals-containing systems are invariably encountered. Electrochemical stripping voltammetry methods offer a simple, quick and cheap way of detecting trace metals such as (Pb, Cu, Cd, Mn, Ag) in water [4, 5].

Biomaterials are an important aspect in the development of biomedical devices and implants and this area of research has been expanding rapidly over the last 50 years. It is the surface of a biomaterial which first contacts with the living tissue when biomaterial is placed in the body. Titanium alloy (Ti–6Al–4V) is well established as a primary metallic biomaterial for orthopedic implants. However, the host response to Ti–6Al–4V is not always favorable, whereby a fibrous layer may form at the skeletal tissue-device interface, resulting in implant failure. Therefore, there is a need to develop novel micro-engineered surfaces to provide better biological outcomes. DLC and carbon nitride CN_x are excellent candidates for use as biocompatible coatings on biomedical implants, which are due to not only their excellent properties but also their chemical composition containing only carbon, hydrogen and nitrogen, which are biologically compatible elements [6].

2. Experimental

Diamond deposition

Deposition of polycrystalline diamond (PCD) over surface was carried out in the double bias enhanced HF CVD reactor described previously [7]. The gas phase was a mixture of 2% CH_4 in H_2, the total pressure in the reactor was 3 000 Pa and flow rates were 6:300 sccm. Gases were activated by 5 tungsten filaments 0.7 mm thick, 120 mm long, heated to 2100 °C. The substrate temperature was maintained at 750 °C (measured by a K-type thermocouple mounted in 80 mm a molybdenum substrate holder with filament-substrate distance of 10 mm). The process of a PCD layer deposition was divided into three stages. The stage *Nucleation* was performed at negative substrate bias of 170 V for 30 min in 2 % gas mixture. The stage *Growth* was enhanced only by dc plasma formed in the region between heated filaments and the above-situated grid (positive grid bias of 100 V with respect to filaments) in 2 % gas mixture for 120 min. The stage *Termination*, methane source was switched off, and for 180 min still termination process took place in H_2 plasma onto polycrystalline diamond for change of electrical properties.

DLC deposition

DLCs were deposited in a UVNIPA-1-001 vacuum system with three sources (gas ion source for cleaning, electric arc source for non-magnetic metal sputtering and pulse arc carbon source for DLC deposition). The pulse sputtering of graphite target is a possible setup in the range of (f = 1, 2, 3, 5, 10, 15, 20 and 30 Hz).

Samples entering were sputtered in one vacuum cycle. All of substrates (microelectrode arrays and medical hips) were cleaned for 10 min with Ar ions. After cleaning the hip was covered with 50 nm Ti interlayer for better adhesion of DLCs and for heated up bulk substrate to temperature about 200 °C. For deposition of MEA (the technological process is described later) is this step missing, but a Ti interlayer is not needed. Consequently the DLC layer ($\sim$ 150 °C) was deposited at low deposition temperature. Nitrogen with 30 sccm flow rate was added during the DLC deposition into a working chamber. The substrates were planetary rotating through all the deposition steps for homogeneous deposition.

MicroElectrode Array

Fig. 3 shows all the technological steps of manufacturing a 1 × 1 mm microelectrode array (MEA) structure consisting of 50 625 microdiscs with 3 μm in diameter and distance of 20 μm between microdiscs on Si with low resistivity (0.008 – 0.024 Ωcm).
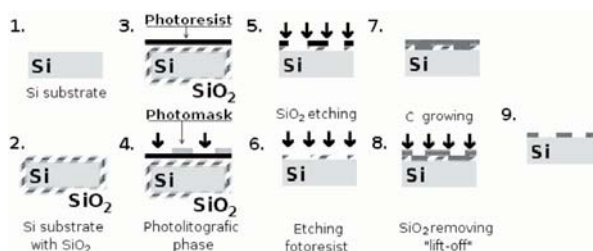
Fig. 3 Technological process of manufacturing a microelectrode array

The 1-st step was to clean the substrate in ultrasonic acetone bath. Then, the 2-nd step, about 300 nm thick SiO_2 layer was created during 6 hours with the substrate at 1200 °C in dry O_2 atmosphere in a furnace. During the standard photolithographic process, as steps 3 to 6, MEA structure in SiO_2 layer was produced through a lithographic mask. After MEA preparation there are two ways for deposition of carbon layers (diamond or DLC), the 7-th step.

After PCD or CN_x deposition the lift off technique is potentially used for SiO_2 removal from the substrate. The overgrown diamond or DLC layer is removed if necessary, the 8-th step. At this stage of the overall process we have a completely prepared MEA for electrochemical measurement, the 9-th step.

Hip replacement joints

Standard biocompatible alloy of Ti–6Al–4V supplied by prof. Zitnansky from the Faculty of Mechanical Engineering of the Slovak University of Technology in Bratislava was used as the substrate. The substrate face corresponds to special human hip replacement joints with the surface roughness after rough machining of about R_a = 10 μm, were 10 min. rinsed in acetone in an ultrasonic bath and than washed in deionized water.

3. Results and discussion

We can see in Fig. 4 SEM images of a deposited layer surface after the complete technological process. In Fig. 4 a) MEA polycrystalline diamond structure, in Fig. 4 b) CN_x layer structure are displayed, both deposited on Si. In case of polycrystalline diamond, the diamond layer was deposited on a freshly etched silicon surface. The areas which act as working electrodes (microdiscs) were defined photolithographically. Finally, the insulating resist mask layer was hardbaked to improve its adhesion. The behavior of a bare electrode array was characterized by cyclic voltammetry at the scan rate of 50 mV/s in 0.1 mol/l KNO_3 (acidified by HNO_3 to pH 2.5). Differential pulse anodic stripping voltammetry was used for determination of Pb^{2+} ions in solution on bare CN_x and polycrystalline electrodes. A preconcentration step was carried out at -700 mV vs Ag/AgCl/Cl$^-$ for 180 s. Lead ions were co-deposited with Hg^{2+} ions (1×10^{-3} mol/l) in 0.1 mol/l KNO_3 (pH 2.5). All the experimental solutions were prepared from chemicals of analytical grade in 18×10^4 Ωm water.
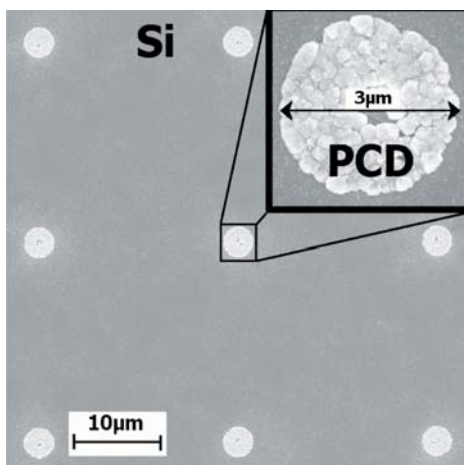
Fig. 4 a) SEM Image of polycrystalline diamond PCD microelectrode array
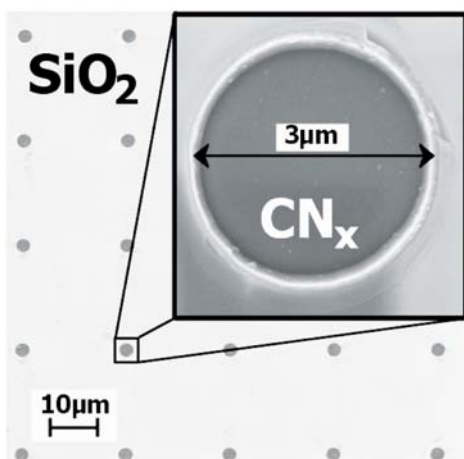
Fig. 4 b) SEM Image of carbon nitride CNx microelectrode array

CN_x microelectrode array for in-situ determination of Pb^{2+} ions was prepared by co-deposition of Pb^{2+} at -700 mV vs. Ag/AgCl/Cl$^-$ in 0.1 mol/l KNO_3 with different content of Pb^{2+} for 180 s preconcentration time under constant magnetic striping. Stripping currents at -566 mV vs. Ag/AgCl/Cl$^-$ from reoxidation of Pb ($Pb^0 \rightarrow Pb^{2+} + 2e$) into the same solution were recorded by DP ASV. The minimum measurable current response to Pb^{2+} concentration on PCD was 1.10^{-4} mol/l, and on CN_x 5×10^{-6} mol/l.

The homogeneity of CNx layer was very high, it can be seen in Fig 5. DLC is in a dense, metastable form of amorphous carbon a–C, or hydrogenated amorphous carbon a–C:H containing a significant number of sp^3 bonds. In other words, DLC consists of amorphous carbon and disordered graphite, and its atomic structure contains mixture of sp^3 and sp^2 sites. The π state of sp^2 controls the electrical properties and sp^3 controls the mechanical properties. Experimentally obtained CN_x films are composed of two phases that have sp^3 and sp^2 bonded structure [8]. Therefore, the concentration of nitrogen in the structure of CN_x coatings is a key factor affecting the coating characteristics, up to now not yet studied.

Fig. 5 Optical image of CNx layer on hip replacement joints

4 . Conclusion

We have demonstrated a very wide range of applications for polycrystalline diamond prepared by the unique HF CVD processing method and for CN_x layer prepared by a pulse arc system.

In an electronic application such as microelectrode array for measurement of heavy metals in water there is a possibility to use an arc system for CNx deposition on a large area substrate with high homogeneity at very low temperature of about 150 °C opposite to 700 °C in HF CVD.

Low deposition temperature opens a new window for many cheaper applications in medicine such as cover layers of hip replacement joints, nails, or cover microscopic glass for research of DNA or any biological tissue growth.

5. Acknowledgement

References

[1] HEIMANN, R. B., EVSVUKOV, S. E., KOGA, Y.: *Carbon allotropes: a suggested classification scheme based on valence orbital hybridization,* Carbon, Volume 35, Issues 10-11, 1997, pp. 1654–1658.

[2] VOJS, M., VESELY, M., REDHAMMER, R., JANIK, J., KADLECIKOVA, M., DANIS, T., MARTON, M., MICHALKA, M., SUTTA, P.: *Double bias HF CVD multilayer diamond films on WC-Co cutting tools*, Diamond & Related Materials 14, 2005, pp. 613–616.

[3] NESLADEK, M.: *Conventional n-type doping in diamond: state of the art and recent progress,* Semicond. Sci. Technol. 20, 2005, R19–R27.

[4] FOORD, J. S., HAO, W., EATON, K.: *Detection of heavy metals in multianalyte solutions using diamond electrodes,* phys. stat. sol. (a) 202, No. 11, 2005, pp. 2116–2121.

[5] LIU, L. X., LIU, E.: *Nitrogenated diamond-like carbon films for metal tracing,* Surface & Coatings Technology 198, 2005, pp. 189–193.

[6] CUI, F. Z., LI, U. D. J.: *A review of investigations on biocompatibility of diamond-like carbon and carbon nitride films*, Surface and Coatings Technology 131, 2000, pp. 481–487.

[7] MALCHER, V., MRSKA, A., KROMKA, A., SATKA, A., JANIK, J.: *Current Applied Physics,* 2, 2002, pp. 201–204.

[8] ROBERTSON, J.: *Pure Appl. Chem. 66,* 1994, pp. 1789–1796.

Libor Hargaš – Miroslav Hrianka – Pavol Špánik *

APPLICATION OF COMMUNICATION SYSTEMS IN BIOMEDICAL ENGINEERING

Picture archiving and communication systems (PACS) in biomedical engineering consist of image and data acquisition, storage, and display subsystems integrated by various digital networks. The standard (DICOM 3) is applicable to a networked or an off-line media environment. It allows development and expansion of PACS system. This Standard has been developed with an emphasis on diagnostic medical imaging as practiced in radiology, cardiology and related disciplines. Also the compression methods suitable for image processing are presented in this article. The compression is often realized by reduction of irrelevance or redundancy. There are described lossless and lossy compression methods which can be used for compression of images in biomedical applications and comparison of these methods based on fidelity criteria.

1. Introduction

Communication is the transport of information between two places, usually by means of some type of medium. A communication standard encompasses detailed specifications of the media, the explicit physical connections, the signal levels and timing, the packaging of the signals, and the high level software required for the transport. A video communication standard describes the characteristics of composite video signals including interlace or progressive scan, frame rate, line and frame retrace times, number of lines per frame, and number of frames per second. In a communication system PACS, the soft copy display is source of video signals; depending on the types of used monitor. These video signals will follow certain standards. At present DICOM 3.0. is standard in a PACS system.

2. Picture Archiving and Communication Systems (PACS)

A picture archiving and communication system (PACS) consists of image and data acquisition, storage, and display subsystems integrated by various digital networks (Fig.1) [1]. Each of PACS modules functioned as an independent island, unable to communicate with other modules. A general multimedia data management system that is easily expandable, flexible, and versatile in its programmability calls for both top-down management to integrate various information systems.

The PACS infrastructure provides the necessary framework for the integration of distributed and heterogeneous imaging systems and makes possible intelligent database management of all related information. The PACS infrastructure consists of a basic skeleton of hardware components (acquisition interfaces, storage devices, host computers, communication networks, and display systems) integrated by standardized, flexible software subsystems for communication, database and storage management, job scheduling, interprocessor communication, and network monitoring.

The PACS infrastructure is physically composed of several classes of computer systems connected by various networks. These include imaging systems, acquisition computers, and the PACS controller with database and archive, and display workstations.

The most troublesome PACS task to date has been the reliable and timely acquisition from an imaging system of images and associated study support text (description of the study, and parameters of acquisition and image processing).

This bottleneck exists mainly because many manufacturers of imaging equipment are not prepared to follow the industry standards developed by, for example, ACR-NEMA and DICOM. To circumvent these difficulties, an acquisition computer can be placed between the imaging system and the rest of the PACS network. The acquisition computer has three primary tasks: it acquires image data from the imaging system, converts the data from the equipment manufacturer's specifications to PACS standard format (header format, byte-ordering, matrix sizes) that is compliant with the proposed ACR-NEMA and DICOM data formats, and forwards the image study to the PACS controller.

PACS display stations should fully use the resources and processing power of the entire PACS network. A station includes communication, database, display, resource management, and processing software.

There are four types of display station: high-resolution monitors, medium resolution stations for conferences, desktop stations, and high-resolution, hard copy print stations.

A basic function of any computer network is to provide an access path by which end users at one geographic location can

* L. Hargaš, M. Hrianka, P. Špánik
University of Žilina, Univerzitná 1, 010 26, Žilina, Slovakia, E-mail: Libor.Hargas@fel.utc.sk, Miroslav.Hrianka@fel.utc.sk, Pavol.Spanik@fel.utc.sk
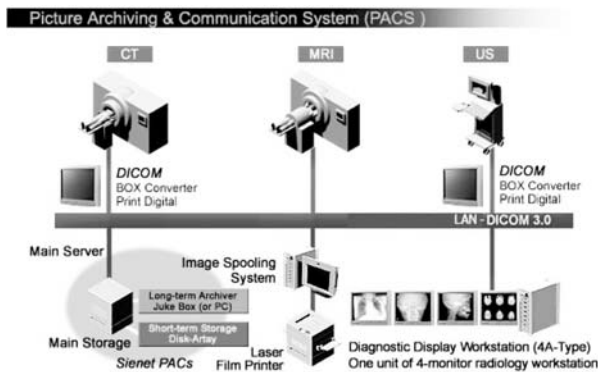
Fig. 1 PACS components

access information (e.g., images and reports) at another location. The most obvious way to characterize a PACS network is to examine the traffic of information between various locations and users. The important networking data needed for system design include location and function of each node, frequency of information passed between any two nodes, cost for transmission between nodes on various speed lines, desired reliability of the communication, and required throughput. The variables in the design include network topology, communication line capacities, and flow assignments.

2.1. Image Acquisition

Automated image acquisition from imaging devices to the PACS controller plays an important role in a PACS infrastructure. The „automatic" part is important because reliance on labor-intensive manual acquisition methods would defeat the purpose of the PACS. Based on existing manufacturers' imaging devices, we categorize the interface methods into five architectural models: sequential chain, direct interface, memory access, shared disk, and interconnected network.

DICOM Standard embodies a number of major enhancements to previous versions of the standard: is applicable to a networked or an off-line media environment; specifies how devices claiming conformance to the Standard react to commands and data being exchanged; is structured as a multi-part document, introduces explicit information objects not only for images and graphics but also for waveforms, reports, printing, etc.

2.2 Goals of the DICOM standard

The DICOM Standard facilitates interoperability of devices claiming conformance. In particular, it:
- Addresses the semantics of Commands and associated data. For devices to interact, there must be standards on how devices are expected to react to Commands and associated data, not just the information which is to be moved between devices;
- Addresses the semantics of file services, file formats and information directories necessary for off-line communication;

- Is explicit in defining the conformance requirements of implementations of the Standard. In particular, a conformance statement must specify enough information to determine the functions for which interoperability can be expected with another device claiming conformance.
- Facilitates operation in a networked environment.
- Is structured to accommodate the introduction of new services, thus facilitating support for future medical imaging applications.
- Makes use of existing international standards wherever applicable, and itself conforms to established documentation guidelines for international standards.

3. Image compression in communication system

Image compression involves reducing the size of image data files, while retaining necessary information. The ratio of the original, uncompressed image file and the compressed file is referred to as the compression ratio. The compression ratio is denoted by [2]:

$$compresion\ ratio = \frac{size_U}{size_C},$$

where $size_U$ – uncompressed file size, $size_C$ – compressed file size.

Compression algorithms are developed by taking advantage of the redundancy that is inherent in image data. Three primary types of redundancy can be found in images: coding, inter pixel, psycho visual redundancy.

If we want to create a successful compression scheme, we must differentiate between data and information. For digital images, data refers to the pixel gray-level values that correspond to the brightness of a pixel at a point in space. Information is an interpretation of the data in a meaningful way. For example, in a binary image that contains text only, the necessary information may only involve the text being readable, whereas for a medical image the necessary information may be every minute detail in the original image.

The compression system model consists of two parts: the compressor and the decompressor. The compressor consists of a preprocessing stage and encoding stage, whereas the decompressor consists of a decoding stage followed by a postprocessing stage. Before encoding, preprocessing is performed to prepare the image for the encoding process, and consists of any number of operations that are application specific. After the compressed file has been decoded, postprocessing can be performed to eliminate some of the potentially undesirable artifacts brought about by the compression process.

3.1 Basic compression technique

Lossless compression methods
Lossless compression methods are necessary in some imaging applications. The most known algorithms are Huffman coding, Run-Length coding, LZW coding (Lempel-Ziv-Welch), arithmetic
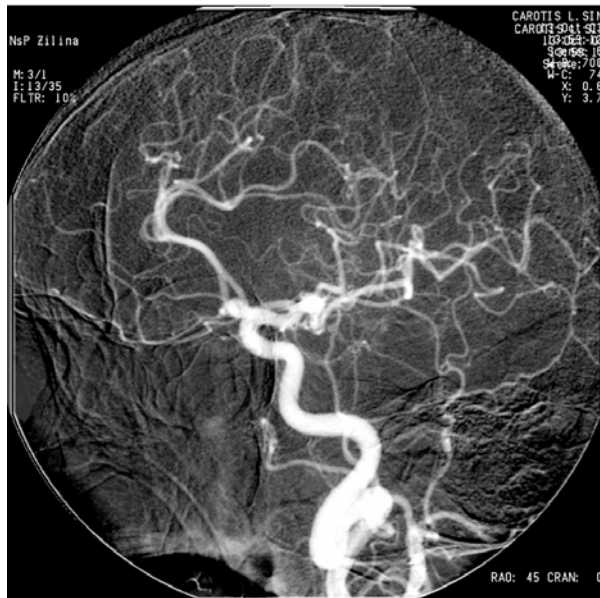
Fig. 2 Original image
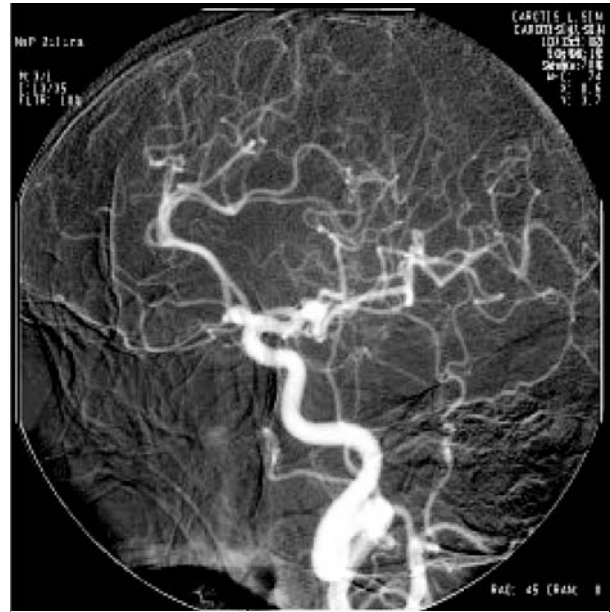
Fig. 3 Predictive BTC compression

coding [2]. In general, the lossless techniques alone provide marginal compression of complex image data, often in the range of only a 10 % reduction in file size. Comparing compression methods are presented by original image Fig. 2 (*Source: Hospital with Policlinic of Žilina*). Many of the lossless techniques were developed for non-image data and, consequently, are not optimal for image compression.

Fig. 4 VQ compression

Lossy compression methods

Lossy compression provides tradeoffs between image quality and degree of compression, which allows the compression algorithm to be customized to the application. With some of the more advanced methods, images can be compressed 10 to 20 times with virtually no visible information loss, and 30 to 50 times with minimal degradation. Many of the methods have adjustable parameters to allow the user to select the desired compression ratio and image fidelity [4]. Block truncation coding (BTC) works by dividing the image into small sub images and then reducing the number of gray levels within each block. This reduction is performed by a quantizer that adapts to the local image statistics. An example is presented in Fig. 3.
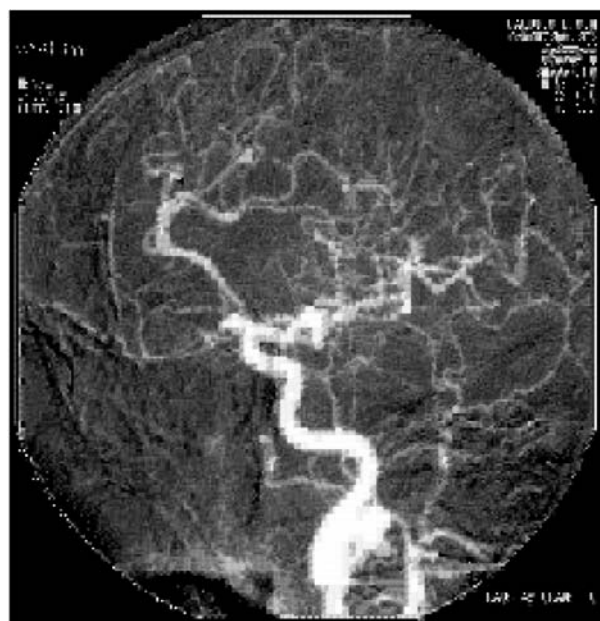
Vector quantization (VQ) is the process of mapping a vector that can have many values to a vector that has a smaller (quantized) number of values. For image compression, the vector corresponds to a small subimage, or block. Vector quantization treats the entire subimage (vector) as a single entity and quantizes it by reducing the total number of bits required to represent the subimage. An example with 3x3 subimage is presented in Fig. 4.

3.2 Fidelity criteria

Fidelity criteria can be divided into two classes: objective fidelity criteria, subjective fidelity criteria. The objective fidelity criteria are borrowed from digital signal processing and information theory and provide us with equations that can be used to measure the amount of error in the reconstructed image. Subjective fidelity criteria require the definition of a qualitative scale to assess image quality. This scale can then be used by human test subjects to determine

image fidelity. The objective criteria, although widely used, are not necessarily correlated with our perception of image quality [1].

Commonly used objective measures are the root-mean-square error e_{RMS}, the root-mean-square signal-to-noise ratio SNR_{RMS}, the peak signal-to-noise ratio SNR_{PEAK}.

$$e_{RMS} = \sqrt{\frac{1}{N^2} \sum_{r=0}^{N-1} \sum_{c=0}^{N-1} [I(r,c) - \hat{I}(r,c)]^2}$$

$$SNR_{RMS} = \sqrt{\frac{\sum_{r=0}^{N-1} \sum_{c=0}^{N-1} [\hat{I}(r,c)]^2}{\sum_{r=0}^{N-1} \sum_{c=0}^{N-1} [I(r,c) - \hat{I}(r,c)]^2}}$$

$$SNR_{PEAK} = 10\log_{10} = \frac{(L-1)^2}{\frac{1}{N^2} \sum_{r=0}^{N-1} \sum_{c=0}^{N-1} [I(r,c) - \hat{I}(r,c)]^2}$$

where $I(r,c)$ is the original image, $\hat{I}(r,c)$ is the decompressed image and $N \times N$ image size.

These objective measures are often used in research because they are easy to generate and seemingly unbiased, but remember that these metrics are not necessarily correlated to our perception of an image.

Subjective testing is performed by creating a database of images to be tested, gathering a group of people that are representatives of the desired population. Subjective fidelity measures can be classified into three categories: impairment, quality and comparison tests [2].

The comparison is done for block truncation coding (BTC) and vector quantization (VQ). In Fig. 5 and Fig. 6 are illustrated lost data, caused by compressions. These images were obtained by comparison of an original image with a compressed image, using function subtraction (contrast is increased for print matter).

4. Conclusion

A PACS module is loosely defined as a self-contained PACS that has some acquisition components: a short-term archive, a database, some display stations, and a communication network linking these components. In practice, the module can function alone, as an individual unit in which the display stations show images from the acquisition components.

There are two categories of preprocessing function. The first is related to the image format - for example, a conversion from the manufacturer's format to DICOM. The second type of preprocessing prepares the image for an optimal viewing at the display station.

Some approaches of image compression methods by the fidelity criteria are presented in these images. These criteria, although widely used, are not necessarily correlated with subjective perception of image quality. Subjective fidelity criteria require the definition of a qualitative scale to assess image quality. This scale can then be used by human test subjects to determine image fidelity.
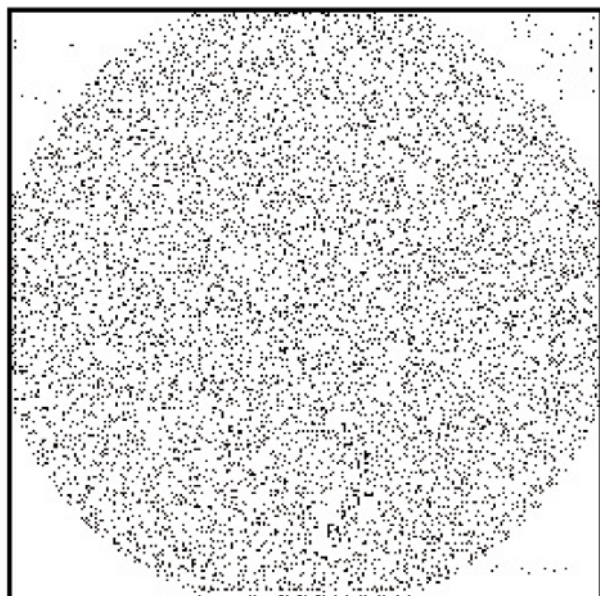
Fig. 5 Difference image Fig. 2 and Fig. 3
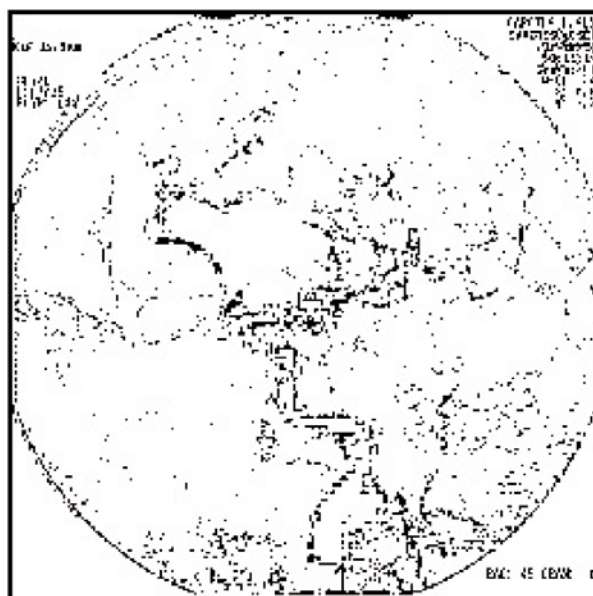
Fig. 6 Difference image Fig. 2 and Fig. 4

References:

[1] HUANG, H. K.: *Picture Archiving and Communication Systems in Biomedical Imaging,* VCH Publishers, Inc., 1996
[2] UMBAUGH, S. E.: *Computer Vision and Image Processing,* Prentice Hall PTR, 1999
[3] CVIP: www.ee.siue.edu/CVIPtools
[4] NEMA National Electrical Manufacturers Association, www.nema.com, *Digital Imaging and Communications in Medicine*, Rosslyn, Virginia, 2003
[5] CASTELMAN, K. R.: *Digital Image Processing*, Prentice Hall, 1996
[6] RUSS, J. C.: *The Image Processing*, CRC Press LLC, 1999

Anna Vojačková *

PROPERTIES OF CARBON NANOTUBES AND THEIR USE IN POTENTIAL APPLICATIONS

Many laboratories in the world are doing research in the field of nanotechnology. Among lot of nanomaterials carbon nanotubes became very popular because of their unique properties which could be used in many applications. But first, lot of problems with their preparation need to be solved.

1. Structure

Carbon nanotubes (CNTs) are very promising material because of their extraordinary properties – electronic, mechanical and optical. These properties are given by the structure of the CNTs. We can imagine a nanotube as a graphite plane rolled up to a cylinder. It can be opened or closed at one or both ends of the cylinder. Each nanotube is characterized by the chiral vector C_h and the chiral angle θ (Fig. 1). The chiral vector: $C_h = na_1 + ma_2$, where a_1, a_2 are the lattice vectors and n, m are integers, is given on the circumference of the nanotube. [1]

There are three types of structures: armchair ($\theta = 45°$, $n = m$), „zig-zag" ($\theta = 0°$, $m = 0$) and chiral ($\theta = 0 – 30°$, $n \neq m$). CNTs are divided into two main groups: Single Wall Carbon Nanotubes (SWCNTs) and Multi Wall Carbon Nanotubes (MWCNTs).
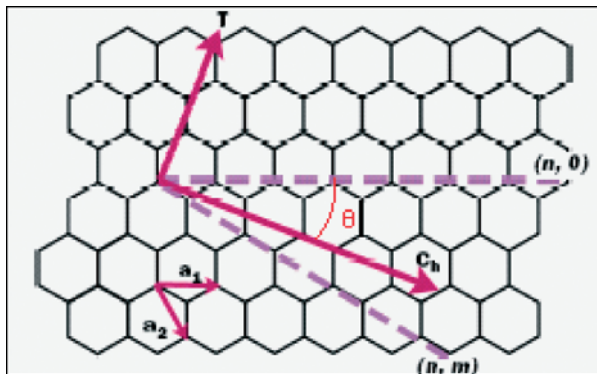
Fig. 1 CNT structure [1]

2. Properties

The most interesting properties of carbon nanotubes and their potential use in some applications are given in Table 1.

Properties of CNTs and their use in potential applications   Table 1

properties	electrical	physical	mechanical
	– field emission – conductivity	– thermally stable – large surface area – cavities	– mechanical strength – elasticity
applications	– electronic nanodevices – emitors for displays – AFM tips – sensors	– gas sensors – hydrogen storage – electrodes for bateries and fuel cells – composit materials	– STM/AFM tips – instruments for nanomanipulation – composit materials

The most important property for the use in the electronic applications is the conductivity of carbon nanotubes. Depending on the structure, they can be either metallic or semiconducting. Because of their small diameter, they represent nearly ideal one-dimensional system. So the nanotubes do not allow the scattering of charge carriers by defects or phonons and they exhibit lower resistivity than conventional systems. Electrical transport in CNTs is supposed to be ballistic, so the energy dissipation in the CNT is minimal and the dissipated power density is lower [2]. CNTs can withstand current densities up to 10^7 A/cm^2 [3]. One of the potential applications is CNTFET, which is an analogue of the silicon MOSFET, where the silicon channel is replaced by a SWCNT. Gold electrodes (source and drain) were fabricated on the SiO$_2$ covered silicon wafer [2]. SWCNT (channel) was then manipulated to bridge the electrodes. The heavily doped wafer with the silicon dioxide served as the gate electrode and gate dielectric. This nanoelectronic device had a lot of disadvantages such as high contact resistance and low on-current. And all transistors, created using one SWCNT, had to be on or off at the same time. These problems were solved by the preparation of top-gated CNTFET and the fabrication of a better metal-CNT contact.

* A. Vojačková
Faculty of Electrical Engineering and Information Technology, Slovak University of Technology, Ilkovičova 3, 812 19 Bratislava, Slovakia
E-mail: anna.vojackova@stuba.sk

Very promising property of carbon nanotubes is their field emission. If voltage is applied to carbon nanotubes in the electric field formed, they emit electrons. This makes nanotubes a very promising material for cold electron emitters. Electron emitters for SEM, TEM, flat displays and cathode ray lamps have to meet some strict criteria (stable emission current, small energy spread). Compared to conventional electron emitters, carbon nanotubes have the best parameters [4]. The next advantage of CNTs field emitters is low voltage needed for field emission. For emission currents of 10^{-7} A applied voltage of 10^2 V is needed [3].

The most interesting mechanical parameter is Young's modulus, which is a measure of material's elastic strength. The modulus is determined by the C–C bonds within the walls. Its value for CNTs is about 1 TPa [3]. Another amazing property is elastic deformation – the deformation disappears when the load, causing this deformation, is removed. This is caused by the ability of carbon atoms in the walls to change their hybridization. An AFM tip with CNT can be fabricated by manually attaching a nanotube to the Si tip or by direct growth of a CNT onto the Si tip. Extremely stable MWCNT tips with small diameters (< 30 nm) were fabricated. The mass production technology of wafer-scale CNT AFM tips was developed [5].

3. Applications

These are just few applications which use the properties of carbon nanotubes. There are many other possible applications such as nanocomposites [6][7], CNTs films for sensor structures [8][9], hydrogen storage medium [10] etc. Most of these applications are under development. The most important step is the efficient preparation of CNTs with the possibility to control their properties with aspect to the desired application.

4. CNTs at FEI STU

At the Department of Microelectronics FEI STU in Bratislava there is a group of researchers trying to prepare arrays of oriented
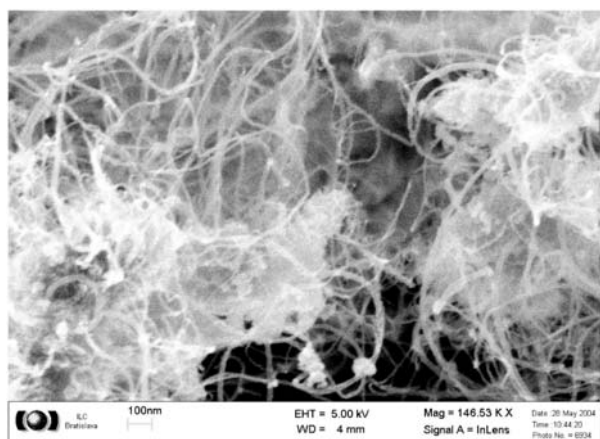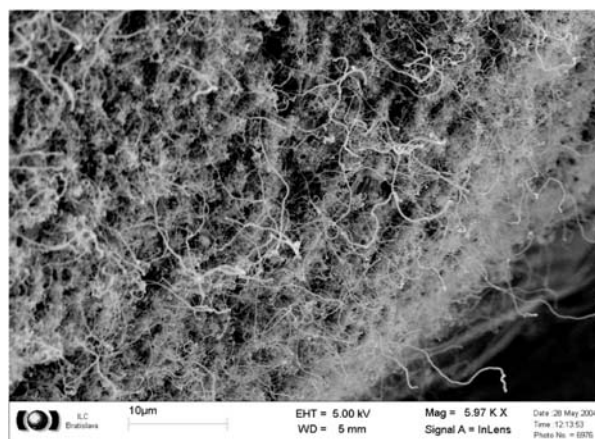
a)   b)

Fig. 2 Carbon nanotubes grown on non-conducting substrates magnified
a) 146 530 x and b) 5 970 x
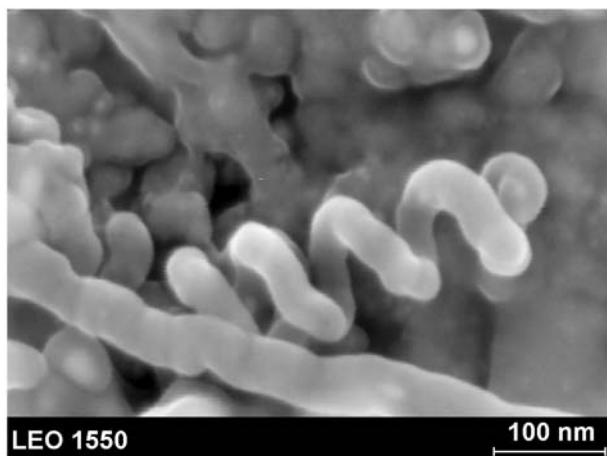
Fig. 3 Carbon nanotubes grown on conducting substrates

carbon nanotubes on various substrates with good emission characteristics. Arrays of non-oriented carbon nanotubes on non-conducting and conducting substrates were prepared (Figs. 2 and 3). On the conducting samples measurements of electron emission were carried out. All the samples were studied using Raman Spec-

troscopy and Scanning Electron Microscopy in cooperation with the International Laser Centre. This work is supported by Grants of the Ministry of Education of the Slovak Republic VEGA 1/3034/06, VEGA 1/2040/05 and VTP 1002/2003.

References:

[1] LERNER, E. J.: *Putting Nanotubes to Work. The Industrial Physicist* [online] December, 1999, Vol. 5, No. 6, 22–25. Available on internet: <http://www.aip.org/tip/INPHFA/vol-5/iss-6/p22.pdf>

[2] AVOURIS, P., APPENZELLER, J.: *Electronics and Optoelectronics with Carbon Nanotubes. The Industrial Physicist* [online] July, 2004, Vol. 10, No. 3, 18–21. Available on internet: <http://www.aip.org/tip/INPHFA/vol-10/iss-3/p18.pdf>

[3] SCHOENEBERGER, CH., FORRÓ, L.: *Multiwall Carbon Nanotubes. Physics World* [online] June, 2000. Available on Internet: <http://physicsweb.org/articles/world/13/6/8>

[4] DE JONGE, N., LAMY, Y., SCHOOTS, K., OOSTERKAMP, T. H.: *High Brightness Electron Beam from a Multi-walled Carbon Nanotube. Nature* [online] November,2002, Vol. 420, 393–395. Available on internet: <http://www.research.philips.com/technologies/light_dev_microsys/carbonnt/ downloads/nature2002_420_393_39.pdf>

[5] NGUYEN, C. V., YE, Q., MEYYAPPAN, M.: *Carbon Nanotube Tips for Scanning Probe Microscopy: Fabrication and High Aspect Ratio Nanometrology. Meas. Sci. Technol.* 16 (2005) 2138–2146. [online] Available on internet: <http://www.iop.org/EJ/S/3/670/ PYt91aqgIfJuoh976 Az3ww/article/0957-0233/16/11/003/mst5_11_003.pdf>

[6] SCHARTEL, B., PÖTSCHKE, P., KNOLL, U., ABDEL-GOAD, M.: *Fire Behaviour of Polyamide 6/Multiwall Carbon Nanotube Nanocomposites.* European Polymer Journal 41 (2005) 1061–1070. [online] Available on internet: <http://www.fibrils.com/PDFs/ P.%20Potschke%20Euro %20Polymer%20Journal%2041(2005)1061.pdf>

[7] ROBEL, I., BUNKER, B. A., KAMAT, P. V.: S*ingle-Walled Carbon Nanotube-CdS Nanocomposites as Light-Harvesting Assemblies: Photoinduced Charge-Transfer Interactions.* Adv. Mater. 17 (2005) 2458–2463. [online] Available on internet: < http://www3.interscience. wiley.com/cgi-bin/fulltext/111090082/PDFSTART>

[8] SOTIROPOULOU, S., CHANIOTAKIS, N. A.: *Carbon Nanotube Array-based Biosensor. Anal Bioanal Chem* 375 (2003) 103–105. [online] Available on internet: < http://lib.store.yahoo.com/ lib/nanolab2000/biosensor.pdf>

[9] PENZA, M., CASSANO, G., AVERSA, P., CUSANO, A., CUTOLO, A., GIORDANO, M., NICOLAIS, L.: *Carbon Nanotube Acoustic and Optical Sensors for Volatile Organic Compound Detection. Nanotechnology* 16 (2005) 2536–2547. [online] Available on internet: <http://www.iop.org/EJ/article/0957-4484/16/11/013/nano5_11_013.pdf>

[10] CHAN, S. P., CHEN, G., GONG, X. G., LIU, Z. F.: *Chemisorption of Hydrogen Molecules on Carbon Nanotubes under High Pressure. Physical Review Letters* [online] November, 2001, Vol. 87, No. 20. Available on internet: http://www.eng.uc.edu/˜gbeaucag/ Classes/Nanopowders/ CarbonBasedNanoPowders/ReistenbergReferences/chemisorption.pdf.

Boris Böttcher *

THE TRANS-EUROPEAN TRANSPORT NETWORK (TEN-T): HISTORY, PROGRESS AND FINANCING

Summing up, the author, M.E.S. (Master in European Studies) MA (International Relations) Dipl.-Ing. (Transport Sciences), presents the basis of his actual doctor thesis about the international and strategic dimensions of the enlargement of the Trans-European Network (TEN) to Russia, the caucasus and Turkey. The article deals with the creation and the development of the TEN-T program of the European Commission. After the description of the history of this program, the progress of the fourteen transport priority projects is shown from the report of the Christophersen group to the European Council in 1994. In addition, the guidelines and the financial rules of the TEN-T are examined, which implemented a regular report from the member states to the Commission. With these data the financial forecast gets more realistic and further amendments about the construction progress could be made. Afterwards, the financing of the infrastructure projects is presented on the basis of the different European, government and private fundings. Finally an outcast is given about the new priority projects of 2004.

1. Introduction

In this article, history, guidelines on how to evaluate projects and budget figures of the European Union (EU) for the financing of the Trans-European Transport Network are presented. The data started with the development of the Common Transport Policy of the EU in the 1950's and continued with the establishment of the Trans-European Networks in 1992. Afterwards the progress of the TEN-T was evaluated. Therefore, the financing of the TEN-T is presented with its different sources, starting from the EU budget up to the different types of funds, loans and guarantees. Finally, there is an outlook from the High-Level group report on the identification of thirty new priority projects up to 2020.

The Trans-European Networks were created with the foundation of the European Union and fixed in the Treaty of Maastricht in 1992. They include different modes of transport and are separated into (1) the TEN for energy and telecommunication and (2) the Trans-European Transport Network. The TEN-T includes air transport as well as road and rail networks. In addition, sea-transport is considered, divided into inland waterways (IWW), ports, and short-sea. Finally, better traffic management and navigation systems are TEN-T objectives. The so-called Intelligent Transport System (ITS) contains road traffic management, the European Rail Traffic management System (ERTS), traffic management and information of inland waterway navigation as well as the Vessel Traffic Management Information System (VTMIS). The ITS is completed by the Air Traffic Management (ATM) and the Global Navigation Satellite System (GNSS), which includes the Galileo satellite system.

2. The History of the Trans-European Transport Network (TEN-T)

The development of the European Common Transport Policy began long before the TEN. The first transport objective was already fixed in the Treaty establishing the European Coal and Steel Community (ECSC) in 1951 before being integrated in the Treaty of Rome, founding the European Economic Community (EEC) in 1957. This objective stated that "measures or practices which discriminate [...] in prices and delivery terms or transport rates and conditions" should "be abolished and prohibited within the Community" (ECSC, 1951, Title I Article 4). Six years later, the EEC went a step further and defined "a common policy in the sphere of transport" (EEC, 1957, Part 1 Article 3 f), which applied to the transport by rail, road and inland waterway, within the territory of the Community as well as to the international transport.

By the beginning of the 1980's, despite decades of economic prosperity and progressive integration of the European Communities (EC), the member states had failed to launch the Common Transport Policy. Therefore, the European Court of Justice, requisitioned by the European Parliament, admonished the Council in 1985 on account of its policy with respect to the liberalisation of the transport market (Kerwer, 2000, 12). According to this judgement the member-states changed their position, and the Council decided in 1988, proposed by the European Commission (COM), to introduce the Internal Market for transport (Bauchet, 1996, 48). But, while the increasing transport in the EU (see Fig. l) necessitated action, further progress in the field of transport had to wait until the foundation of the European Union.

* **B. Böttcher**
C.E.I.E. (Centre d'études internationales et européennes), Université Robert Schuman, Strasbourg, France; E-mail: Boris.Bottcher@eturs.u-strasbg.fr
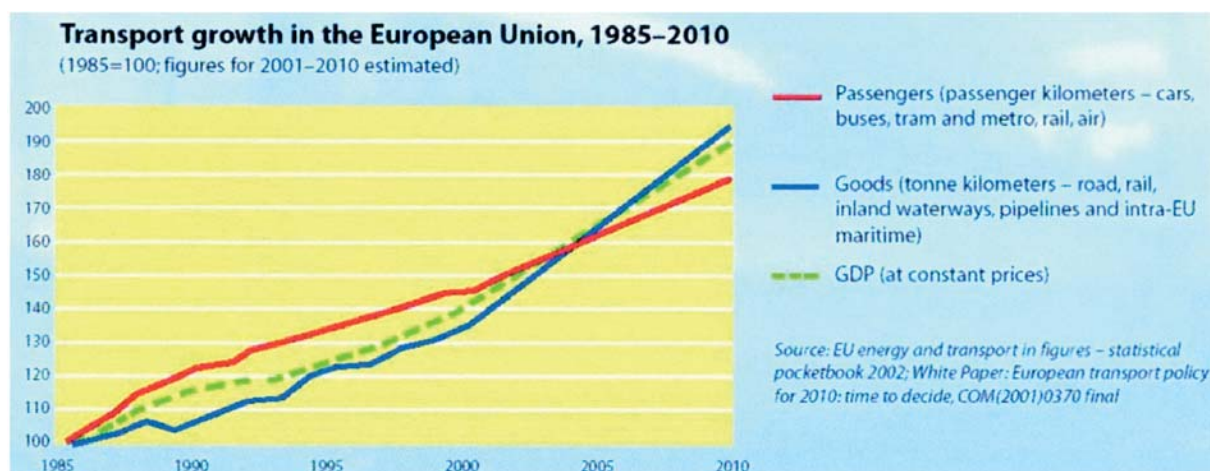
Fig. l: Trans-European Transport Network (COM, 2002, 5)

3. The Progress of the Trans-European Transport Network

Although some projects had begun previously, most of them were not started until the foundation of the European Union in 1992 (COM, 2004a). Due to the insertion of the Trans-European Networks in the treaty, the liberalisation of the transport market should be reached by promoting "the interconnection and inter-operability of national networks as well as access to such networks" (EU, 1992, Article 129b). Therefore, coordination was needed, and the Council ordered a special group of national experts, led by the Vice-President of the Commission, Mr. Christophersen, to examine the possibilities to speed the progress of the TEN-T. In 1994, the propositions of the High-Level group included fourteen priority projects (EU, 1995a, Annex I, 254) as well as possible solutions for how to ease the rules of construction measures within the

member-states and raise the needed financial aid. They were adopted in 1996.

Launching the network character of the measures, the amendments were focused on cross-border links and on projects that connect peripheral regions with the centres of the European Union. In particular, the high-speed train network was targeted with one of the main objectives, because the policy of the EU introduced the Strategic Environmental Assessment (SEA) in 1992, which strengthened the more durable transport modes. Fulfilling an obligation of the Article 129c of the Treaty of Maastricht (EU, 1992, Article 129c), the Community guidelines for the development of the Trans-European Transport Network were introduced in 1996 with the Decision 1692/96/EC (EC, 1996). This directive specified that the network must insure "sustainable mobility of persons and goods within an area without internal frontiers under the best

Total TEN-T support 1996 – 2001 in million € per mode (Planco, 2003, 95)   Tab. 1

	1996	1997	1998	1999	2000	2001	TOTAL
Rail	163.70	176.29	269.75	263.80	343.13	283.85	1,500.52
Road	27.77	49.82	59.50	62.96	73.40	83.00	356.46
Iww	1.50	4.00	8.50	18.24	15.80	9.81	57.85
Airports	3.78	21.45	28,60	29.36	11.10	14.73	109.02
Ports	3.10	4,70	6.07	3.04	2.50	10.11	29.52
Combined transport	0,31	0,00	1.80	9.40	1.50	1.30	14.31
Multimodal transport	26.20	56.20	24.00	45.27	34.00	2.00	187.67
Air traffic management	18.97	18.60	21.10	12.39	14.70	10.97	96.73
Road traffic management	20.50	24,38	16JO	15,68	32.13	25.29	134.89
Rail traffic management	10.23	9.00	22.80	22.05	35.00	0.00	99.08
GNSS	10.80	6.60	9.65	14.10	12.00	110.00	163.15
\/TMIS (Vessel TM)	2.14	0.96	5.34	1.30	0.90	0.00	10.64
TOTAL per year	289.00	372.00	474.01	497.58	576.17	551.07	2,759.83

possible social and safety conditions" (EC, 1996, Section 1 Article 2 (2a)) and provided several other prerequisites to get accepted as priority projects of the TEN-T. Furthermore an "optimum combination and integration of the various modes of transport" should be guaranteed, so that all of these different modes of transport would be represented within the TEN-T. In addition to the willingness to strengthen the railways, every other mode was also supported directly by the Community budget (see Tab. 1).

4. Financing of the Trans-European Transport Network

Moreover, the decision of 1996 laid down in its Article 18 (3) the obligation to make an implementation report every two years and, from 1998 on, every four years. These reports had two main objectives. On the one hand, they present the figures about the progress of the projects, and, on the other hand, they expose the difficulties of one project or the changes in the circumstances. In this case, especially if financing of one project is in danger, the guidelines or the list of priority projects could be amended and updated. In the 2001 report, the Commission emphasized that, between 1996 and 2001, a total of € 172 billion had been invested in the TEN-T with the sum for the railway being twice that of the total for the route infrastructure (COM, 2004b, p.8). The main question about all these infrastructure and technical measures is: how to finance all these projects? The Community policy is very strict with the direct financial aid: only 50 % of the cost of preliminary studies (feasibility studies) and 10 % of the cost of the work could be financed by the EU budget (EU, 1995b). Even though it

was raised to 20% from 2003 (Regulation 1655/99), it is still far from full financing by the European Union.

Consequently, other Community resources must be found. In the first category of financing are different kinds of funds. The European Regional Development Fund (ERDF) had already existed when the Treaty of Maastricht established a Cohesion Fund effective at the end of 1993. This fund enabled EU financing of projects in countries in Objective 1 such as Portugal or Greece, which had a GDP below seventy five percent of the average EU-GDP, but also in the regions of the former GDR, at up to 100% of the project cost. In addition, loans and guarantees could be generated, like the newly created European Investment Fund (EIF), which could also be used for some transport projects. Overall, it was a great amount of money from Community funds to launch the TEN-T projects, primarily in the form of loans from the European Investment Bank (EIB), especially targeting the Central and Eastern Europe Countries (CEEC) – (see Tab. 2).

5. The Current Situation and Outlook of the Trans-European Transport Network

To summarize, the European Commission made great efforts to improve the European infrastructure, but the results for the Trans-European Transport Network in comparison to the forecast are disappointing. Two main problems are responsible for this development. On the one hand, the enlargement of the European Union widened the financial needs for the TEN-T. On the other

Community funding of TEN-T projects in million € (see sources above)   Tab. 2

Financing/ Year	TEN-T Budget (DG7)	Cohesion Fund (DG16) (1993–1995 calculated	EIF (loans/ guarantees)	EIB (loans) (1991–1994 with CEEC)	PHARE	ERDF (DG16)	Total of year or period
1991		for transport		2633			2633
1992		55% of total)		4868			4868
1993	185	825		4292	73		5375
1994	200	963		4500	230		5893
1995	216	1100			240		1316
1991–1995	**601**	**2888**		**16293**			**19782**
1996	280	1224	303	3504	240	–	5311
1997	352	1251	55	4943	240	–	6601
1996–1997	**632**	**2475**	**358**	**8447**		**1050**	**12962**
1998	474	1337	72	4415	240	–	6298
1999	497	1523	266	5977	240	–	8263
1993–1999					1503		1503
2000	580	1287	117	4010		–	5994
2001	563	1318	–	5161		–	7042
1998–2001	**2114**	**5465**	**455**	**19563**		**3000**	**30597**
1991–2001	**3347**	**10828**	**813**	**44303**	**1503**	**4050**	**64844**
Sources:		(Damien, 1999, 46-47)		(COM, 2001a, 25)		(COM, 2004c, 25)	

hand, and more importantly, historical privileges of national authorities for the planning of projects and policies of their national leaders often leave the projects uncompleted at the last miles before the border. As the Commissioner of Energy and Transport Loyola de Palacio pointed out in 2002, the problems are still not solved, and she resumed that "the resulting delays affect cross-border projects in particular. At the present rate, and without additional financing, further 20 years will be needed just to complete the work planned for 2010" (COM, 2002, 3). In addition, the financing remained difficult and insufficient (see supported actions COM, 2004d). While the European Commission often promoted only the beginning of transport projects, the planning or preliminary studies, the main efforts of the construction process were left for the member states. Therefore, the new proposal 2004/0154 (COD) of the Commission laying down general rules for the granting of Community financial aid wants "to change the co-financing rate to a maximum of 30% for certain sections of the priority projects, and that in exceptional cases for cross-border sections, to change the rate to a maximum of 50 %" (COM, 2004e).

For futher information about the TEN/T financing and perspectives see the recently published report (COM, 2005).

Substantial challenges remain. In 2003, only three of the old priority projects were finished and another five should be finished before the fixed date in 2010. But the rest of them will not be terminated by the 2010 goal, and 22 new priority projects are already in the pipeline, due to the report of the High-Level group. The costs for all these priority projects are estimated at up to € 235 billion and the total sum for all Trans-European Networks through 2020 should be about € 600 billion (all data COM, 2003). Summing up, beneath the challenge of the financial forecast, great efforts must also be made with regards to political decisions. While unanimity is no longer required in the transport sector, good consensus is more important than ever to safeguard a real network character of the TEN-T with the support of all EU countries.

References

[I] *Treaty establishing the European Coal and Steel Community,* 18 April 1951

[2] *Treaty establishing the European Community,* 25 March 1957

[3] KERWER, D., TEUTSCH, M.: *Elusive Europeanisation – Liberalising Road Houlage in the EU,* p. 12, http://www.mpp-rdg.mpg.de/pdf_dat/00011.pdf , 23 Feb 2005

[4] BAUCHET, P.: *Les transports de 1'Europe – La trop lente integration,* Paris, Economica, 1996, p. 48

[5] EUROPEAN COMMISSION: *Trans-European Transport Network,* p. 5, http://europa.eu.int/comm/ transport/themes/network/doc/2002_brochure_ten_t_en.pdf, 17 Feb 2005

[6] *http://europa.eu.int/comm/ten/transport/actions/supported_actions_en.pdf,* 28 Feb 2005

[7] *Treaty on the European Union* (Title XII Article 129b), 29 July 1992, http://europa.eu.int/eur-lex/lex/en/treaties/dat/! 1992M/htm/l 1992M.html, 13 Feb 2005

[8] EUROPAISCHE UNION: *Transeuropaische Netze,* Amt fur amtliche Veroffentlichungen der Europaischen Gemeinschaften (Afa), Luxemburg, 1995, p. 254

[9] PARLIAMENT AND COUNCIL: *Decision No 1692/96/EC*, 23 July 1996, http://europa.eu.int/eur-lex/lex/LexUriServ/LexUriServ.do?uri=CELEX:31996D1692:EN:HTML, 06 Jan 2005

[10] PLANCO, et. al.: *TEN-Invest - Final report*, planco, Essen, 2003, p. 95, 06 Feb 2005 http://europa.eu.int/comm/ten/transport/documentation/doc/2003_ten_invest_en.pdf

[11] EUROPAISCHE KOMMISSION, DG VII, Dienststelle TEN-V: *Durchführung der Leitlinien* 1998–2001, (Afa), Luxemburg, 2004, p. 8

[12] *Regulation (EC) n° 2236/95 of the Council about TEN financial aid*, 18 Sep 1995, http://europa.eu.int/smartapi/cgi/sga_doc?smartapi!celexplus!prod!DocNumber&lg=fr&type_doc=Regul ation&an_doc=1995&nu_doc=2236, 7 July 2005

[13] DAMIEN, M.-M.: *La politique europeenne des transports,* Paris, puf, 1999, pp. 46–47

[14] EUROPEAN COMMISSION: *TEN-T report 1996–1997*, 2001, p. 25, 16 Jan 2005, http://europa.eu.int/comm/transport/themes/network/english/hp-en/grepdocs/bimprep.htm

[15] EUROPEAN COMMISSION: *TEN-T report 1998–2001*, 2004, p. 25, 11 Feb 2005, http://europa.eu.int/comm/ten/transport/documentation/doc/sec_2004_0220_en.pdf

[16] *http://europa.eu.int/comm/ten/transport/actions/supported_actions_2004_en.pdf*, 28 Feb 2005

[17] COMMISSION OF EC: P*roposal amending Reg. (EC) n° 2236/95*, 14 July 2004, 28 Aug 2005, http://europa.eu.int/eur-lex/lex/LexUriServ/site/en/com/2004/com2004_0475en01.pdf

[18] EUROPEAN COMMISSION: *TEN-T report with up to 2020*, 2003, 06 March 2005, http://europa.eu.int/comm/ten/transport/revision/hlg/2003_report_kvm_en.pdf

[19] EUROPEAN COMMISSION: *Networks for peace and development – Extension of the major trans-European transport axes to the neighbouring countries and regions,* 13 December 2005, http://europa.eu.int/comm/ten/transport/external_dimension/doc/2005_12_07_ten_t_final_report_en.pdf

Marcus Einbock *

THE INTRODUCTION OF THE AUSTRIAN TOLL SYSTEM FOR TRUCKS – EFFECTS ON COMPANIES

This paper deals with effects of the Austrian road pricing system on enterprises. Trucks are charged per kilometre driving on Austrian motorways with the amount depending on the number of axles. Therefore, enterprises whose trucks use motorways are confronted with higher transport costs. These costs can be generally divided into direct and indirect ones. The main cost categories concerning indirect costs are costs for pre-financing, for bad debts losses and for toll-control. In this contribution these kinds of costs are assessed and the cost effects in different industries are evaluated. Further, empirical evidence based on a survey conducted in June 2005 is included, where Austrian enterprises were asked about their assessments concerning consequences of road pricing on their company.

Keywords: road pricing toll, consequences on enterprises, Austria, effects on costs, strategies.

1. Introduction

The idea of charging the transport infrastructure is very old. [7] The usage of special roads was combined with paying a fee already in ancient times. [3,12] Today, two kinds of toll systems can be distinguished. On the one hand, there exist a lot of time-dependent road toll systems. On the other hand, kilometre-based road pricing systems will become more important in future. Time dependent toll systems are characterised by the right to use a defined road network within a certain period. For influencing behaviour of road users, these time-dependent fee systems are not sufficient. They do not discriminate between frequency and temporal-local demand of road users. [10,11] In contrast to this kilometre-based road pricing systems are able to regulate demand on a road network in a better way. Such kilometre-based systems can be already found in freight and/or passenger transport in some European countries, i.e. France, Italy or Slovenia. [4] Perhaps the most prominent one is the "Leistungsabhängige Schwerverkehrsabgabe" for all trucks on all roads in Switzerland, established in 2001. In Austria, a kilometre-based system for trucks was introduced in January 2004, with Germany following in 2005.

2. Description of the Road Toll System in Austria

The era of kilometre-based road pricing started at the beginning of 2004. The government decided upon the implementation of a kilometre-based charging system on all motorways for trucks from 3.5 tons maximum weight on in 2002. As shown in Table 1, the fees range in amount from 13 Cents to 27.3 Cents per kilometre and are dependent on the number of axles.

These Austrian road fees are the highest ones within the European Union. In comparison with Germany, the Austrian fees are

Amount of road fees in Austria (exclusive 20 % VAT) Table 1

	2-axles	3-axles	4- and more axles
Category	2	3	4
Amount	13.0 Cent / km	18.2 Cent / km	27.3 Cent / km

2.23 times higher for trucks with four or more axles. Moreover, crossing the Alps (i.e. via Brenner, Tauern-motorway, Arlberg-motorway) come along with further tolls and duties for trucks. Unlike Germany, emission classes of vehicles are not considered in this present charging system. But it's expected that a more ecological design of Austrian road fees considering different external costs will happen in the nearer future. This would deliver incentives for buying vehicles with less pollutant emissions. [9]

The charged roads in Austria are depicted in Figure 1. Revenues are disposed for reconstruction and extension of motorway network all over Austria. The enlargement of the European Union in May 2004 reinforced the necessity of investments in the Austrian motorway system. For example, there is up to now no direct motorway link from Vienna to the Austrian-Czech border or to the nearby Slovakian capital Bratislava.

The charging process is based on the microwave-technology. The fundamental components are portals located between two exits of the motorway and the OBU (on-board-units) attached at the front-window of the vehicles. The portals send signals by microwave and if a vehicle passes a portal, the signal will be send back for registration. The registration data will be transferred to a central server recording the process.

* M. Einbock
  Institute of Transport Economics and Logistics, Vienna University of Economics and Business Administration, 1090 Vienna, Austria,
  E-mail: Marcus.Einbock@wu-wien.ac.at

3. Kind of Consequences on Austrian Enterprises

3.1. Overview

The kilometre-based charging has several effects on enterprises in Austria. First of all, a new kind of costs arises – charges for using motorways which in turn contribute to transport costs. Further, companies react to their changing environment and take measures in order to reduce logistics system costs. In the following the most important effects will be discussed focusing on the consequences on costs, competitive ability and on the planning system of companies.

For the assessment of these direct and indirect consequences, an empirical study was conducted in June of 2005, 17 months after the road pricing system came into effect. The survey was carried out in co-operation with the Austrian Federal Chamber of Commerce. Over 1.000 companies were chosen for a structured sample of companies from economic sectors, which regarded to be heavily influenced by kilometre-based charging systems. Enterprises were asked about their assessment of consequences on their company. Within the sample industrial enterprises, trading companies and logistics service providers were considered. At the end, 105 companies took part in the survey, whereof 3 forms could not be taken into further consideration, as the answers therein were not plausible or valid. The respondent's affiliation were for 46 industrial enterprises, 38 traders (wholesalers and retailers) and 47 logistics service providers (forwarders or carriers), multiple answers were possible.

3.2. Effects on Costs

As already indicated above, accounting of companies using the Austrian motorway system is confronted with a new type of costs, the toll charges. These costs are a component of transport costs which can be separated between direct and indirect ones. Direct toll costs are expenses resulting directly from the payment of the charge determined by the number of axles and the distance on the charged roads. They are emphasised in current discussions

Fig. 1. Charged motorways in Austria, source: ASFINAG

about charging in practice. Indeed, this kind of costs seems to be the predominant part of toll costs. But companies are confronted also with indirect costs which are not negligible. [6] Indirect toll costs are costs arising for logistics service providers and shippers, which are no direct toll costs but stand in a close relationship with the charging process. In general they can be divided into three categories:
- costs for pre-financing,
- costs for bad debts losses and
- costs for toll-controlling.

Indirect toll costs arise either permanently or one-time whereas costs for pre-financing and for bad debts losses belong to the permanent cost category. Regarding the costs of toll-controlling, there exist cost-types pertaining to permanent or one-time costs.

Costs for pre-financing will typically arise if the time of out-payment for goods or services is earlier than the date of in-payment. It is a form of bridge-financing resulting from the late in-payment of customers. In Austria, customers usually pay transport costs up to 60 days after shipment. The out-payment occurs regularly about 10 or 14 days after carriage in the widespread post-paid-procedure. So there is a need to finance the time-gap between the two dates. Generally costs for pre-financing correspond to costs for an over-draft credit. Costs for pre-financing amount about 2 to 3 % of the direct toll costs in Austria.

Costs for bad debt losses are a second important component among the multitude of indirect toll costs especially borne by freight forwarders and carriers. If a carrier for example transports goods for a customer and after the transport the customer will go to insolvency, the carrier will have to bear basically all the direct costs for this special customer. Due to this fact, it is necessary to consider the risk of bad debt losses including full / partial depreciation, administration costs, and insurance costs, too. All in all, costs of bad debts losses account to less than 0.1 % of direct costs in Austria. This cost type is consequently less important. One of the reasons for such a low figure is an overall high probability of shipper's in-payments.

The third category covers the costs for toll-controlling. Toll-controlling deals with all processes regarding setting aims, planning and monitoring resulting from the implementation of the kilometre-based charging system. The general goal of toll-controlling comprises the keeping of the management abilities for co-ordination, reaction and adaptation despite charging-induced changes in the environment of companies. The implementation of toll-controlling is especially relevant for logistics service providers confronted with high direct toll costs. As the profit margin in the Austrian logistics service sector is very low with an average of the net operating ratio of 0.24 % [13], the establishment of a toll-controlling-system is recommended.

Direct and indirect toll costs lead to higher transport costs. The increase of transport costs vary considerably between indus-

try sectors, as Table 2 shows. The study documented a wide range from average 4.3 % in the construction industry and materials and up to average 10.1 % increase in paper and printing. In general, the average among industrial enterprises is 8.2 %. The reason for such a relatively wide span seems to lie in different needs for transport. In addition to this heterogeneous logistics systems are established in the branches. The structure of the fleet, the kind of transport (short distance vs. long-distance), the fraction of road transport of overall transportation in a company or the real utilisation of the fleet are all components influencing the increase of toll-based costs.

Road toll based increase of transport costs   Table 2

Industry	Increase of transport costs
Earths, Stones, Ceramics	9.3 %
Construction industry and Materials	4.3 %
Paper and Printing	10.1 %
Wood	9.5 %
Food and Beverages	6.1 %
Trading Companies	5.3 %
Logistics Service Providers	9.1 %

Bearing all the additional costs alone can significantly reduce the profit margin and the financial results.

If companies give the additional toll costs to their customers, the sales-price for goods will rise. That seems to be an important point as opponents of such road pricing systems in politics refer to negative effects on prices. The average rise of sales-prices is shown in Table 3.

Average increase of sales-prices in different branches   Table 3

Branch	Average rise of sales-prices
Industrial Enterprises	1.2 %
Traders	3.5 %
Logistics Service Providers	7.0 %

Companies see clearly sales-price increases. Especially logistics service providers estimate a pretty strong average rise of 7.0 %. This shows clearly their cost burden. However, these figures state nothing about price changes for the ultimate customer. As companies are involved in supply chains, the effect on final sales-prices can only be estimated. A precise examination of supply chains and the transport links between the stages in the supply chain is required to find out price changes for the ultimate customer. Another method would be the use of Input-Output-Tables for estimating price changes. An estimation on the basis of such tables revealed minor changes between 0.09 and 0.63 % for Austria. [5]

3.3. Effects on Competitiveness

Charging of road infrastructure means also consequences for the competitive ability. Competitiveness can be improved or deteriorated. But there are a lot of enterprises too, seeing no changes in their competitive ability. The shifting of competitiveness can be discussed for four different levels:
- opposite to Austrian competitors in Austria,
- opposite to Austrian competitors outside Austria,
- opposite to foreign competitors in Austria and
- opposite to foreign competitors outside Austria.

This differentiation allows an exposure of discrepancies according to the considered level. It can be assumed that there exist differences regarding the reference object. The results concerning the levels are to been seen in Table 4 for industrial enterprises.

Regarding Table 4, industrial enterprises supposed different effects on their competitive ability dependent from the kind of level. Most respondents realised no significant changes on their competitiveness – only their position related to foreign competitors outside Austria is realised explicitly to worsen. About 40 % of the

companies assume a negative influence on their competitiveness in export. This shows that the enterprises saw a deterioration of their ability to export products, as they see that the price of products will rise to a not-acceptable level leading to a decrease in demand. Their foreign competitors do not have to bear the additional toll costs; that is why they saw this level negative. The spreading indicates also, that general statements assuming a global decrease in competitiveness are absolutely wrong. A further point is the estimation of some enterprises realising an increase in competitive ability. It is explainable by the fact that certain companies are much nearer to the customer than the domestic or foreign competitors resulting in advantages for delivery. Otherwise this shows, that most of the companies do not consider the road pricing system as a protective tariff.

3.4. Effects on Planning Systems

Defining adequate goals for minimising the total costs with corresponding strategies is especially relevant for companies having a high fraction of transport costs on turnover and a strong toll-based increase in transport costs. Minimising the toll-based increase

Expectations about the change of competitiveness for each level, industrial enterprises Table 4

Level	Strong improve-ment of competitive-ness	Improve-ment of competitive-ness	Constant competitive-ness	Worsening of competitive-ness	Strong worsening of competitive-ness
Opposite to Austrian competitors in Austria	0 %	3 %	74 %	20 %	3 %
Opposite to Austrian competitors outside Austria	0 %	0 %	76 %	17 %	7 %
Opposite to foreign competitors in Austria	0 %	0 %	74 %	20 %	6 %
Opposite to foreign competitors outside Austria	0 %	3 %	57 %	20 %	20 %

Importance of strategies in the field of transport and packaging, industrial enterprises Table 5

Strategy	Very probably	Probably	Medium probably	Less probably	Im-probably
Reorganisation of transport logistics	6 %	25 %	25 %	19 %	25 %
Intensified using of non-tolled roads	9 %	6 %	30 %	21 %	34 %
Intensified using of non-tolled vehicles	3 %	21 %	12 %	12 %	52 %
Intensified using of smaller, lower tolled vehicles	3 %	12 %	9 %	30 %	46 %
Intensified using of bigger vehicles	10 %	13 %	10 %	23 %	44 %
Transfer to other transport modes (Railway)	6 %	18 %	12 %	18 %	46 %
Intensified co-operation with other shippers	0 %	0 %	25 %	19 %	56 %
Intensified outsourcing of transport services	15 %	12 %	18 %	21 %	34 %
Intensified using of non-returnable packaging	3 %	6 %	3 %	21 %	67 %

of total logistics system costs cannot be equated with minimising toll costs. Pursuing just minimising toll costs does not necessarily mean a minimisation of increase in logistics system costs, as they could possibly rise other cost types in the logistics system. A frequency-reduction of road transport for example leads to a decrease in toll costs, but on the other side a rise in inventory and storage cost arises, apart from longer delivery times (Concerning this kind of total cost thinking see [1, 2, 8]).

Definition of goals is a prerequisite for planning strategies. Concerning road toll system there exist a lot of possible strategies to diminish increase in logistics system costs:
- Strategies in the field of procurement,
- Strategies in the field of distribution,
- Strategies for improvement of the location structure in logistics networks and
- Strategies in the field of transportation and packaging.

All these kind of strategies can support a minimisation of total logistics system costs including toll costs. Especially the last strategy group can help to reduce logistics system costs.

As Table 5 shows, the importance of different strategies in the field of transport and packaging is very variable for industrial enterprises. Strategies like reorganisation or outsourcing are relevant for some companies. Other strategies like cooperation with other shippers or intensified using of non-returnable packaging play only a minor role for industrial companies.

4. Summary

In January 2004, a road pricing system on all motorways was introduced in Austria. All vehicle (trucks and buses) from 3.5 tons overall weight have to pay a certain fee extending from 13 Cent/km to 27.3 Cent/km. This road toll system leads to different effects on enterprises in Austria. At first accounting is confronted with a new cost type. Toll costs can be separated into direct and indirect toll costs. Both result in an increase of transport costs depending on the industry. Higher transport costs can have an influence on the competitive ability in Austria and in foreign countries compared to inland and foreign companies. It is a general goal to reduce the toll-based rise of logistics system costs which cannot be equated with minimising toll costs. Enterprises can pursue strategies in the field of procurement and distribution, changing the logistics network or in the scope of transportation and packing.

References

[1] BALLOU, R.: *Business Logistics / Supply Chain Management*, Upper Saddle River, 2004
[2] Bowersox, D., Closs, D., Cooper, B.: *Supply Chain Logistics Management*, Boston, 2002
[3] CASSON, L.: *Travel in the Ancient World*, London, 1974
[4] HERRY, M. U., JUDMAYR, S.: *Finanzielle Belastung der Straßenbenutzer in Europa*, Part 1: Lkw, Wien, 2000
[5] KRATENA, K., PUWEIN, W.: *Road Pricing for Heavy Goods Vehicles Transport*, Wien, 2002
[6] KUMMER, S. U., EINBOCK, M.: *Auswirkungen der Einführung der fahrleistungsabhängigen Lkw-Maut in Österreich – Ergebnisse einer empirischen Umfrage*, Wien, 2003
[7] NIELSEN, S. M.: *Beiträge des Verkehrssystem-Managements zum stadtverträglicheren Straßenverkehr*, Berlin, 2000
[8] PFOHL, H. CHR.: Logistiksysteme, 7.ed, Berlin,
[9] ROTHENGATTER, W., DOLL, K.: *Anforderungen an eine umweltorientierte Schwerverkehrsabgabe für den Straßengüterverkehr*, Berlin, 2001
[10] SCHEELE, U.: *Privatisierung von Infrastruktur*, Köln, 1993
[11] THALLER, O.: *Impact Analysis of Urban Road-Use Pricing on Travel Behaviour*, the Environment and the Economy, Wien, 2000
[12] VITON, P.: *Private Roads,* Journal of Urban Economics, 37(3), pp. 260 –289, 1995
[13] VOITHOFER, A., SCHUBERT, P.: *Untersuchung der Ertrags-, Kosten- und Finanzlage der Österreichischen Verkehrsunternehmen*, Wien, 2004.

Heda Hansenova – Ho Thi Thu Hoa *

INTERMODALITY – TRANSPORTATION SOLUTION FOR GLOBAL TRADE

World trade has been growing at an average rate which is considerably greater than the growth rate of GDP (Gross Domestic Production). Policies aimed at the reduction of tariffs and quotas have led to an increase in the bilateral trade flows between countries. Increasing global trade also means that opportunities of transportation are growing. The efficient transportation solutions for global trade really offer demand for transport market by sea because of its satisfaction in long-distance routes as well as mass quantity of transported freight. Increasing business relations of two continents EU and Asia (especially ASEAN plus 3 named APT)[1] are obviously creating potential trends for transportation network and corridors. One of the very important sea transport routes between ASEAN + 3 and EU can link up the Danube river. While traditional transportation used to separate individual modes of transportation, intermodalism creates unbroken door-to-door transport chains.

1. Global trade and modalities of transport

Nowadays, a number of important developments affecting international flows of goods and international logistics are: globalization (globalization of the production process), the empowered consumer (growing competition in international trade, time-based competition), power shift in the supply chain (supply chain management strategies), technology (growth of computerization, electronic data interchange „EDI" and global e-commerce) and deregulation (elimination of quotas or embargoes and freight rates is more flexible according to the laws of supply and demand).

The globalization of world trade not only increases the significance of international logistics but also has an impact on the behaviour of all those who are directly or indirectly involved in organizing this logistical process. First and foremost, there is a growing trend towards providing an integral door-to-door intermodal transportation services. At the same time, efforts are also made to sell additional value-added logistics services. Why can we confirm that Intermodality must become transportation solution for global trade?

According to the definition of OECD, intermodalism implies the use of at least two different modes of transport in an integrated manner in a door-to-door transport chain. The intermodal concept is therefore an integral part of the global logistics chain concept. Intermodal transportation allows each mode to play its role in building transport chains which overall are more efficient, cost-effective and sustainable. Thus it provides a solution that combines individual modes of transport and enters into a global
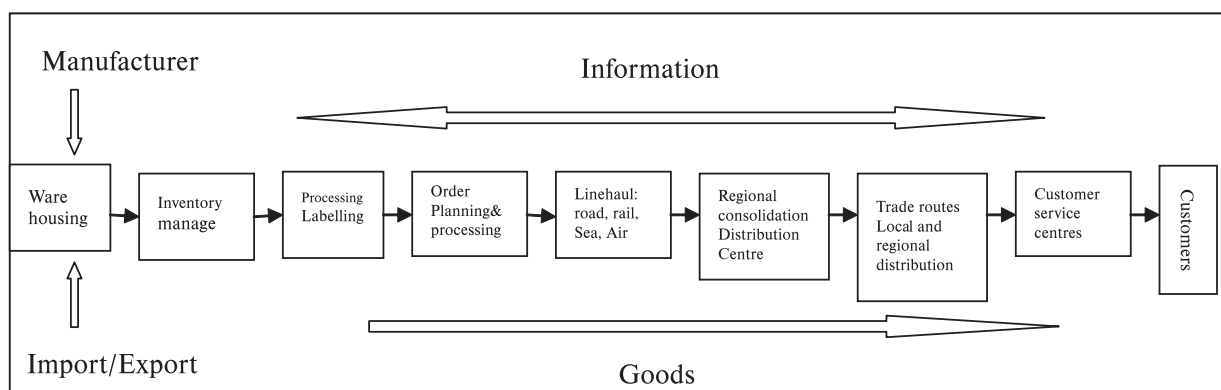
Source: Review of development in transport and communications in ESCAP-2001, United Nations

Fig. 1 Supply chain services: A contemporary Western view of logistics

* **H. Hansenova, Ho Thi Thu Hoa**
  Department of International Business, Faculty of Commerce, University of Economics in Bratislava, Slovak Republic

[1] ASEAN +3 (APT) includes 10 Asia South East Nations (Brunei, Cambodia, Myanmar, Laos, Singapore, Thailand, Vietnam, Malaysia, Philippines, Indonexia) and South Korea, Japan, China.

logistics chain which is not necessarily the result of each mode of transport performed individually. It can be confirmed that intermodal transportation is the smart transport combination.

Providing an integral door-to-door intermodal transportation is a typical example of a logistics chain approach (shown in Fig. 1), how one considers the totality of costs from the point of raw material to the destination of consumption.
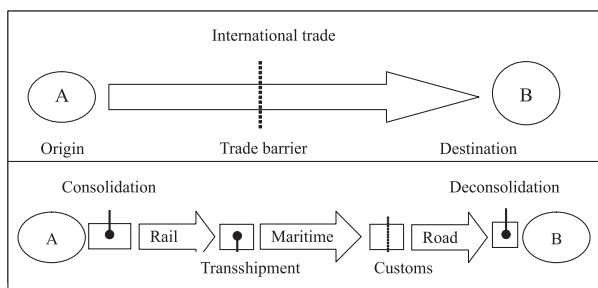
Source: www.people.hofstra.edu/geotrans
Fig. 2 International trade and Transportation chains

Transportation can be carried out in many ways and forms. Transportation techniques or transport modalities are considered as manner of road, rail, inland water, ocean shipping, air, pipeline. The choice of suitable transport modes is depending on several factors as characteristics of goods, transport distances, requirements of shippers, etc ...

In contemporary transportation, shippers are more interested in the end result from transportation than with using a specific mode of transportation. So long as the shipper's service requirements are satisfied, they are essentially indifferent as to the mode used to provide the transportation.[2] The pattern of these transportation services is model of door-to-door intermodal transporta-
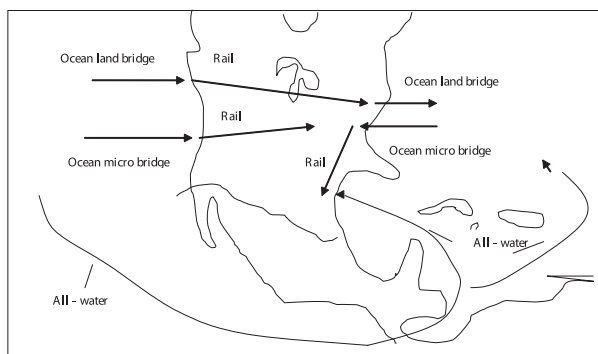
Source: The Management of Business Logistics, AMACOM 2002, p.153
Fig. 3 Types of International Intermodalism

[2] International Logistics, p. 431.
[3] Review of Maritime 2004.
[4] Review of Maritime 2004, see chapter 4.

tion – using different transport modalities with preferably: one organiser, one document, one responsibility, one price and in unbroken chain transport (shown in Fig. 2).

A prime example of international intermodalism is a land bridge which occurs on the trade route between Japan and Europe. The all-water route takes anywhere from the twenty-eight to thirty-one days. If the shipment travels by water from Japan to Seattle (ten days), then by rail to New York (five days), and by water from New York to Europe (seven days), we have a total shipping time of approximately twenty-two days (shown in Figure 3).

2. Trade boom and the demand of transportation between ASEAN + 3 and EU

On routes from EU to APT and on opposite, demand of transportation is not only in cargoes movements but also in passenger transport and tourism (shown in Fig. 4). EU people are discovering the natural material resources, business opportunities in new dynamic markets and tropical landscapes of Asia as well as APT countries.
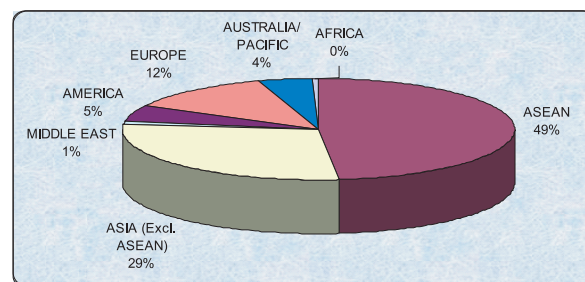
Source: www.aseansec.org/tour_stat
Fig. 4 Major market share by region of international visitor arrivals to ASEAN (2004)

On the Europe-Asia trade route, the transportation from Asia increased by 10 times the increase in the opposite direction.[3]

The coming cargoes from APT countries need sustainable transport system with cost effective and efficient operation. The event of quota elimination in garment imports from China, Vietnam and other countries in ASEAN perfectly contributes in increasing cargo exports from APT to EU members. Liberalization of trade without quota barriers forecasts necessary demand on transportation and services. The movements of cargo exports from APT to EU such as garments, shoes, electronic components, agricultural and aquatic products, furniture and flows of cargo imports of APT from EU as industrial equipment, chemical products, finished automotive products absolutely need the efficient solution for transportation of cargo between two areas[4]. However, unbalance in merchandise trade (shown in Fig. 5) between the EU and APT will bring challenges for shipping carriers.
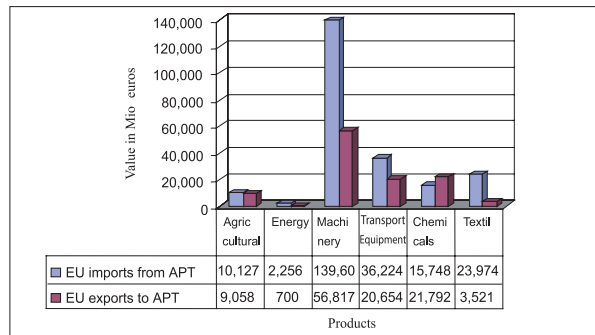
Source: EUROSTAT, 2004
Fig. 5 EU25 merchandise trade with APT by product (2004)
(Mio Euros)

While considering statistics of cargo flows along major trade routes as following: Asia – USA, Asia – Europe and USA – EU, we can realize the fact that cargo flows on route Asia – EU and Asia – USA have two or three times larger than that on route USA – EU (shown in Fig. 6), for example, Western-Central China exported over 132,000 TEU to Europe.
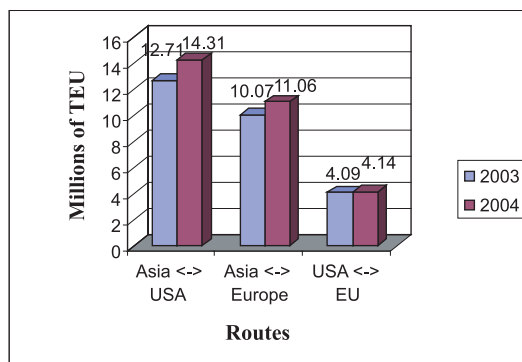
Source: Review of Maritime, 2004
Fig. 6 Cargo flows along major trade routes (millions of TEU)

APT is one of the most dynamic integrated economic zones which includes China and Vietnam – two economies with the highest growth rate of GDP in the world. Almost countries in APT have export – oriented economic policies, especially such as export value ratio to GDP of Vietnam achieved 57.4 %, of China reached 34.5 %. Therefore, EU – 25 enlargement with new ten potential markets will benefit for foreign trade activities of APT.

3. Possibilities of freight transportation on routes between ASEAN + 3 – EU

The expansion in trade has benefited transportation on routes connecting between ASEAN + 3 and EU. Intermodality will be the best solution for this situation. So which possibilities are considered for choice of corridors and combination of transport modalities on routes Asia – Europe and ASEAN + 3 – EU?

In 2004, at Kiev they discussed about use of rail transit capacities for intermodal freight transport for passage from China to Europe via Kazakhstan, Turkmenistan, Iran, Russian Federation, Belarus, the Caucasus States, Ukraine and Turkey.

The Trans-Siberian Railway is one of the most attractive transport routes in the world. This railway line running over 10,000 kilometres, one of the world's longest lines, leads from Russia's western border to its Pacific ports in East Siberia. Built in the years 1895–1916, the line runs via Moscow, Ryazan, Samara, Chelabinsk, Omsk, Novosibirsk, Krasnoyarsk, Irkutsk, Chita and Khabarovsk to Vladivostok. Its branch lines lead towards Kazakhstan. Uzbekistan, China and other countries.

However, the sea transport routes have more cost-efficient because they are very well established, accounting for two-thirds of all international movements[5]. There are several transport corridors Asia – Europe which concentrate on shipping by sea.

From 2000, Russia, Iran and India signed an agreement in St. Petersburg laying out a vision for a North-South Transport Corridor. The corridor stretches from ports in India across the Arabian Sea to the southern Iranian port of Bandar Abbas, where goods then transit Iran and the Caspian Sea to ports in Russia's sector of the Caspian. From there, the route stretches along the Volga River via Moscow to northern Europe. On the 13–15th May 2004 Turkey, Russia and Central Asia Transport, Maritime and Railway Ministers met at regional Caspian Transport Summit in Istanbul. Ministers discussed a variety of intermodal transportation and logistics issues including the goods flows, capacity and direction of energy transportation from the Caspian region to Europe via the Black Sea as well as the potential of maritime transport between Central Europe and Black Sea region via the Danube.

The world economy is proving record price of fuel (increasing price from USD 40 until USD 60 per oil barrel). The fluctuation of fuel price has seriously impacted on transportation market and price of goods. The requirements of environment preservation and greenhouse effect have influenced on the pattern of choice modes of cargo transport. While road or rail transport have flexible advantages in short – distance routes, maritime transport is main transport mode which take part in long - distance routes as well as satisfy demand of mass cargo quantity shipping. Therefore, sea transport has become the major transport mode for cargo movement on route EU – ASEAN + 3 and has to be a link connecting to another transport mode to establish integrated door-to-door intermodal transport chain. When transport network is planned connecting sea transport and inland water way between Asia and EU, it will contribute in development of maritime and river trade of EU countries, such as Slovakia. Until now, over 90 % of EU external trade and some 43% of its internal trade goes by sea; more than 1 billion tonnes of freight a year are loaded and unloaded in EU ports.[6] Maritime companies belong to European Union nationals control one third of the world fleet, and some 40 % of EU trade is carried on vessels controlled by EU owners.

[5] The Management of Logistics Business, p. 163.
[6] http://europa.eu.int/scadplus/leg/en/s13000.htm

One of the very important sea transport routes between ASEAN + 3 and EU can be described as follows:

The shipments from APT -> Strait of Malacca via Port of Singapore (the second largest sea port in the world) ->Indian Ocean -> Red Sea via Suez canal -> Mediterranean Sea -> Black Sea -> sea ports of Europe -> inland waterway intra EU via Danube river.

The strait of Malacca, linking the Indian and Pacific Oceans. More than 50,000 vessels per year transit the Strait of Malacca. With Chinese oil imports from the Middle East increasing steadily, the Strait of Malacca is likely to grow in strategic importance in coming years.

The Danube River is the second longest river in Europe.[7] The Danube has always been an important route between Western Europe and the Black Sea. One reason for this is the fact that it is the only major European river to flow west to east. The source of the river is located in the Black Forest area of Germany, from there, it flows about 1,770 miles to the east.

There are many important cities that the Danube flows through. They include Passau, Vienna, Budapest, Bratislava, Belgrades. With the aid of canals, the Danube is connected to the Main, Oder, and Rhine Rivers. This waterway connects the North and Black Seas. For commercial transportation, the Danube is extremely valuable.

Transport network between ASEAN + 3 countries and EU states will establish more effective routes for shipping cargoes from APT to EU west countries through means of sea transport between Pacific and Indian Ocean as well as inland waterway en route intra EU via Danube river. This network will also contribute to development of maritime and river trade of EU countries, such as Slovakia. It is no doubt that these situations are creating the opportunities for cargoes movements between two continents-especially development in shipping cargo, promoting for routes by sea transport between two continents and inland waterway intra EU. The biggest advantages of these corridors are to reduce transit time and lead lower cost, and that is very good news both for transport operators and customers.

Intermodality is also the effective combination of transport modes: sea – air, sea – rail, rail – road, etc. Therefore, it is very necessary to improve infrastructure of rail, road transports as well as intermodal transportation terminals. In Europe, the integration of transport routes into the Trans European Networks and the development of alternative transport corridors including the North-South corridor from Russia and North Eastern Europe to Iran have created linking corridors to Asia. Europe and Asia have also been discussed with inter-regional parties involved in the projects including the European Commission, European Commission for Energy and Transport (Trans-European Networks), International Road Federation, International Union of Railways, United Nations and the Organisation for Railway Co-operation.

Conclusion

The combination of different modes of transport to offer better links has been known as intermodality. Transportation has derived from the demand of cargo and passenger movements. The global trade has been increasing quickly , cargo flows are moving to and from dynamic economies. ASEAN and EU have gradually become essential trade partners, economic co-operation and trade relations are also major issues between these areas. However, increasing trade requires efficient means of transport for shipping cargo smoothly and cost-effective. How can we link modes of transport into unbroken transportation chain with the aid of modern informatics technique, EDI and logistics to serve for trade purposes on route ASEAN - EU? The answer is intermodality, this transportation solution will promote for developing maritime transport between ASEAN and EU as well as inland waterway transport en route intra EU via Danube river (contributing on commercial activities of cities along Danube river included Bratislava).

References

[1] BALÁŽ, P. a kol: *Medzinárodné podnikanie,* Sprint, Bratislava, 2005, ISBN: 80-89085-51-2.
[2] HANSENOVA, H., HOA, H. TH. TH., HLAN, T.: *Effect of intermodal transportation for exportable and global marketing of companies,* proceedings of 8th international conference EUROKOMBI-INTERMODAL 2005 – development of combination transport after EU enlargement, Zilina – Slovakia, 14-15/06/2005, pp. 69–73.
[3] HOA, H. TH. TH.: *Influences of EU southeastwards expansion on ASEAN + 3 trade and transport network,* international scientific conference in the framework of VEGA project 1/2640/05 „European Union – the enlargement towards southeastern", University of Economics, Bratislava 11/11/2005.
[4] WOOD, D.F., BARONE, A. P., MURPHY, P. R., WARDOW, D. L.: *International Logistics*, AMACOM, 2002.
[5] Review of Maritime 2004, chapter 4.
[6] COYLE, J. J. et al.: *The management of Business Logistics,* South Western Thomson, 2003.
[7] www.people.hofstra.edu/geotrans
[8] //europa.eu.int/scadplus/leg/en/s13000.htm

[7] Along its way, the Danube flows through countries (Germany, Austria, Slovakia, Hungary, Croatia, Serbia and Montenegro, Bulgaria, Romania, Ukraine)

Anna Černá – Jan Černý *

A NOTE TO NON-TRADITIONAL SYSTEMS OF PUBLIC TRANSPORT

The paper deals with the following non-traditional (from the Czech point of view) solutions of public transport: • free competition of several providers, • use of heterogeneous rolling stock, • Dial-a-Ride systems and • integration with other systems.

1. Introduction

First, we have to say that in the case of the Czech Republic the public transport system is said to be *traditional* if the following conditions hold:

T1: In the given area, the whole bulk of services is run by a unique provider. This is usually completely valid in the case of rail or trolley-bus systems. In the case of bus transport it is valid with the exception of buses coming from outside.

T2: In the bus (or trolley-bus) service, the prevalent size of buses is the standard one for about 80 passengers (sitting and standing together). If needed, some few articulated buses for about 120 passengers are added.

T3: These vehicles do not perform any other transport service (post delivery, transport of goods to shops etc.) during their trips with passengers.

T4: The service has a fixed schedule i.e. the vehicles move on compulsory routes through compulsory stops arriving/departing to/from them at precisely determined times.

The service is called *non-traditional*, if any of T1–T4 conditions does not hold.

Czech (as well as foreign) transport specialists argue in favor of the use of non-traditional systems mainly in case of a weak demand. We speak about a *weak passenger demand*, if the traditional transport system service, applied to satisfy the demand, might be extremely inefficient (i.e. the difference between cost and fare revenue is extremely high).

Further, we are going to present several types of non-traditional services and we shall discuss their suitability for the Czech scene. We shall deal with road transport mainly, because its role is highly prevalent in the Czech Republic.

The topics we are going to deal with are not new neither in the CR as one can see in [1] – [5], [7], nor abroad – [6]. Now we intend to present some facts which are not important only from the theoretical point of view, but we hope they may be interesting for the readers among employees of public authorities and transport providers.

2. Free Competition of Service Providers

The case of several service providers is in opposition to condition T1. One cannot expect to meet an absolute free competition of providers. It is more probable to have an oligopoly formed by two or more providers. It is well known from the economic theory that in the oligopolistic case one can expect smaller declared costs than in the monopolistic one.

We can distinguish the following alternatives:

2.1 One Major and One Minor Provider

Some time ago there were two very similar Czech districts, let us call them X and Y. They had very similar rural bus routes using similar vehicles and connecting villages of similar size having similar distances. However, there were two big differences to be noticed:

- in the *X* district, there was only one monopolistic provider and in the *Y* one there existed a minor provider (providing about 15 % of the service) beside the major one,
- in the *Y* district, the declared cost of one vehicle kilometer was 24 CZK and in the *X* it was 30 CZK!

This example clearly shows that even a minor provider can have a non-negligible influence on the declared costs and consequently on the required subsidy.

2.2 Oligopoly of Two or More Providers

In another Czech district there were two (almost balanced) providers. Their services covered the district overlapping in some areas. The district authorities decided to optimize the vehicle and

* A. Černá, J. Černý
Faculty of Management, University of Economics, Prague, E-mail: cerny@fm.vse.cz

crew scheduling of both companies keeping the timetable and the rolling stock unchanged. Two approaches were used:

a) each provider's scheduling was optimized independently,
b) a common optimization was elaborated neglecting the assignment of bus journeys to providers.

The results were surprising. The optimization a) led to the saving of 8 % and b) led to 15 %! Almost twice as much.

This promotes the following conclusion: If the regional authority wants to get profit from the oligopolistic situation, it is necessary to optimize the total service first and only then to assign vehicle daily duties to the individual providers. Of course, the better way of that assignment is an open competition.

3. Heterogeneous Rolling Stock

Regarding their size, the buses can be divided into the following classes:

- *articulated buses* for approx. 120 passengers,
- *standard buses* for approx. 80 passengers
- *midibuses* for approx. 40 passengers,
- *minibuses* for approx. 20 passengers,
- *microbuses* for approx. 10 passengers.

As one can find in the book [4], the rural bus service in the Czech Republic is based on standard buses (more than 80 %). The average capacity of all used buses is about 75 passengers, but the average number of passengers on board is only 19. It is obvious that the corresponding mean capacity of vehicles need not exceed the double of this figure, i.e. 38, only a half of the present value. This is an evident disproportion!

The transportation theory is able to give a tool optimizing the fleet (see [4], part 14.2.3). One can expect savings of about 10–15 % of costs after having been applied.

Many Czech providers use pure fleet consisting of standard buses only, although the demand does not correspond to it. This sticking to the "traditional" alternative causes significant economical damages and the use of „non-traditional" heterogeneous fleet is an obvious necessity.

4. Flexible Systems of Public Transport

As we have already said, a "traditional" public transport system has a fixed schedule i.e. the vehicles move on compulsory routes through compulsory stops arriving/departing at/from them at precisely determined times. It does not reflect the topical passenger demand at all.

The opposite is the so called "Demand Responsive Transport" (briefly DRT). The extreme case of the DRT is the traditional taxi-cab service serving individually to any demanding passenger (or small groups of 2–4 passengers travelling together).

Between these two extremes – the traditional public transport system and the taxi-cab system – there are several forms of public transport DRT's.

4.1 Fixed Schedule with Demand Responsive Journeys

Such a system uses a fixed time table where several journeys have a footnote "The journey is worked out only in case of x passengers (x tickets sold)." These systems are quite common at mountain cable ways. Beside that one can find them in the Czech Republic at the following places:

- Near Rychnov nad Kněžnou, several scheduled rural bus journeys run only in case of a sufficient passenger demand.
- Passengers can order an evening train connection between Bezdružice and Konstantinovy Lázně in West Bohemia if they buy about 60 tickets.

The authors were informed by their Italian colleagues that similar type of journeys can be found in Italy as well. However, the home and foreign experts do not consider this type of DRT suitable for the areas with a weak passenger demand.

4.2 Hail-a-Ride Systems

This type of system is suitable for (strongly demanded) routes with fixed time tables passing through weak demand areas. There could be request stops used only occasionally by hailing passengers. It is possible to admit hailing on the other place as well, but there must be a possibility of safe stopping of a vehicle and boarding of passengers.

4.3 Systems with Fixed Routes and Optional Stops outside them

The system consists of fixed routes with compulsory or request stops and moreover there is a set of optional stops outside the routes. The time tables do not precise the departures (e.g. 6:26) but hey contain „time windows" (e.g. 6:26–6:34) for each compulsory or request stop on the routes where a passenger can come, wait and board. If the passenger wants to board at an optional stop he/she has to ring up the provider's dispatcher who may accept the demand (and promise the arrival of the vehicle) or refuse it or suggest another stop for the boarding of the passenger.

Transportation experts consider this system very promising. The authors recommend it to regional and municipal authorities. However, the transportation theory has not yet solved all problems connected with the preparation and operation of it. Therefore the providers and public authorities will have to improvise if they want to prove this solution of a weak demand problem in practice.

4.4 Fully Flexible Dial-a-Ride Systems

This type of service is close to the taxi-cab one. We can mention only two differences:
- the cabs are usually for 3 or 4 passengers, but these Dial-a-Ride systems operate usually micro-buses for 8-10 passengers,
- a cab transports a passenger or a small group individually from the origin to the destination but a dial-a-Ride bus has passengers with different origins and destinations on board in the same time simultaneously.

5. Non-Traditional Integration with Other Systems

In this part we should like to mention several other alternatives of a non traditional solution of public transport services in areas with a small passenger demand. However, in the Czech Republic there is no or hardly any experience with them and we recommend to think about these possibilities.

5.1 Combined Passenger-Freight Transport

There is only small experience with this type of integration in the Czech scene:
- on several Czech private railways one can see trains consisting of both passenger wagons and freight ones,
- during short periods of extreme frosts, foodstuffs were transported to rural shops by buses as „heated vehicles".

However, the idea, not yet put into practice, is the following: The bus takes milk and bread to rural shops during its first morning trip from the town to the surrounding villages, then it transports workers to the town, afterwards it turns to the villages with other goods and brings pupils to schools in the town. In the afternoon the inverse operations can be performed bringing back empty shipping boxes.

5.2 Combined Passenger-Post Transport

This solution is very well known in Austria and the authors cannot understand why it has not been put into practice yet in the Czech Republic.

5.3 Car Sharing

For a foreign observer, it could be surprising that Czech public authorities do not promote any form of car and ride sharing, even in areas with a small passenger demand. It is due to the opinion of many lawyers that any car owner financially subsidized for sharing his/her car ought to meet all complex conditions of a public transport provider.

The authors agree with that. But there is another solution – not to subsidize the car owners, but to subsidize individual passengers (mainly the pupils) for "solving their transport problems themselves without any demand for public transport". One can expect that passengers (or their parents) will organize some private car sharing in that situation. Of course, the financial expenses for such a subsidy would be much smaller than the necessary subsidies for the traditional bus service.

6. Conclusion

The paper has presented several non-traditional alternatives for the transportation services mainly in areas with a weak passenger demand. The authors hope that it could be interesting mainly for regional and municipal authorities. The highest importance can be expected in the solutions described in parts 2, 3, 4.3 and, maybe, 5.3 as well.

References

[1] ČERNÁ, A., ČERNÝ JAN. *Non-traditional solution of transport services in rural areas* (in Czech). Územní samospráva v praxi. pp. 13–18, No. 14, (1997).
[2] ČERNÁ, A., ČERNÝ JAN. *Semiadaptive systems of public transport and transport service in areas with smaller demand* (in Czech). Scientific papers of the University of Pardubice B,No. 4 pp. 183–186 (1998) .
[3] ČERNÁ, A. *A remark on the regular inland transport efficiency (excluding urban mass transport)* (in Czech). Manažerské rozhledy, FM VŠE Praha (2000).
[4] ČERNÁ, A., ČERNÝ JAN. *Theory of control and decision-making in transportation systems* (in Czech).Monograph, Institut Jana Pernera (2004).
[5] ČERNÝ, JIŘÍ. *Interactive systems of Transport services* (in Czech), Scientific Papers of the University of Pardubice B, No. 4 (1998).
[6] MALUCELLI, F.- NONATO, M.- PALLOTTINO, S.: *Demand adaptive systems: Some proposals on flexible transit*, in: Operational Research in Industry (T. A. Ciriani et al. Editors), (1999), McMillan Press, London, pp. 157–182.
[7] ŠIROKÝ, J. *Dial-a-Bus – a new mode of regional public passenger transport service.*, Scientific Papers of the University of Pardubice B, No. 4, pp. 201–206 (1998).

Jerzy M. Wolanin *

CHOSEN ELEMENTS OF CIVILIZATIONAL SELECTION THEORY THIS IS WHY UNWILLING EVENTS ARE UNAVOIDABLE

Man has always lived in two spaces, natural environment and civilizational space. Civilizational space has been formed by man, is built up of all human activities, and has been created among others as human response to hazards. Variability of civilizational space causes the necessity of keeping up with changes. Things that were good yesterday today are of no value, which means they no longer protect from unwilling events. Description delay in relation to its constant change in civilizational space along with its complexity causes difference in interpretation. Occurrence of unwilling event is a sign that the accepted solution was bad and needs improvement. Thus, civilizational space is a source of hazards.

Man has always lived in two spaces. The first one, being the beginning of all that happened on Earth, has been created by natural environment. Here, it will be called natural space. The other space, civilizational, has been formed by man. Civilizational space, at first serving as a shield against blind forces of nature, has transformed along with civilizational development into independent existence. It was isolated out of natural environment characteristic of people only. The essence of the environment are human relations supported by science and technology. Without the civilizational space there would be no development of civilization. Creation of the civilizational space is an answer to hazards of life in natural environment in consequence of which people lost their lives. Building human relations was probably connected with ability to communicate among group individuals of first people. Common overcoming of hazards connected with famine, protection against stronger plunderer or the division of functions among the members of the society helped it to survive, that means it worked. Other solutions might have been checked, however, nothing can be said about them, as the societies no longer exist. That means their solutions did not work. Making assumption that such unsuccessful attempts had taken place is well justified. An observation of evolution of societies throughout their historical growth implies that such attempts have always been made. Some of them are exceptionally cruel but they are unavoidably verified by the civilizational evolution. Unavoidability is a common phenomenon in many domains. Natural selection is a good example here. Individuals unadapted to natural environment must suffer a defeat. There are no exceptions to this rule. Life in natural environment unavoidably made them create first organized societies. As mentioned before, it was a defensive reaction against challenges of natural environment. That was the right way to respond. To put it into modern terms, those people employed the strategy of response, which depends on mutual "stimulus-response" relations. The correct reaction protects against the effects of a given stimulus as long as the consequences are negative. The appropriate reaction to hazards caused by natural environment allowed man to survive. On account

of what has been said so far it may be stated that the strategy of response is the original one in comparison to other reactions that have ever been observed. It may be said that this strategy is an inborn ability of humans and societies they constitute. Till present days it has brought exceptionally good results, however, as will be shown later, not always sufficient.

The correct reaction to hazards of nature influenced better organization of groups. Yet even then it was observed that reaction in "stimulus-response" relation only was not enough. How to react to hazards that are yet to come? Here magic appeared. People felt safer and were more self-assured in their actions knowing that all had been done to assure them succeed. Setting souls at rest through fulfilling rituals had a great advantage. It provided certainty of action as people deeply believed they were supported by supernatural forces. Such positive attitude worked well in fight with blind forces of nature. It was a good solution that lasted and transformed. The strategy of misfortune avoidance appeared. Hence, along with the strategy of response the strategy of prevention surfaced. The former one is said to be connected more with tools while the latter one with the spirit and its evolution. Both strategies have succeeded and exist up till now. They constitute the foundations of the civilizational space. Partially the strategy of prevention also helped man to detach from and become independent of nature. Building cities is a good example here.

A number of people feels comfortable in a city. It has its undeniable advantages. What is more, cities turned out to be a good solution for man and all the societies so far. Rural areas, even though closer to nature, also constitute oasis of human settlements. Natural disasters are no longer as dangerous as they used to be. Nevertheless, they are able to break manmade barriers and verify them often enough. The boundaries of the civilizational space created by man and natural space are in a state of flux. They change and in consequence they strive for balance of mutual adjustment. Each shift of balance always leads to disasters. It should be remem-

* **J. M. Wolanin**
 The Main School of Fire Service, Warsaw 01-629 Slowackiego 52/54 Poland, E-mail: Jerzy.Wolanin@sgsp.edu.pl

bered that natural space is primary and in consequence it provides the right direction to the evolution of civilizational space. The civilizational space will not replace natural space permanently. Even though the civilizational space influences the natural one the latter marks the direction of mankind development. Degradation of forests leads to floods, industrial gases destroy ozone in the atmosphere, and nuclear energy may be a cause of threats connected with radioactive contamination of environment. Those examples of interaction between the civilizational and natural space explicitly indicate obvious predominance of natural space in the struggle for search of the best solutions. Unfortunately the results come in form of disasters. How to avoid them? It is hard to give up on civilizational progress as such solution, negative in its nature, would also lead to disasters. There is some hope, however, in specific characteristics of struggle between civilization and nature. The idea is that on different levels of those struggles their effects are delayed in time. They occur after some time giving us the same a chance to undertake activities enabling counteraction to excessive civilization expansion. The chance can be used by researching mechanisms of concurrent phenomena of civilizational development and its influence on natural environment. Engaging in scientific research and making certain decisions may but do not have to lead to soothing the conflict between civilization and nature. The last claim does not have to refer to phenomena in global dimension. It stretches on each and every level and functions in local communities as well. Thus certain inertia of tension effects created on the point of junction of civilizational development and protection of natural environment allows better phenomena recognition and better performance of particular actions. It should be stressed here that symptoms of catastrophes appear much earlier in such cases. The whole problem is to be able to observe it at the right time and interpret adequately. For such reasons safety policy should be created no only in global dimension but in local one as well.

Undoubtedly safety policy belongs to the human sphere of action in the civilizational space. Appropriate safety policy assures people security. But on the other hand, how can we know that a given policy is appropriate? Only its functioning in thecivilizational space can verify it. It is helpless to hazards either natural or civilizational, as sooner or later tragedy will occur. Wrongly applied safety policy will always be negatively verified unlike correctly applied one which will last till it becomes insufficient and only then it will be negatively verified. All the considerations concerning safety policy that man has always employed refer to each and every aspect of human life. So the question is whether each human activity, as in the case of employing safety policy, is verified? And does negative verification always cause misfortune?

The analysis of the civilizational space characteristics will bring answers to those questions. The civilizational space is built up of all human activities. As it was mentioned before, it has been created as human response to hazards. This role is still present today. Complexity of human activities in the material as well as in spiritual sphere generates similar complexity in the civilizational space. Being independent, a single man creates his own existence. The distinctive feature of existence is its constant change. It is trans-

formed by a constant activity of billions of people. Millions of tiny changes cause continual civilizational development. Some of those changes are more permanent than others. They bring certain things into the civilizational space but under the influence of other changes they simply disappear. Due to the civilizational space variability things that were good yesterday today are of no value and when they are no longer valued they just stop serving their turn. They do no longer protect from unwilling events or they do not fulfill requirements. Unfulfilling requirements causes discomfort which is categorized as one of less severe effects of unwilling events.

An unwilling event is defined as an event hazardous to life and/or human health, possession, environment as well as all social, economic and cultural relations of a given society or an event that does not achieve aims of undertaken actions.

Variability of the civilizational space causes the necessity of keeping up with the changes. Observing changes of natural environment around,is an everyday reality. Even in "safe" civilizational surroundings in order to survive one has to follow changes and adapt to them. Lack of p[ermanent adjustment always reveals unwilling events around. To avoid this humans incessantly investigate their surroundings and then analyze and describe it, i.e. they share experience with others. Description of civilizational settings may employ different forms, as many as the civilizational space has itself. Those can be scientific descriptions with research method records that aim at generalizing the binding laws. A description of reality is also expressed through all kinds of artistic forms. Does not classical music describe of sounds or is not a form of a world description in general? Actually, to description of setting belongs each information that is transformed in any way and any form. A description is a collection of gathered observations. This extremely differentiated means of sharing observations unfortunately has one fundamental feature. The result of civilizational space research influences the space itself and is strongly connected with it. At the time of exchanging given information the civilizational space described by the info is being transformed. It is due to the fact that the info has been spread around and has been functioning in minds of many people not mentioning the change in their consciousness. When multiplying this dependence by the infinite number of information exchanged in the whole world at any moment there is in fact a delay of knowledge about the civilizational space in relation to its factual state. Time is needed to describe a new reality. A new description changes unavoidably data described before. The process is continuous and ongoing. An analogy from physics can be helpful here. To see where exactly the electron is, first a photon reflected from the electron must be perceived by an eye. However, the photon reflecting from the electron moves it to another position. Hence, when one thinks he/she sees the electron it actually is already somewhere else. It may be said that phenomena occurring on an elementary particle level transform themselves to a description of the civilizational space. Just like in physics the principle of indeterminacy applies here. Thus, the civilizational space is elusive in its nature.

Description delay in relation to its constant change in the civilizational space along with its complexity causes difference in

interpretation. Consequently, those differences influence adoption of various solutions concerning the civilizational space. Unfortunately, most of them are inadequate. Such a statement can be accepted with a high level of accuracy if the number of functioning solutions remaining in responsible time in relation to the number of solutions ever thought about is taken into consideration. Occurrence of an unwilling event is a sign that the accepted solution was bad. Accepting a bad solution is a result of elusive nature of the civilizational space. Unfortunately, this statement implies the following conclusion:

Principle of indeterminacy in civilizational space description was, is, and will always be a source of hazards.

So the civilizational space is a source of hazards. A space that has been created by humans to protect them became itself a source of hazards. Yet it is not the fault of man that he/she does not know how to use achievements of the civilizational space. Humans in their civilizational development have to accept bad solutions as they lack knowledge about the space because of the binding principle of indeterminacy. Lack of such knowledge causes that accepted solutions often do not fit into civilizational space and are negatively verified. Then negative selection takes place and causes that solutions are more adjusted to civilizational space. Such a phenomenon can be called civilizational selection.

Civilizational selection is a natural process of verification of accepted solutions depending on rejection of solutions not fitting into civilizational space and revealing through occurrence of unwilling events.

Civilizational selection is an unavoidable phenomenon due to the binding principle of indeterminacy. Unluckily, it also causes unavoidability of unwilling events occurrence on different scale. On the other hand, civilizational selection forces better accommodation to civilizational space. So for these reasons it is a phenomenon stimulating progress. The dynamics of changes in civilizational space influences the space itself. Vast variability of civilizational space accelerates civilizational selection. Unfortunately, acceleration means increase in the number of unwilling events occurrence that is often dramatic. For this reason every revolution is accompanied by such a great number of misfortunes. There is no difference whether it is industrial, social or political revolution. The dynamics of changes is high enough to be observed at once.

All that defines the essence of civilization is adjusted to civilizational space especially man and whole societies. Unacquainted with technology humans, when brought in contact with it, con-stitute an overt example of hazards. Civilizational space includes mutual relations between people. Here hazards may also occur when those relations are not fitted into civilizational surroundings, e.g. to well-established laws. Ideologies, organizational concepts, ways of handling business, forms of human organizational groups with common aims as well as cultural activity and media are all subjects to civilizational space adjustment. All human activities need to be accommodated into civilizational space. Each failure indicates lack of adjustment. Those facts even stronger confirm that civilizational space is a source of hazards itself.

Negative selection is not the only characteristic of civilizational selection. Civilizational selection is a stabilizer of proper solutions. Of course, ''proper solution'' is a relative notion and fits into the category of the best adjusted solution to civilizational space at a given time. However, some solutions are permanent while others are modified. It shows the existence of some universal laws in civilizational space. Such solutions become stable in consequence of civilizational selection. Very often history verifies stabilized solutions. Nevertheless, it does not deny commonly bounding civilizational selection. On the contrary, historical verification is a sign of civilizational selection. The connection between time and bad solution existence is hard to establish. Most probably it is connected with nature of the very thing being a bad solution. The longest ones of bad solutions to hold are ideologies. The reasons for that are subject to another inquiry.

Concluding, it may be claimed that there are several main reasons for developing hazards that are inseparably connected with surrounding reality. Firstly, the source of hazards are forces of nature always verifying ill-thought concepts. Secondly, the source of hazards is boundary of civilizational and natural space created by human beings. In this case nature verifies everything itself warning against bad solutions causing its devastation. Thirdly, the source of hazards is an immanent for civilizational space elusiveness arising in consequence of explicit inability to being described. It is a "genetic" feature of this space causing inadequacy of accepted solutions to its actual state. Fourthly, the source of hazards is the space itself due to psychological adjustment process to new civilizational conditions. Finally, the source of hazards are interpretations of observations concerning the conditions of civilizational space which are connected with constant monitoring by people and what follows accepting inadequate solutions. The latter occurs mostly on an individual decisions level.

The article was written after reading the Polish edition of "The End of Science" by John Horgan. I was inspired by chapter V: "The End of Evolutional Biology".

COMMUNICATIONS – Scientific Letters of the University of Žilina
Writer's Guidelines

l. Submissions for publication must be unpublished and not be a multiple submission.

2. Manuscripts written **in English language** must include abstract also written in English. The submission should not exceed 7 pages (format A4, Times Roman size 12). The **abstract** should not exceed 10 lines.

3. Submissions should be sent: **by e-mail** (as attachment in system Microsoft WORD) to one of the following addresses: *holesa@nic.utc.sk* or *vrablova@nic.utc.sk* or *polednak@fsi.utc.sk* **with a hard copy** (to be assessed by the editorial board) **or on a 3.5″ diskette** with a hard copy to the following address: Zilinska univerzita, OVaV, Moyzesova 20, SK-10 26 Zilina, Slovakia.

4. Abbreviations, which are not common, must be used in full when mentioned for the first time.

5. Figures, graphs and diagrams, if not processed by Microsoft WORD, must be sent in electronic form (as GIF, JPG, TIFF, BMP files) or drawn in contrast on white paper, one copy enclosed. Photographs for publication must be either contrastive or on a slide.

6. References are to be marked either in the text or as footnotes numbered respectively. Numbers must be in square brackets. The list of references should follow the paper (according to **ISO 690**).

7. The author's exact **mailing address of the organisation where the author works, full names, e-mail address or fax or telephone number,** must be enclosed.

8. The editorial board will assess the submission in its following session. In the case that the article is accepted for future volumes, the board submits the manuscript to the editors for review and language correction. After reviewing and incorporating the editor's remarks, the final draft (before printing) will be sent to authors for final review and adjustment.

9. The deadlines for submissions are as follows: September 30, December 31, March 31 and June 30.

10. Topics for the next issues: 2/2006 – Energetic machines and equipment, 3/2006 – Informative and communication tools for decision-making support, 4/2006 – Fatigue and endurance of constructional materials, 1/2007 – Mechatronics in electrotechnical systems.

POKYNY PRE AUTOROV PRÍSPEVKOV DO ČASOPISU
KOMUNIKÁCIE – vedecké listy Žilinskej univerzity

1. Redakcia prijíma iba príspevky doteraz nepublikované alebo inde nezaslané na uverejnenie.

2. Rukopis musí byť **v jazyku anglickom**. Príspevok by nemal prekročiť 7 strán (formát A4, písmo Times Roman 12 bodové). K článku dodá autor **resumé** v rozsahu maximálne 10 riadkov (v anglickom jazyku).

3. Príspevok prosíme poslať: **e-mailom**, ako prílohu spracovanú v aplikácii Microsoft WORD, na adresu: *holesa@nic.utc.sk* alebo *polednak@fsi.utc.sk* príp. *vrablova@nic.utc.sk* (alebo doručiť na diskete 3,5″) **a jeden výtlačok** článku na adresu Žilinská univerzita, OVaV, Moyzesova 20, 010 26 Žilina.

4. Skratky, ktoré nie sú bežné, je nutné pri ich prvom použití rozpísať v plnom znení.

5. Obrázky, grafy a schémy, pokiaľ nie sú spracované v Microsoft WORD, je potrebné doručiť buď v digitálnej forme (ako GIF, JPG, TIFF, BMP súbory), prípadne nakresliť kontrastne na bielom papieri a predložiť v jednom exemplári. Pri požiadavke na uverejnenie fotografie priložiť ako podklad kontrastnú fotografiu alebo diapozitív.

6. Odvolania na literatúru sa označujú v texte alebo v poznámkach pod čiarou príslušným poradovým číslom v hranatej zátvorke. **Zoznam použitej literatúry** je uvedený za príspevkom. Citovanie literatúry musí byť **podľa STN 01 0197 (ISO 690)** „Bibliografické odkazy".

7. K rukopisu treba pripojiť **plné meno a priezvisko autora a adresu inštitúcie v ktorej pracuje, e-mail adresu** alebo číslo telefónu event. faxu.

8. Príspevok posúdi redakčná rada na svojom najbližšom zasadnutí a v prípade jeho zaradenia do niektorého z budúcich čísiel podrobí rukopis recenziám a jazykovej korektúre. Pred tlačou bude poslaný autorovi na definitívnu kontrolu.

9. Termíny na dodanie príspevkov do čísiel v roku sú: 30. september, 31. december, 31. marec a 30. jún.

10. Nosné témy ďalších čísiel: 2/2006 – Energetické stroje a zariadenia, 3/2006 – Informatické a komunikačné nástroje na podporu rozhodovania, 4/2006 – Únava a životnosť konštrukčných materiálov, 1/2007 – Mechatronika v elektrotechnických systémoch.